Dysferlin and its role in the pathogenesis of muscular dystrophy

Dissertation

In partial fulfillment of the requirements for the degree
“Doctor rerum naturalium (Dr. rer. nat.)”
in the Molecular Medicine Study Program
at the Georg-August University Göttingen

submitted by Julia Hofhuis

born in Bremen

Göttingen 2013

Reviewers/Members of the Thesis Committee:

1. Thesis Committee Member

Prof. Dr. Jutta Gärtner

Department of Pediatrics and Adolescent Medicine

University Medical Center Göttingen, University of Göttingen

2. Thesis Committee Member

Prof. Dr. Peter Schu

Department of Biochemnistry II

University Medical Center Göttingen, University of Göttingen

3. Thesis Committee Member

Prof. Dr. Wolfgang Brück

Department of Neuropathology

University Medical Center Göttingen, University of Göttingen

Date of Disputation:

Affidavit

I hereby declare that I wrote my doctoral thesis entitled "Dysferlin and its role in the pathogenesis of muscular dystrophy" independently and with no other sources and aids than quoted.

Göttingen, September 2013

_____

(Signatur)

Contents

Abstract

Dysferlin is a multi C2 domain protein that belongs to the ferlin family and is localized to the T-tubule system in skeletal muscle fibers. It is involved in skeletal muscle membrane repair, regeneration and T-tubule biogenesis. The precise biochemical function of dysferlin has not been discovered so far, but mutations in the dysferlin gene lead to mucular dystrophy. Preliminary data demonstrated that dysferlin induces tubulated membranes when heterologeously expressed in non-muscle cells. These observations suggested a role of dysferlin in membrane tubulation, and it was the aim of this thesis to further examine the biochemical and cell biological of dysferlin

Analysis of dysferlin-induced tubules in non-muscle cells revealed that these structures share biochemical and morphological similarities to T-tubule membranes as they incorporate T-tubule phospholipids and invaginate from the plasma membrane. Full-length dysferlin was required for membrane tubulation, and pathogenic mutations impaired membrane deformation capacity. In vitro, dysferlin induces liposome tubulation which provides direct morphological evidence for a powerful membrane tubulation capacity.

In this thesis it was further demonstrated that the alteration in T-tubule morphology of dysferlin-deficient muscle lead to increased Ca^{2+} release probably through excitation-coupled Ca^{2+} entry. This effect was not due to a secondary alteration of triad- or T-tubule associated proteins and resulted in increased exercise capacity in juvenile dysferlin-deficient mice similar to the phenotype of presymptomatic patients affected by dysfelin-deficient muscular dystrophy.

Also in heart muscle dysferlin was required for a morphologically and functionally intact T-tubule system. Functional alterations in Ca^{2+} homeostasis were compensated under normal physiological conditions but induced severe arrhythmogenic events in stress situations.

Taken together, we provide direct evidence that dysferlin induces membrane tubulation defining a novel function of this protein. The abnormal T-tubule system affects Ca^{2+} homeostasis in skeletal and heart muscle. These findings may have important clinical implications, and modulation of Ca^{2+} homesostasis in dysferlin-deficient muscular dystrophy should be investigated as a possible translational therapeutic approach.

List of figures

Abbreviations

AM	acetomethyl ester
BCA	bicinchonic acid
BDM	2,3-butadionemonoxime
ß-ME	2-mercaptoethanol
BSA	bovine serum albumin
BTS	N-benzyl-p-toluene sulphonamide
cAMP	cyclic adenosine monophosphate
CaSpF	Ca^{2+} spark frequency
CPVT	catecholaminergic polymorphic ventricular tachycardia
Cyto D	cytochalasin D
DAPI	4′,6-Diamidin-2-phenylindol
DGC	dystrophin-glycoprotein complex
dH_2O	distilled water
ddH_2O	double distilled water
DHPR	dihydropyridine receptor
Di8ANEPPS	di-8-butyl-aminonaphthyl-ethylene-pyridinium-proply-sulfonate
DMSO	dimethyl sulfoxide
DNA	desoxyribonucleic acid
dNTP	deoxyribonucleoside triphosphate
DTT	dithiothreitol
ECCE	excitation-coupled Ca^{2+} entry
EC-coupling	excitation contraction-coupling
EDTA	ethylenediaminetetraacetic acid
EGTA	ethylene glycol tetraacetic acid
ER	endoplasmatic reticulum
F	fluorescence
F_0	baseline Fluorescence
FCS	fetal calf serum
FDAR	frequency-dependent acceleration of relaxation
FDB	flexor digitorum brevis
FDHM	full duration at half maximum
FKBP12	12 kDa FK506 binding protein
F_{max}	maximal fluorescence
F_{min}	minimal fluorescence
FWHM	full-width at half maximum

GAPDH	glyceraldehyde-3-phosphate dehydrogenase
GFP	green fluorescent protein
HA	hemagglutinin
HCl	hydrochloric acid
HEPES	2-(4-2-hydroxyethyl)-piperazinyl-1-ethansulfonate
HRP	horseradish peroxidase
IF	immunofluorescence
IPTG	isopropyl β-D-1-thiogalactopyranoside
ISO	isopropanol
JP 1	junctophilin 1
KCl	potassium chloride
K_d	dissociation constant
KO	knock-out
LB	luria broth
LGMD2A	limb-girdle muscular dystrophy type 2A
LGMD2B	limb-girdle muscular dystrophy type 2B
LGMD2C	limb-girdle muscular dystrophy type 2C
LiCl	lithium chloride
MeOH	methanol
$MgCl_2$	magnesium chloride
MI	myocardial infarction
MM	Miyoshi Myopathy
Mn	manganese
NaCl	sodium chloride
NaOH	sodium hydroxide
NBD	7-nitro-2-1,3-benzoxadiazol-4-yl
NCX	Na^+/Ca^{2+}-exchanger
Orai1	Ca^{2+} release-activated Ca^{2+} channel protein 1
PBS	phosphate buffered saline
PCR	polymerase chain reaction
PDI	protein disulfide isomerase
PE	phosphatidylethanolamine
PFA	paraformaldehyde
PH domain	pleckstrin homology domain
PIP	phosphatidylinositol phosphate
PIP2	phosphatidylinositol 4,5-bisphosphate
PIP2 kinase	phosphatidylinositol 4-phosphate 5-kinase

PIP3	phosphatidylinositol 3,4,5-trisphosphate
PI3P	phosphatidylinositol 3-phosphate
PI4P	phosphatidylinositol 4-phosphate
PMCA	plasma membrane Ca^{2+} ATPase
PMSF	phenylmethylsulfonyl fluoride
PR 30	post 30 s rest
PTA	phosphotungstic acid
RFP	red fluorescent protein
RT	relaxation time
RyR	ryanodine receptor
RyR1	skeletal ryanodine receptor
RyR2	cardiac ryanodine receptor
SDH	succinate dehydrogenase
SDS	sodium dodecylsulfate
SEM	standard error of the mean
SERCA	sarcoplasmatic reticulum Ca^{2+}-ATPase
SOCE	store-operated Ca^{2+} entry
SR	sarcoplasmatic reticulum
ss	steady-state
STIM1	stromal interaction molecule 1
TAE	tris-acetate-EDTA
TBST	tris buffered saline with 1 % tween 20
TEMED	N, N, N´, N´-tetramethylethylenediamine
TM	transmembrane domain
Tris	tris-(hydroxymethyl)-aminomethane
TRPC3	transient receptor potential cation channel 3
vs.	versus
WB	Western blot
WT	wild-type

Units

b	base
ºC	degree Celsius
Da	dalton
g	gram
h	hour
Hz	hertz
l	liter
m	meter
M	molar
min	minute
mol	mol
OD_{600}	optical density at 600 nm
%	percentage
% (v/v)	percent by volume
% (w/v)	percent by weight
rpm	rounds per minute
s	second
U	unit

Unit prefix

c	centi
k	kilo
m	milli
µ	micro
n	nano

1. Introduction

1.1 The muscular dystrophies

Muscular dystrophies are a heterogenous group of inherited disorders of skeletal muscle which can manifest in any age from childhood to adolescence. These diseases are characterized by progressive muscular weakness and wasting due to degeneration and loss of muscle fibers. Most muscular dystrophies lead to a massive increase of serum creatine kinase and muscle pathology with de- and regenerating fibers with centralized nuclei, inflammation, increase in fiber size variation and replacement of intact muscle fibers by fat and fibrous tissue. Several genes could be identified in the last decades that are responsible for these diseases, but most of the underlying pathomechanisms leading to muscle degeneration are still unknown and therefore no curative treatment is available. A major step towards the identification of the molecular mechanisms behind these disorders was the discovery of dystrophin (Koenig et al., 1988) and its association with the dystrophin-glycoprotein complex (DGC). Mutations in the dystrohin gene lead to the most common muscular dystrophy, Duchenne muscular dystrophy. The DGC is a multisubunit complex which links the subsarcolemmal actin cytoskeleton with the extracellular matrix thereby stabilizing the plasma membrane (Laval and Bushby, 2004). Loss of dystrophin or other proteins associated with the DCG lead to plasma membrane destabilization. Muscle fibers are permanently exposed to mechanical stress due to shearing forces that work on the plasma membrane of the muscle fibers during the process of contraction and relaxation. Therefore, muscle fibers with destabilized DGC due to mutations of DGC genes are prone to membrane ruptures which then lead to degeneration of the muscle fiber (Staub and Campbell, 1997). This emphasizes the crucial role of an intact plasma membrane in skeletal muscle physiology.

1.2 Dysferlin-deficient muscular dystrophy

Mutations in the dysferlin gene were found to be the cause of three clinical diseases, autosomal recessive limb-girdle muscular dystrophy type 2B (LGMD2B; OMIM# 253601, Bashir et al., 1998), Miyoshi Myopathy (MM; OMIM# 254130, Liu et al., 1998) and distal anterior compartment myopathy (OMIM #606768, Illa et al., 2001). As the number of patients affected with dysferlinopathies is estimated between 1/100,000 and 1/200,000 (Moore et. al., 2006) it is a rare muscular dystrophy. Patients present with muscle pain and muscle weakness in either proximal (LGMD2B) or distal (MM) muscles. During the course of the disease with typically slow progression the phenotypes overlap and muscle degeneration spreads from distal to proximal muscles

and vice versa so that all limb-girdle muscles are affected. Age of disease onset is very heterogeneous but most patients show first symptoms in the second decade of life. Bansal et al. showed that dysferlin is distinct from the DGC as dysferlin-null mice developed a slowly progressive muscular dystrophy but maintained a functional dystrophin-glycoprotein complex. Furthermore they showed that absence of dysferlin leads to defects in the plasma membrane repair system (Bansal et al., 2003). Therefore it was concluded that defective membrane repair but not instability and defects of the plasma membrane structure lead to loss of muscle fibres in dysferlinopathy. This was a first hint towards a different pathomechanism as compared to DGC deficiencies. The role of dysferlin in membrane repair was substantiated by the fact, that patient muscles show accumulation of vesicles in sub-sarcolemmal regions (Piccolo et al., 2000, Cenacchi et al., 2005). Furthermore, dysferlin-deficient muscle fibres show defective muscle differentiation due to delayed expression of myogenin (De Luna et al., 2006). In contrast to patients with other forms of musclular dystrophy dysferlinopathy patients show increased levels of fitness before onset of symptoms (Klinge et al., 2009). So far this observation is not understood but it leads to the hypothesis that the molecular pathomechanism underlying the disease is not sufficiently resolved. Muscle tissue is permanently exposed to mechanical stress and therefore plasma membrane ruptures. As patients are initially without symptoms and have a high level of fitness, it seems unlikely that the disease is based on a defective membrane repair system alone. McNeil and Steinhardt claimed that membrane repair is a prerequisite for evolutional development of force generating tissue which further hints towards other molecular pathomechanisms underlying the disease.

1.2.1 The dysferlin gene an its orthologues

The dysferlin gene is located on chromosome 2p13. The most common transcript encoded by the dysferlin gene includes 55 exons and alternative splicing leads to several isoforms (Aoki et al., 2001). Among them, isoform 8 is commonly used to describe the dysferlin gene. With 90 % sequence similarity between mouse and human dysferlin is well conserved among the mammals (Vafiadaki et. al., 2001).

Mutations of the dysferlin gene are scattered throughout the whole coding sequence without any apparent hotspot. Mainly point mutations and small insertions or deletions are found but larger exonic deletions or duplications do also exist. Many dysferlin mutations lead to degradation through the nonsense-mediated mRNA decay process (Wenzel et al., 2006) and others lead to truncated or unstable versions of the protein that are degradated by autophagy or the endoplasmatic reticulum (ER) associated

degradation system (Fujita et al., 2007). Furthermore, no genotype-phenotype correlation was found (Krahn et al., 2009, Klinge et al., 2008, Klinge et al. 2009).
The dysferlin protein translated from isoform 8 is a 230 kDa protein which belongs to the ferlin family. The ferlins are named after their homology to Fer1 which was originally identified in *C. elegans*. Fer1 mediates Ca^{2+}-dependent fusion of membranous organelles to the plasma membrane in developing spermatids (Achanzar and Ward, 1997, Washington and Ward, 2006). Human orthologues of dysferlin are otoferlin, myoferlin and FER1L5. Otoferlin is located in the inner ear at the inner hair-cell and is known to play a role in exocytosis of synaptic vesicles and is needed for Ca^{2+}- dependent vesicle-plasma membrane fusion (Roux et al., 2006). Myoferlin is most related to dysferlin and is highly expressed in fusing myoblasts. It is known to be involved in myoblast-myoblast and myoblast-myotube fusion which are critical events during muscle development and repair (Davis et al., 2000, Doherty et al., 2005). Additionally, myoferlin and also FER1L5 were demonstrated to interact with vesicle recycling proteins EDH1 and EDH2 (Doherty et al., 2008, Posey et al., 2011). Loss of function mutation of otoferlin leads to nonsyndromic deafness (Yasunaga et al., 1999) but so far no human pathologies have been described for myoferlin and FER1L5. In human and mouse genomes two further genes are present, FER1L4 and FER1L6, but not much is known about their function or protein expression.

1.2.2 The dysferlin protein and its C2 domains

All proteins of the ferlin family have a very similar protein structure (see figure 1.2.2). They all are type II transmembrane proteins and have a carboxy-terminal transmembrane domain. Furthermore, they all contain multiple copies of C2 domains which are known to play a role in phospholipid interaction (Davis et al., 2002). C2 domains were first described in proteinkinase C where they are involved in Ca^{2+}-dependent membrane binding. Most of the C2 domain proteins have maximal three C2 domains. Besides the ferlins only two gene families have been described with three or more C2 domains; the multiple C2 domain and transmembrane region proteins (Shin et al., 2005) and the extended synaptotagmins (Min et al., 2007) but the precise function of multiple C2 domain proteins remains so far unknown. Dysferlin contains seven C2 domains that show high similarity to the synaptotagmin VII C2 domains which are involved in Ca^{2+}-triggered fusion of synaptic vesicles with the plasma membrane in neurons (Sutton et al., 1995). The classical function of C2 domains is Ca^{2+}-dependent lipid binding but some C2 domains are involved in membrane trafficking and signal transduction by mediating protein-protein interaction without Ca^{2+}-binding abilities (Nalefski and Falke, 1996). C2 domains form an eight-stranded antiparallel ß-sandwich

consisting of two four-stranded ß-sheets which are connected by highly variable surface loops in terms of amino acid composition and conformation (Rizo and Südhof, 1998). Two different topologies of C2 domains were shown which seem to be important for protein function (Nalefski and Falke, 1996). Dysferlin C2A, C2B and C2E domains have topology I like the C2A domain of synaptotagmin I and the other four C2 domains belong to the type II topology domains like the C2 domain of proteinkinase Cδ (Therrien et al., 2006). The Ca^{2+} binding site is built of three Ca^{2+} binding loops which reside on one end of the sandwich and contain negatively charged residues that are responsible for Ca^{2+} binding thereby influencing the electrostatic potential of the membrane as a prerequisite for phospholipid binding (Shao et al., 1997). Additionally, the residue composition of the loop provides the specificity for the targeted membranes as it influences the phospholipid selectivity (Cho et al., 2006). Despite the fact that to date the purpose of multiple C2 domains is unknown it should be mentioned that sequence analysis of the ferlin C2 domains reveals a great diversity. Each domain seems to be more similar to its counterpart in paralogs than to the other C2 domains of the same ferlin (Washington and Ward, 2006, see figure 1.2.2) leading to the hypothesis, that all C2 domains of dysferlin are different and are therefore needed for proper protein function.

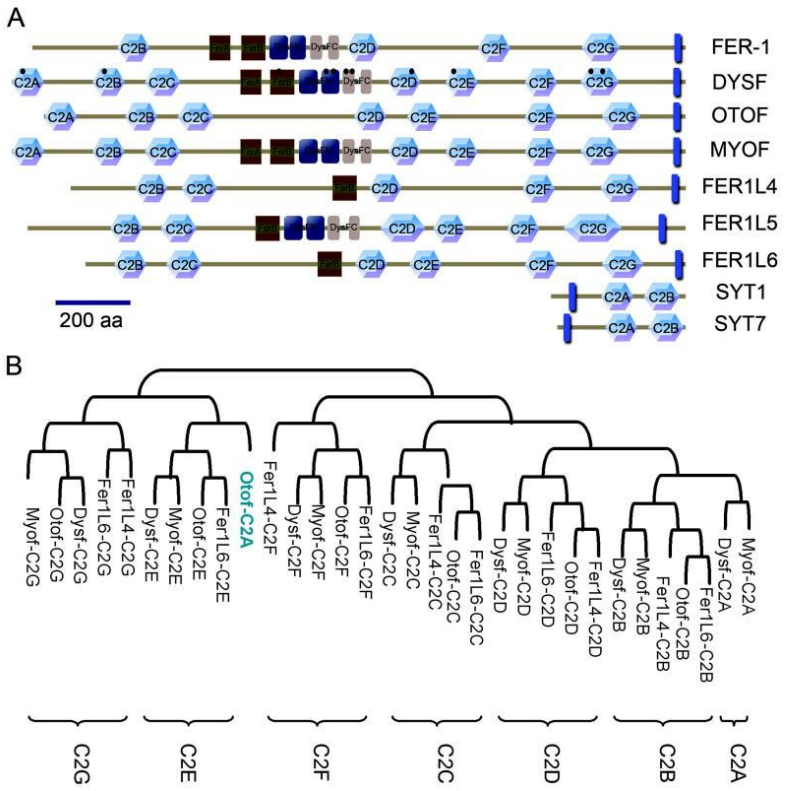

Figure 1.2.2: Domain structure of ferlins and phylogenetic tree of C2 domains A) Domain structure of Fer1 and mammalian ferlin-like proteins. B) Phylogenetic tree based on alignment of ferlin C2 domains (from Han and Campbell, 2007).

So far phospholipid binding ability was shown for the C2A domain of dysferlin. This domain binds negatively charged phospholipids in a Ca^{2+}-dependent manner which is abolished by mutations in this domain (Davis et. al., 2002). Furthermore, the C2A domain was shown to bind phosphatidylinositol 4-phosphate (PI4P) and phosphatidylinositol (4,5)-bisphosphate (PIP2) in presence of Ca^{2+} (Therrien et al., 2009). Much less is known about the other C2 domains of dysferlin. Like C2A they seem to bind phosphatidylserine, but the binding affinity seems to be much weaker and independent of Ca^{2+} (Therrien et al., 2009). Only recently it was published that the C2 domains of dysferlin as well as oto- and myoferlin are able to alter the packaging of membrane vesicles indicating a membrane sculpting function of the dysferlin C2 domains (Marty et al., 2013).

The dysferlin gene contains two further motifs, the DysF sequences which are conserved between orthologues and the ferlin domains. For both of the motifs no function could be established so far. Ferlin domains are present in all ferlin family proteins, but the DysF domain can be found as an unusual nested repeat in only three of the ferlins. Further it is present in yeast peroxisomal proteins where it is important for regulation of peroxisome size and number (Yan et al., 2008). The structure of the myoferlin DysF domain has already been solved and showed two long antiparallel ß-strands (Patel et al., 2008). Proper folding of the DysF domain seems to be important for proper protein function, as many disease-causing mutations can be found in this region. Additionally, PEST sequences, which are known to play a role in protein-protein interaction and protein degradation by the proteasome (Rechsteiner and Rogers, 1996) and nuclear localization signals are present in the dysferlin gene. The dysferlin protein typically does not localize to the nucleus, but these sequences may be relevant for truncated versions of the protein.

1.2.3 Binding partners of dysferlin

To date, several binding partners of dysferlin could be identified. The first interaction partner of dysferlin that has been discovered is caveolin 3 (Matsuda et al., 2001). The protein is the crucial structural component of caveolae localized at the plasma membrane and at the intersection between T-tubule network and the sarcolemma in skeletal and heart muscle and is involved in T-tubule biogenesis (Murphy et al., 2009, Parton et al., 1997). Mutations in the caveolin 3 gene lead to LGMD1C and rippling muscle disease. Caveolin 3-deficient patients show reduced sarcolemmal localization of dysferlin, therefore a role of caveolin 3 in recruiting dysferlin to plasma membrane and to the T-tubules was proposed (Hernandez-Deviez et al., 2006). Affixin, a focal adhesion molecule and annexin I and II, Ca^{2+} and phospholipid binding proteins, were

also shown to interact with dysferlin in skeletal muscle (Lennon et al., 2003, Matsuda et al., 2005) but are not directly involved in any human disease. It was proposed, that Ca^{2+}-dependent interaction of dysferlin with the annexins is needed for aggregation and fusion events after membrane injury (Lennon et al., 2003). Two proteins involved in cytoskeleton regulation are known to interact with dysferlin; calpain 3 and AHNAK (Anderson et al. 2000, Huang et al. 2008, Huang et al. 2007). Calpain 3 is skeletal muscle specific Ca^{2+}-dependent cysteine protease whose substrates are mainly cytoskeleton components. The role of calpain 3 is therefore thought to be regulation of cytoskeleton structure and interaction of cytoskeleton and plasma membrane. Furthermore, calpain 3 is a triad-associated protein and interacts with ryanodine receptor (RyR). Absence of the protein leads to decreased Ca^{2+} release from the SR which probably explains muscle weakness in calpain 3-deficient patients (Kramerova et al., 2008). Mutations of calpain 3 lead to LGMD2A and underlying pathomechanisms involve deregulation of sarcomere structure due to lack of calpain 3-mediated proteolysis (Duguez et al., 2006). As AHNAK is not present in T-tubule membranes, it colocalizes with dysferlin at the sarcolemma (Huang et al., 2007). The large protein localizes at large-scale vesicles called enlargeosome which are involved in cell membrane differentiation and repair and signal transduction through interaction with other proteins (Haase et al., 1999, Borgonovo et al., 2002) but the exact function of this protein is unknown so far and the protein is not directly involved in any human disease. In vitro interaction of dysferlin and mitsugumin 53 was reported but so far no in vivo evidence is available (Cai et al., 2009). It was proposed that mitsugumin 53 recruits dysferlin to the side of injury as mitsugumin 53 acts as sensor for extracellular oxidative molecules which enter the cell on the side of injury and mitsugumin 53 containing vesicles are transported to these sites (Cai et al., 2009).

1.3 Therapeutic approaches

Several studies addressing therapy of dysferlinopathies have been published but until now no curative therapy could be established. Studies testing different pharmacological substances have been conducted, but none of these could improve muscle pathology. Dysferlin-deficient patients show an increased immune response including infiltration and increased phagocytic activity of monocytes in their muscles (Gallardo et al., 2001, Nagaraju et al., 2008) and it was proposed that the aggressive immune response may play a role in disease progression. Therefore studies using a Rho-kinase inhibitor were performed as it limits the inflammatory response due to inhibition of the rho-pathway which plays a crucial role in many immune cell activities. Nevertheless, the decreased immune response did not lead to increased muscle strength or inhibition of

degeneration (Rayavarapu et al., 2010). In contrast to that, inhibition of B cells by rituximab© leads to a slight increase in muscle force indicating a possible role of B cells in muscle pathology (Lerario et al., 2010). Dantrolene is known to inhibit excitation contraction coupling by binding to the (RyR) and inhibiting Ca^{2+} release from the sarcoplasmatic reticulum (SR) (Krause et al., 2004). The exact mechanism is still unknown but interestingly, dantrolene was able to increase the disease course in two dysferlin-deficient patients (Hattori et al., 2007). In addition to these immunological approaches, gene therapy could be a possible way to overcome muscle pathology in dysferlin-deficiency. Neverthesless, gene therapy by transfer of the dysferlin gene is not a trivial method as dysferlin is a large protein of about 230 kDa and encapsulation size of adeno-assosiated viruses is normally restricted to 4 kb. Therefore two independent viruses had to be used to express dysferlin. One vector carried the 5' part of the cDNA and a donor splice site in an intronic sequence, the other vector carried the 3' part of the sequence and an intronic sequence containing a donor splice site. Injection of both vectors in muscle of dysferlin-deficient mice leads to expression of full-length dysferlin due to formation of intermolecular circular concatamers between the two independent vector genomes (Lostal et al., 2010). Using this method it was possible to improve membrane repair and locomotor activity in treated mice. Another possibility to overcome size limitations in gene transfer is transfer of minigenes. Krahn et al. identified a minidysferlin gene in a patient with late onset and moderate dysferlinopathy which was used for injection into dysferlin deficient mouse muscles via AAV mediated gene transfer (Krahn et al., 2010). The minidysferlin protein was correctly localized to the sarcolemma and the T-tubule system and was demonstrated to efficiently repair membrane lesions. Nevertheless, the minidysferlin seems not to be completely functional, as no histological improvement of treated muscles was observed. This further indicates that the disease is not based on a defective membrane repair alone.

1.4 Mouse models of dysferlinopathy

Several dysferlin-deficient mouse models are available to study the disease. First of all, two naturally occurring mice strains have been observed, which reveal dystrophic phenotypes. The SJL/J mouse carries a splicing mutation of the dysferlin gene making it a model for MM and LGMD2B (Bittner et al., 1999, Vafiadaki et al., 2001). One disadvantage of this mouse strain is the fact that the mouse is very susceptible to autoimmune diseases like inflammatory muscle disease and experimental autoimmune encephalomyelitis, lymphoma and virus infections and influences on skeletal muscle can not be excluded. The A/J mouse presents with a mild progressive muscular

dystrophy and was shown to contain a retrotransposon insertion in the dysferlin gene (Ho et al, 2004). A matched control strain is not available for both of these mouse strains, therefore genetically engineered dysferlin knock-out mice strains have been established (C57BL/10.SJL-Dysf, B6.129-Dysftm1Kcam, B6.A/J-*Dysfprmd*) which probably are better models for dsyferlinopathy (Bittner et al., 1999, Bansal et al., 2003, Ho et al., 2004). B6.129-Dysftm1Kcam mice which were used in this thesis develop a slowly progressive muscular dystrophy that starts with the age of two month with appearance of single necrotic fibers. All typical features of dystrohphic muscle are present at the age of 8 month (Bansal et al., 2003).

1.5 Dysferlin and its role in T-tubule biogenesis

The dysferlin protein is expressed mainly in heart and skeletal muscle but can also be found in monocytes and macrophages, brain or lung tissue or in the placenta (Bashir et al., 1998, Liu et al., 1998, Ho et al, 2002, Vandre et al., 2007). In skeletal muscle, dysferlin expression can be detected from 5 to 6 weeks of human embryonic development, the time, when limbs start to show regional differentiation (Anderson et al., 1999) and the dysferlin protein was localized to the plasma membrane and the T-tubule system (Anderson et. al., 1999, Ampong et al., 2005, Klinge et al., 2008). It was demonstrated that dysferlin associates to the T-tubule system in differentiating myotubes in vitro and in vivo and translocates to the sarcolemma after muscle fiber injury (Klinge et al., 2007). This lead to the suggestion, that dysferlin is involved in T-tubule biogenesis. Furthermore, during regeneration dysferlin was localized to the T-tubule system and only in later stages of regeneration it translocated to the sarcolemma. The proposed role of dysferlin in T-tubule development was further substantiated by the fact, that dysferlin-deficient mice are characterized by a highly abnormal configuration of the T-tubule system with dilated and longitudinally oriented tubules (Klinge et al., 2010). Additionally, the dysferlin C2A domain was demonstrated to bind to PIP2, a highly negatively charged phospholipid that is present in T-tubule membranes (Milting et al., 1994). The T-tubule system is an extensive membranous system of skeletal and heart muscle which is necessary for propagating the action potential into the interior of the muscle fiber thereby initiating the process of excitation contraction coupling (EC-coupling) which results in Ca^{2+} release from the SR and

following contraction of the muscle fiber. Further, the T-tubule system is involved in intracellular membrane transport and provides a membrane reservoir for the plasma membrane in muscle fiber regeneration (Engel and Franzini-Armstrong, 2004).

1.6 Biogenesis of the T-tubule system

Biogenesis of the T-Tubule system is a complex mechanism which is not completely understood so far. One model of T-tubule development suggests that tubules derive from the plasma membrane trough a mechanism similar to endocytosis (Ishikawa, 1968). Another model suggests development of tubules through addition of new membranes by a mechanism similar to exocytosis (Schiaffino et al., 1977). The real mechanism of T-tubule development may also involve features of both models, so that plasma membrane vesicles are endocytosed and subsequently fused to T-tubules invaginated from the plasma membrane. In developing mouse muscle T-tubules are first identified after fusion of myoblasts to multinucleated myotubes at E15. They invaginate from the sarcolemma and extend within the myofiber appearing as longitudinal orientated membranes. Later they develop short transverse segments but until birth stay predominantly longitudinal (Veratti, 1961, Kelly, 1980). Two weeks after birth a rearrangement of tubules takes place and tubules appear now mainly in a transverse orientation. Final maturation of tubules is completed in mouse 3 weeks after birth (Takekura et al., 2001a, Franzini-Armstrong, 1991). T-tubule membranes form anatomical triad junctions with the longitudinally oriented sarcoplasmatic reticulum which are already established before birth (see figure 1.6). Therefore, the mature orientation of the T-tubule system is reached only after the triad formation has occurred.

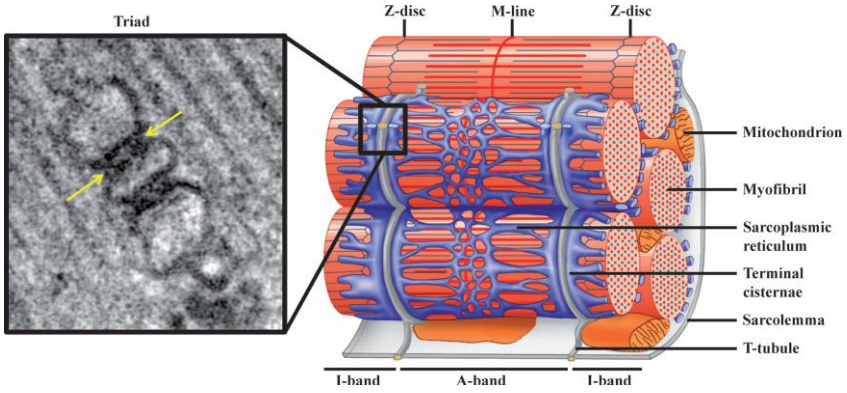

Figure 1.6: T-tubule system and triad organization in skeletal muscle. a) Electron micrograph of a triad junction. A central T-tubule is flanked on both sides by a terminal cisternae element from the SR. Arrows indicate electron-dense junctional feet corresponding to the RyR-DHPR complex. b) Schematic representation of a skeletal muscle sarcomere and surrounding membranes (from Al-Qusairi and Laporte, 2011).

1.6.1 Other proteins involved in T-tubule biogenesis

Besides dysferlin, two further proteins have been implicated in T-tubule biogenesis; Bin1, also known as amphiphysin II and caveolin 3. Caveolin 3 associates to the developing T-tubule system; therefore caveolae and caveolin 3 have been postulated to play a role in T-Tubule biogenesis (Parton et al., 1997). This was substantiated by the fact, that caveolin 3 knock-out mice reveal T-tubule abnormalities with dilated and longitudinal oriented tubules (Galbiati et al., 2001, Minetti et al., 2002). Later it was demonstrated that caveolin 3 also localized to the T-tubule system in mature muscle fibers where it is clustered in so called hot spots at the opening of the T-tubules immediately beneath the sarcolemma (Murphy et al., 2009). The altered structure of the T-tubule system after loss of caveolin 3 leads to alteration of the Ca^{2+} homeostasis as it was shown that L-type Ca^{2+} channel function is reduced in caveolin 3 deficient mice (Couchoux et al., 2007). The fact that the T-tubule system in caveolin 3 null mice shows abnormalities, but is still present and at least has no overt influence on mortality, further proteins seem to be involved in T-tubule biogenesis. One of these is the bar domain protein Bin1 which is known to induce membrane invaginations (Frost et al., 2008), and as it is distributed on the T-tubule system it seemed to be involved in tubulogenesis (Lee et al., 2002). By Lee et al. it was shown that the N-terminal BAR domain of Bin1 is able to induce deformation of membrane bilayers through its interaction with cell membrane phospholipids (Lee. et al., 2002). It was demonstrated in CHO cells that Bin1 is able to induce membrane tubules which was abolished by mutation of the Bin1 BAR domain. Furthermore, a disrupted T-tubule system was detected in Drosophila melanogaster after Bin1 knockout (Razzaq et el., 2001), in adult skeletal muscle fibers after Bin1 knockdown (Tjondrokoesoemo et al., 2011) and in muscle biopsies of Bin1-deficient patients (Toussaint et al., 2011). This implicates a role of Bin1 not only in T-tubule development but also in maintenance of intact membrane structure. The disrupted T-tubule system in Bin1 knockdown muscle fibers leads to disruption of L-type Ca^{2+} channel, also known as dihydropyridine receptor (DHPR) and RyR coupling which influences Ca^{2+} homeostasis. Reduced Ca^{2+} release and breaks in Ca^{2+} transient amplitudes were detected in Bin1-deficient muscle fibers (Tjondrokoesoemo et al., 2011). Mutations of Bin1 lead to centronuclear myopathy which was claimed to be due to the defective T-tubule remodeling (Nicot et al., 2007). A disrupted T-tubule system was also detected in mitsugumin 29- (Nishi et. al., 1999), myotubularin 1- (Al-Qusairi et al., 2009) and junctophilin 1-deficient muscles (Ito et al., 2001, Komazaki et al., 2002). These proteins have not been implicated in biogenesis of the T-tubule system but seem to be important for maintenance or formation of the triad structure.

1.7 The triad and the process of EC-coupling

The triad is an anatomical structure where T-tubule system and the terminal cisternae of the SR interface (see figure 1.6). Here, a close contact is established between the voltage sensitive DHPR at the T-tubule membrane and the RYR, a Ca^{2+} release channel at the SR membrane which allows coupling of the neuronal signal along the T-tubules and the Ca^{2+} release from the SR with following muscle contraction. Interestingly in DHPR and in RyR KO mice a normal triad structure was detectable (Takekura et al., 1995, Flucher et al., 1993). This suggests that both proteins are not needed for proper triad formation but other proteins have to be required for normal formation of the triad. The triad proteins junctophilin 1, which provides a structural basis for triad formation as it bridges the SR to the T-tubular membrane (Takeshima et al., 2000), mitsugumin 29 and myotubularin 1 have already been implicated in the process of triad structure formation or maintenance. Interestingly, most of the proteins mentioned above, which are proposed to be involved in triad formation or T-tubule biogenesis have been shown to influence the process of EC-coupling and therefore deficiency of one of these proteins leads to alterations in Ca^{2+} homeostasis.

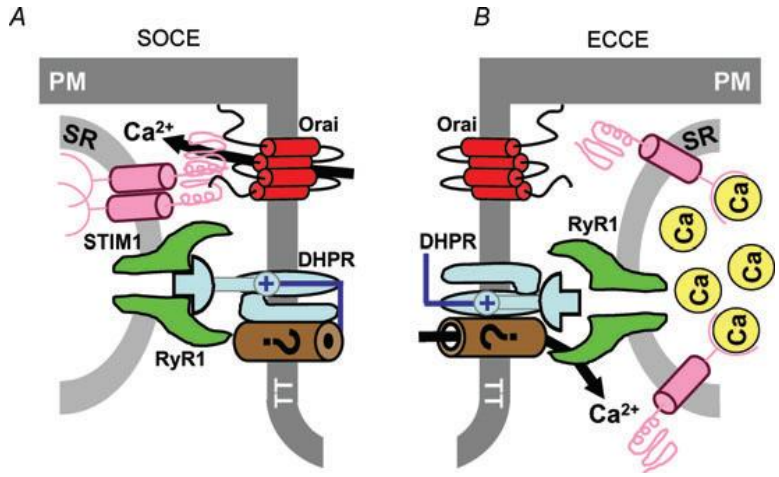

Figure 1.7: Proposed models for store-operated Ca^{2+} entry (SOCE) and excitation-coupled Ca^{2+} entry (ECCE) a) The Ca^{2+} sensor STIM1 at the SR membrane is required for opening of Ca^{2+}-permeable ORAI1 channels in the T-tubule membrane. b) ECCE requires interaction of DHPR and RyR but the exact channel for Ca^{2+} entry remains to be identified (from Lyfenko and Dirksen, 2008).

The process of EC-coupling in skeletal muscle starts with propagation of the action potential along the T-tubular membrane into the interior of the muscle fiber where it opens the DHPR. This leads to influx of Ca^{2+} into the cytoplasm and to conformational change of the DHPR and thereby activation of the RyR1 which results in rapid Ca^{2+}

release from the SR and initiation of muscle contraction (reviewed in Dulhunty, 2006). The rise in global intracellular Ca^{2+} leads to binding of Ca^{2+} to troponin C and activationof contraction. Ca^{2+} is then transported back into the SR by the sarcoplasmatic reticulum Ca^{2+} ATPase (SERCA) and outside of the cell by plasma membrane Ca^{2+} ATPase (PMCA) and sarcolemmal Na^{2+}/Ca^{2+} exchanger (NCX) thereby terminating the process of contraction. Inside the SR the free Ca^{2+} concentration is kept low by Ca^{2+} binding proteins like the main skeletal muscle Ca^{2+} buffer calsequestrin. This is necessary to provide a pool of Ca^{2+} that is available to maintain free Ca^{2+} levels and to minimize Ca^{2+} leakage through the RyR and energy waste of SERCA. Additionally, calsequestrin modulates RyR1 Ca^{2+} release from the SR (Royer and Rios, 2009). The coupling of DHPR and RyR is bidirectional, meaning DHPR controls RyR-mediated Ca^{2+} release in orthograde direction and in turn RyR mediates Ca^{2+} flux through DHPR in retrograde mode (Nakai et al. 1996). Two further Ca^{2+} entry mechanisms have been demonstrated so far. Store-operated Ca^{2+} entry (SOCE) was detected, when Ca^{2+} was re-added to the extracellular medium of muscle fibers with previously depleted SR Ca^{2+} store and fibers started to refill their SR stores (Kurebayashi and Ogawa, 2001, figure 1.7). Several proteins are proposed to be involved in this process but the exact mechanism remains to be identified. Most studies favor a model of SOCE involving interaction of stromal interaction molecule 1 (STIM1) with Ca^{2+} release-activated Ca^{2+} channel protein 1 (ORAI1). STIM1 is localized at the SR and has Ca^{2+} sensing properties. In response of SR Ca^{2+} content decrease, Ca^{2+} dissociates from STIM1 which leads to conformational changes and clustering of STIM1 molecules at the SR membrane. ORAI1 channels which are localized at the T-tubule membrane in close vicinity to the SR membrane become activated upon STIM 1 oligomerization and mediate Ca^{2+} entry into the cell (Dirksen, 2009). Therefore, efficient SOCE can only be provided through close contacts of SR and T-tubule membranes at the triad junction which is primarily mediated by junctophilin 1. Further models that require interaction of RyR or inositol-3-phosphate receptor with transient receptor potential canonical type 3 have been proposed but seem not to play a major role in SOCE. Later, a store-independent mechanism of Ca^{2+} entry was identified which was dependent on prolonged or repetitive depolarization and was termed excitation-coupled Ca^{2+} entry (ECCE; Cherednichenko et al., 2004, figure 1.7). This mechanism requires interaction of DHPR and RyR but the channel responsible for Ca^{2+} entry is still under debate. Bannister et. al. claimed that the DHPR itself is the main and perhaps only contributor for Ca^{2+} entry during ECCE (Bannister et al., 2009).

1.7.1 Influence of abnormal T-tubule morphology on EC-coupling

As mentioned above, several proteins were identified that are involved in T-tubule biogenesis or maintenance of triad structure and their absence leads to disorganized T-tubule morphology. Due to the altered morphology of the T-tubule system most of these proteins have influences on Ca^{2+} homeostasis of the skeletal muscle fibers. Bin1 knockdown in murine flexor digitorum brevis (FDB) muscles leads to reduced Ca^{2+} transient amplitudes and reduced SR Ca^{2+} content probably due to compromised coupling of DHPR and RYR. Furthermore induction of Ca^{2+} sparks after osmotic shock was decreased because of compromised DHPR activation (Tjondrokoesoemo et al., 2011). Similar to Bin1 also myotubularin-deficient muscle fibers show defective RyR1-mediated Ca^{2+} release from the SR combined with a decrease of RyR1 protein level (Al-Qusairi et al., 2009) and loss of caveolin 3 reduces the amplitude of DHPR Ca^{2+} current (Couchoux et al., 2007). On the other hand, an abnormal triad structure has been shown to influence the process of SOCE as mitsugumin 29-deficiency leads to dysfunction of SOCE making the muscle fibers highly susceptible to fatigue (Pan et al., 2002) and junctophilin 1-deficiency also leads to reduced SOCE (Li et al., 2010). These results indicate that abnormal T-tubule biogenesis and therefore abnormal T-tubule structure or an abnormal formation of the triad structure have direct influences on Ca^{2+} homeostasis.

1.8 Dysferlin and cardiomyopathy

As mentioned above, besides its expression in skeletal muscle dysferlin is highly expressed in heart muscle. Patients with dysferlin-deficient muscular dystrophy present primarily with defects of the skeletal muscle, but cardiomyopathies have also been described (Guglieri et al., 2008; Wenzel et al., 2007). In mouse models of dysferlin-deficiency it was found that stress induced by isoprenaline treatment leads to development of cardiomyopathy (Wenzel et al., 2007). Furthermore, dysferlin deficient mice develop mild dilative cardiomyopathies when getting old which are further impaired by stress exercise (Han et al., 2007). A role of dysferlin in heart function has not been extensively examined so far but observations from patients and animal models suggest a role of dysferlin in heart function.

1.8.1 EC-coupling in cardiomyocytes

The mechanism of EC-coupling in cardiomyocytes is similar to the one in skeletal muscle. One major difference is the coupling of DHPR and RyR2 which is not mechanical but mediated by Ca^{2+}. Upon myocyte membrane depolarization, Ca^{2+} enters the cell through the DHPR and this leads to and is absolutely required for

opening of RyR2. Ca^{2+} is therefore released from the SR by Ca^{2+}-induced Ca^{2+} release (Bers, 2002). After initiation of contraction, Ca^{2+} is pumped back into the SR by SERCA2a and out of the myocyte by PMCA and NXC which is also able to act in reverse mode which then contributes to Ca^{2+} influx in systole (Bers, 2002). The exact amount of Ca^{2+} released into the cytosol by DHPR and NCX has to be exported again out of the cell mainly by NCX and to a lesser extent by PMCA. The amount of Ca^{2+} released from the SR hast to be transported back by SERCA2a. A further difference between cardiac and skeletal EC-coupling is the mechanism of SOCE which probably plays only a minor role in healthy cardiomyocytes. Many studies have reported STIM 1 and the mechanism of SOCE to be present in neonatal cardiomyocytes and further, SOCE was demonstrated to play a role in cardiac hypertrophy (Luo et al., 2012), but its contribution to normal Ca^{2+} homeostasis and its relationship to the mechanism of EC-coupling remains poorly understood. In present accepted models of Ca^{2+} homeostasis the mechanism of SOCE is not included (Bers 2002, Kho et al., 2010, figure 1.8.1).

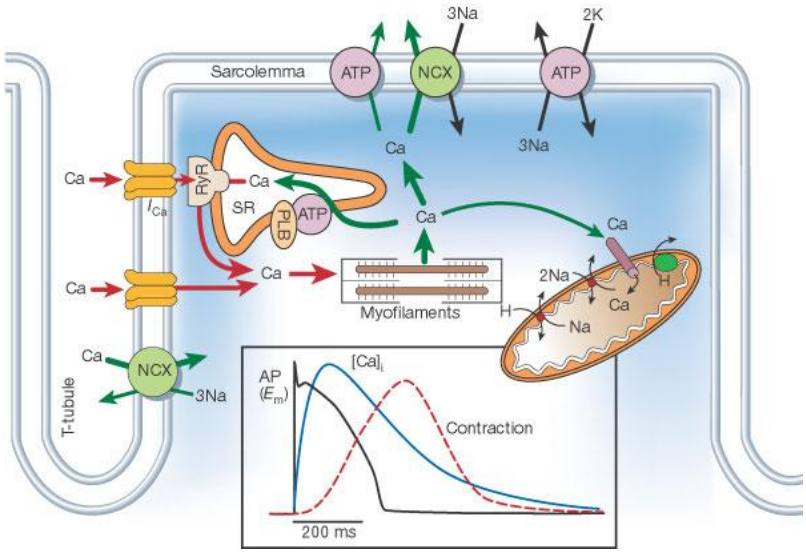

Figure 1.8.1: Excitation-contraction coupling in cardiomyocytes. Due to the action potential voltage gated DHPR channels open and Ca^{2+} entry leads to opening of RyR. This is followed by Ca^{2+} release into the cytoplasm where contraction is initiated. Ca^{2+} is transported back by SERCA, NCX and PMCA. Inset shows time course of action potential, Ca^{2+} release and contraction (from Bers et al., 2002).

At the triad junction, about 25 DHPR molecules are coupled to about 100 RyR proteins forming a so called Ca^{2+} release unit (Bers and Guo, 2005). Spontaneous Ca^{2+} release from a single release unit is called a Ca^{2+} spark. These Ca^{2+} sparks appear during rest as well as during EC-coupling. During EC-coupling thousands of Ca^{2+} sparks appear synchronized by the action potential thereby establishing a uniform Ca^{2+} transient. Ca^{2+}

sparks that occur during diastole are totally normal but if the frequency of these sparks increases this leads to a severe SR Ca^{2+} leak which increases the probability of arrhythmias (Wehrens et al., 2003). Ca^{2+} release can be mediated by sympathetic activation of ß-adrenergic receptors. Activation of ß-receptors by epinephrine or norepinephrine activates GTP-binding proteins leading to cAMP production by adenylyl cyclases. cAMP in turn activates proteinkinase A and the kinase phosphorylates several proteins involved in EC-coupling thereby enhancing their function. Among these proteins are the DHPR, the RyR2, phospholamban, a negative regulator of SERCA, the myosin binding protein C and troponin I. This leads to enhanced Ca^{2+} influx through the DHPR, increased SERCA function leads to increased SR Ca^{2+} content and therefore to increased available Ca^{2+}. All these effects enhance the Ca^{2+} transient amplitude.

1.8.2 Influences of abnormal T-tubule structure in cardiomyocytes

As in skeletal muscle, a highly organized T-tubule structure is also important in cardiomyocytes as disorganized T-tubule structure or loss of T-tubules involves impaired Ca^{2+} homeostasis presenting as desynchronized and impaired Ca^{2+} transients (Lyon et al., 2009, Louch et al., 2006) and may lead to acute heart failure. As mentioned above, many proteins have been found to be involved in biogenesis of the skeletal muscle T-tubule system. So far, much less is known about the role of these proteins in biogenesis of the cardiac T-tubule system and the maturation of the cardiac T-tubule system at all. Junctophilin 2 and Bin1 are the first proteins implicated in this process. Junctophilin 2, the cardiac isoform of junctophilin is required for normal structure of cardiac dyads and absence of the protein leads to reduced and unstable Ca^{2+} transients (Takeshima et al., 2000). Later it was demonstrated that junctophilin 2-deficiency leads to acute heart failure due to disruption of the T-tubule structure (Van Oort et al., 2011). This leads to impaired coupling of RyR and DHPR and therefore alteration of Ca^{2+} homeostasis due to reduced Ca^{2+}-induced Ca^{2+} release. Bin1 is also expressed in heart muscle and deficiency of the protein leads to hypertrophic cardiomyopathy and therefore prenatal lethal Bin1-deficient mice (Muller et al., 2003). It was demonstrated that Bin1 is responsible for trafficking of critical Ca^{2+} handling proteins, for example the DHPR, to the dyads in cardiamyocytes (Hong et al., 2010). In failing cardiomyocytes Bin1 expression is significantly decreased and knockdown of Bin1 leads to severely altered Ca^{2+} transient amplitudes in mouse cardiomyocytes (Hong et. al., 2012). Interestingly, the protein is involved in a process called “reverse remodeling” of the T-tubule system in hearts after recovery from heart failure (Lyon et al., 2012). This indicates that Bin1 and junctophilin 2 are involved in Ca^{2+} homeostasis

in cardiomyocytes. Its role in T-tubule biogenesis in cardiomyocytes remains to be investigated.

1.9 Abnormal Ca^{2+} handling in muscular dystrophy

In several studies it was demonstrated that the presence of muscular dystrophy can also have influences on Ca^{2+} homeostasis of muscle fibers. Dystrophin-deficient mdx mice show increased sarcolemmal Ca^{2+} permeability which leads to accumulation of Ca^{2+} in the cytosol and this activates proteases and induces necrosis of muscle fibers. The mechanism of Ca^{2+} entry is still under debate. It was discussed that Ca^{2+} enters through microtears due to instability of the plasma membrane or by a more active mechanism involving nonselective cation channels (Fong et al., 1990) or mechanosensitive channels (Franco et. al., 1990). Also SOCE seems to be increased in mdx muscle (Edwards et al., 2010). SOCE is activated upon SR Ca^{2+} store depletion which could be due to increased SR Ca^{2+} leak. Wang et al. demonstrated that dystrophic mdx muscle reveals an increased SR Ca^{2+} spark frequency which is probably due to membrane deformation (Wang et al., 2005). Additionally a reduced SERCA1 activity has been detected in mdx mice which probably further increases intracellular Ca^{2+} levels (Kargacin et al., 1996). It was demonstrated that overexpression of SERCA1 enhances SR Ca^{2+} uptake thereby decreasing intracellular Ca^{2+} levels and this leads to improvement of muscular dystrophy in these muscles (Goonasekera et al., 2011). Decreased SERCA activity in combination with increased Ca^{2+} sparks and following increased SOCE probably leads to increased intracellular Ca^{2+} levels which result in the dystrophic phenotype. Similar findings have been published for ß sarcoglycan-deficient mice, which show decreased exercise capacity due to increased RyR Ca^{2+} leak resulting in decreased Ca^{2+} release (Andersson et al., 2012). These results clearly indicate that muscular dystrophy in skeletal muscle influences intracellular Ca^{2+} homeostasis.

2. Aim of the study

This thesis aims to identify the cellular function of dysferlin and its role in the pathology of dysferlin-deficient muscular dystrophy. So far direct evidence of the main cell biological role of dysferlin is missing and therefore the main function of the dysferlin protein is still unknown. Mediation of plasma membrane repair was shown to be one function of dysferlin but as dysferlinopathy patients are without symptoms and have a high level of fitness until their second decade of life, this can not be the whole basis of the disease. Furthermore, overexpression of myoferlin in dysferlin-deficient mice rescues plasma membrane repair but does not alter the development of muscular dystrophy (Lostal et al., 2012). The association of the dysferlin protein to the developing T-tubule system and the finding that dysferlin-deficient mouse muscle is characterized by a highly abnormal configured T-tubule system (Klinge et al., 2010) suggested a functional role in the biogenesis of the T-tubule system. The fact that dysferlin shows high homology to Fer1, a protein mediating vesicle fusion and the fact that dysferlin contains several C2 domains, which are known to mediate phospholipid binding support a role of the protein in T-tubule development and further hint towards a role of dysferlin in membrane organization. Previous unpublished work demonstrated that dysferlin is able to induce membrane tubules upon heterologous expression in non-muscle cells and that these tubules are a newly induced membrane networks. This finding further supported the hypothesis that dysferlin is involved in membrane organization. In this thesis, the cellular and biochemical function of dysferlin with respect to membrane organisation and its role in tubule formation was investigated. The aims of this thesis were as follows:

- Cellular investigation of dysferlin, truncated dysferlins and pathogenic dysferlin mutants in muscle and non-muscle cells with respect to localization and function and comparison to other ferlins.
- Analysis of T-tubule- and triad-associated protein expression to detect potential alterations due to the abnormal T-tubule morphology
- Biochemical analysis of membrane binding and membrane tubulation properties of the dysferlin full-length protein, truncated or mutated dysferlin proteins and single C2 domains
- Identification of dysferlin localization in cardiomyocytes and potential influences of dysferlin-deficiency on the cardiac T-tubule system
- Investigation of potential influences of dysferlin-deficiency and abnormal T-tubule structure on cardiac and skeletal muscle Ca^{2+} homeostasis

3. Materials and Methods

3.1 Materials

3.1.1 Mice

Dysf^{tm1Kcam} mice were provided by Kate Bushby (Newcastle, UK; Bansal et al. 2003). Mdx mice were provided by Jens Schmidt (UMG). Male Dysf^{tm1Kcam} mice, mdx mice and respective age matched wild-type controls were used. All animals received human care in accordance with the institution's guidelines, the German Convention for Protection of Animals and the National Institutes' of Health guidelines.

3.1.2 Cell culture

Mammalian cell lines

Cos 7 green monkey kidney, fibroblast-like cells
HeLa human cervical cancer cell line
C2C12 mouse myoblast cell line

Mammalian cell culture medium

DMEM (PAA Laboratories)
10 % Fetal calf serum (FCS)
1 % Penicillin/streptomycin
1 % L-glutamine

Freezing medium

DMEM high glucose
20 % FCS
1 % Penicillin/streptomycin
1 % L-glutamine
10 % Dimethyl sulfoxide (DMSO)

Transfection reagent

Effectene Transfection Reagent	Qiagen
0.05 % Trypsin	PAA Laboratories
Phosphate buffered saline (PBS)	PAA Laboratories

3.1.3 Strains and cells

Bacterial cells

Escherichia Coli:

BIOBlue Chemically Competent Cells	Bioline
BL21-RIL (DE3)	Stratagene
BL21-RIL star (rosetta plasmid)	provided by Achim Dickmanns (UMG)

Bacterial culture media

Bacterial media were autoclaved and supplemented with antibiotics prior to use.
LB Medium and LB Agar were purchased from Roth.

Antibiotics

Kanamycin	25 mg/ml
Ampicillin	100 mg/ml
Chloramphenicol	30 mg/ml

3.1.4 Molecular cloning

Vectors and constructs

Vectors

Vector name	Purchased from
pcDNA4/TO/myc His B	Invitrogen
PST884/pET41a	Novagen
pGEX6p1	GE Healthcare
pGEX6p2	GE Healthcare

Constructs

Construct name	Genotype	Provided by
pcDNA4-GFP	mammalian expression vector containing GFP	AG Klinge
pcDNA4-GFP-DYSfl	GFP-tagged dysferlin	AG Klinge
pcDNA4-GFP-Dysfl-Mut-1 (G299W)	GFP-tagged dysferlin mutation in C2B domain	AG Thoms/Klinge
pcDNA4-GFP-Dysfl-Mut-2 (R959W)	GFP-tagged dysferlin mutation in C2C domain	AG Thoms/Klinge
pcDNA4-GFP-Dysfl-Mut-3 (R1331L)	GFP-tagged dysferlin containing mutation not within C2 domain	AG Thoms/Klinge

pcDNA4-GFP-Dysfl-Mut-4 (L1341P)	GFP-tagged dysferlin mutation in C2C domain	AG Thoms/Klinge
pcDNA4-GFP-Dysfl-V67D	GFP-tagged dysferlin mutation in C2A domain	this thesis
pcDNA4-Dysfl-Myc/His6	C-term Myc/His6-tagged dysferlin	AG Thoms/Klinge
pcDNA4-His6-Dysfl	N-term His6-tagged dysferlin	AG Thoms/Klinge
pcDNA4-GFP-C2FG	GFP-tagged truncated dysferlin	this thesis
pcDNA4-GFP-C2FGTM	GFP-tagged truncated dysferlin	this thesis
pcDNA4-GFP-DysΔTM	GFP-tagged dysferlin without TM domain	AG Thoms/Klinge
pcDNAa-GFP-Minidysferlin	GFP-tagged truncated dysferlin	Martin Krahn, (France)
pcDNA4-GFP-Minidysferlin3	GFP-tagged truncated dysferlin	this thesis
ECFP-N1-mOtoferlin-eGFP	C-term. GFP-tagged otoferlin	Ellen Reisinger, (UMG)
pcDNA3.1-Myoferlin-HA	N-term. HA-tagged myoferlin	Addgene
pET41aΔN-B-His6-Dysfl	E.coli Expression vector containing N-term. His6-tagged dysferlin	this thesis
pGEX6p1-GST-Dysfl	E.coli Expression vector containing N-term. GST-tagged dysferlin	this thesis
pET41aΔN-B-His6-DysflV67D	N-term. His6-tagged dysferlin mutation in C2A domain	this thesis
pET41aΔN-B-His6-DysΔTM	N-term. His6-tagged dysferlin without TM-domain	this thesis
pGEX6p1-Minidysferlin3	GST-tagged truncated dysferlin	this thesis
pGEX6p1-C2A-Kl1	GST-tagged C2A domain	this thesis
pGEX6p1-C2B-Kl1	GST-tagged C2B domain	this thesis
pGEX6p1-C2C-Kl1	GST-tagged C2C domain	this thesis
pGEX6p1-C2D-Kl1	GST-tagged C2D domain	this thesis
pGEX6p1-C2E-Kl1	GST-tagged C2E domain	this thesis
pGEX6p1-C2F-Kl1	GST-tagged C2F domain	this thesis
pGEX6p1-C2G-Kl1	GST-tagged C2G domain	this thesis
pGEX6p1-C2A-V67D	GST-tagged mutated C2A domain	this thesis
pGEX6p2-Bin1	GST-tagged Bin1	this thesis
GFP-Rab7	GFP-tagged Rab7	Addgene
PH-ACT-YFP	YFP-tagged PH-ACT (PIP sensor)	Mikael Simons, (UMG)
PH-PLC-GFP	GFP-tagged PH-PLC (PIP sensor)	
RFP-PIP2-kinase	PIP2 kinase	
RFP-synaptojanin 1	Synaptojanin 1 (PIP2 phosphatase)	

Enzymes and buffers

Enzymes and buffers for restriction digestion were purchased from NEB.

Pfu DNA polymerase	Promega
Precisor DNA polymerase	BioCat
T4 ligase	Fermentas
Proteinase K	Qiagen
Phenol/Chloroform	Roth

Miniprep buffers

Buffer P1

50 mM	Tris/HCl (Roth), pH8.0
10 mM	EDTA (Roth)
100 µg/ml	RNAseA (Calbiochem)

Buffer P2

200 mM	NaOH
1 % (v/v)	SDS (Roth)

Buffer P3

3 M	Potassium acetate, pH 5.5

Lysis buffer for genotyping

50 mM	Tris, pH 8
100 mM	NaCl (Roth)
1 % (v/v)	SDS
1 mM	EDTA

Agarose gel electrophoresis

GeneRuler DNA Ladder Mix	Fermentas

Agarose gel

1 % agarose (Bioline), 0.5 µl / 80 ml GelRed (Biotium) in TAE-buffer

TAE-Puffer:

40 mM	Tris-HCl, pH 8.0
0.1 % (v/v)	Acetic acid
1 mM	EDTA

Oligonucleotides

Primer name	Sequence
Primers for genotyping	
P1 sense	5’-GCCAGACAAGCAAGGTTAGTGTGG-3’
P2 antisense	5’-GCGGGCTCTCAGGCACAGTATCTGC-3’
P3 antisense	5’-GCTGACTCTAGAGCTTGCGGAACC-3’
Sequencing primers	
pGEX 5’ primer (Invitrogen)	5’-GGGCTGGCAAGCCACGTTTGGTG3’
pGEX 3’ primer (Invitrogen)	5’-CCG-GGAGCTGCA TGT GTC AGAGG-3’
T7 promoter primer (Novagen)	5'-TAATACGACTCACTATAGGG-3'
T7 terminator primer (Novagen)	5'-GCTAGTTATTGCTCAGCGG-3'
Sequencing primers dysferlin	
IC1	5’-GCT CAG CTG ACG GAT GAG C-3‘
IC2	5’-GAT CTC AGC CAA ATG GAA GC-3'
IC3	5’-CTC TTC ATG GAA GTG ATG C-3'
IC4	5’-GCA GCC AGA CAT CGA GC-3'
IC5	5’-CAG CCA AGA AGT GCT CCT TGG-3'
OST583	5’-CAA AGC GGA GGC CCG C-3'
OST584	5’-GCA ACC TGC TCC GGC C-3'
OST585	5’-CAG GCT TCC CAG ACC C-3'
OST586	5’-GGG GAC ACC GGG CCT C-3'
OST587	5’-CCG CCC AGC ATT GTG G-3'
OST602	5’-CCT GTG GTG GGC GAG TG-3'
OST603	5’-CAT CCC CTG CAC GCT GG-3'
OST604	5’-CCT GGA TGA CCT GAG C-3'
Primer for mutagenesis	
OST 616, ΔTM mutation, sense	5’-CATGAAGTTCATCCTGTGACGGCGTTTCCG GTGGG-3'
OST 617, ΔTM mutation, antisense	5’-CCCACCGGAAACGCCGTCACAGGATGAACT TCATG-3’
OST 907, mutation V67D, sense	5’-CCAGGGCTCTGAGCTTCATGATGTGGTCAA AGACC-3'

OST 908, mutation V67D, antisense	5’-GGTCTTTGACCACATCATGAAGCTCAGAGC CCTGG-3'
JH12, truncated dysferlin, sense	5’-GTACCGAATTCATGGAGGAAGAGTTCA TCGAT-3'
JH3, truncated dysferlin, antisense	5’-GTACCGCGGCCGCTCAGCTGAAGGG CTTCA-3'
JH10, truncated dysferlin ΔTM, antisense	5’-GTACCGCGGCCGCTCACCGGAAACG CCGCC-3'
JH53, minidysferlin 3, sense	5’-CTAGAAAGCTGCTGTCAGACAAACCGCAGGT GATTGGTGAATTTAAGGGCCTCTTC-3'
JH54, minidysferlin 3, antisense	5’-GAAGAGGCCCTTAAATTCACCAATCACCTGC GGTTTGTCTGACAGCAGCTTTCTAG-3'

PCR protocols

DpnI mediated mutagenesis

10 ng	template DNA
2.5 µl	10x Pfu DNA polymerase buffer
1.5 µl	sense primer (10 µM)
1.5 µl	antisense primer (10 µM)
1.35 µl	dNTP mix (3.75 mM)
0.5 µl	Pfu DNA polymerase
ad 25 µl	ddH_2O

1. 95°C	30 s
2. 95°C	30 s
3. 55°C	1 min
4. 68°C	2 min/kb of plasmid length 18 cycles
5. 10°C	pause

DpnI digest

25 µl	PCR product
1 µl	DpnI

Sequencing PCR

0.2-0.3 µg	DNA
0.5 µl	primer (10 µM)
2 µl	BigDye 5x Sequencing buffer (Applied Biosystems)
1 µl	BigDye Sequencing Ready Reaction Premix (Applied Biosystems)
ad 10 µl	ddH_2O

1. 96°C 10 s
2. 60°C 4 min / 24 cycles
3. 10°C pause

Genotyping PCR

5 µl	5x GC buffer
0.13 µl	$MgCl_2$ (50 mM)
1.4 µl	dNTPs (3.75 mM)
0.5 µl	primer P1 (10 µM)
0.5 µl	primer P2/P3 (10 µM)
0.25 µl	Precissor polymerase
ad 25 µl	ddH_20

1. 98°C 3 min
2. 98°C 30 s
3. 65°C 30 s
4. 72°C 90 s / 34 cycles
5. 72°C 5 min
6. 4°C pause

3.1.5 Biochemical experiments

Western Blotting

Homogenization buffer

12.5 mM	Sucrose
0.3 mM	NaN_3
10 mM	$NaHCO_3$, pH 7.0
0.1 mM	Phenylmethylsulfonyl fluoride (PMSF, AppliChem)

Complete protease inhibitors (Roche)

TBST

200 mM	Tris
1.5 M	NaCl
1 % (v/v)	Tween 20

Blocking Solution

4 % (w/v) non fat dry milk powder in TBST

Blotting buffer

48 mM	Tris
39 mM	Glycin (Roth)
0.04 % (v/v)	SDS
10 % (v/v)	MeOH (J.T.Baker)

Sample Buffer (4x)

160 mM	Tris/HCl pH6.8
8 % (v/v)	SDS
20 % (v/v)	Glycerol (Sigma)
0.01 g	Bromphenolblue (Merck)
100 mg/ml	DTT (Serva)

SDS running buffer

3.03 g	Tris
14.4 g	Glycine
50 ml	20 % SDS
Ad 1000ml	dH_2O

8 %/12 % SDS separating gel

8 %/12 % (v/v)	Polyacrylamide (BioRAD)
0.39 M	Tris/HCl, pH 8.8
0.1 % (v/v)	SDS
0.1 % (v/v)	Ammonium persulfate (Roth)
0.1 % (v/v)	TEMED (Roth)

SDS stacking gel

5.1 % (v/v)	Polyacrylamide
0.13 M	Tris/HCl, pH 6.8
01 % (v/v)	SDS
0.1 % (v/v)	Ammonium persulfate
0.1 % (v/v)	TEMED

Protein ladders

PageRuler Prestained Protein Ladder	Thermo
PageRuler Plus Prestained Protein Ladder	Thermo

Detection

Lumi-Light western blot substrate	Roche

Transfer membrane

Nitrocellulose transfer membranes	GE Healthcare

Protein expression

Lysis buffer

300 mM NaCl in PBS, pH 7.3

Washing buffer

2 mM 2-mercaptoethanol (ß-ME) (Sigma) in lysis buffer

Elution buffer

50 mM	Tris/HCl, pH 8
150 mM	NaCl
10 mM	reduced Glutathione (Sigma)
2 mM	ß-ME

Lysis-buffer C2 domains

20 mM	Tris/HCl pH 7.4
150 mM	NaCl
3 mM	DTT
0.4 % (v/v)	Triton X-100
0.4 % (w/v)	Sodium-deoxycholate

8 M urea-buffer

20 mM	Tris/HCl, pH 7.4
150 mM	NaCl
3 mM	DTT
8 M	Urea

1 M NDSB201

20 mM	Tris/HCl pH 7.4
150 mM	NaCl
3 mM	DTT
1 M	NDSB201

Complete protease inhibitors without EDTA	in PBS, Roche
Lysozyme 10mg/ml	Roche
PMSF	in isopropanol, AppliChem
DNAse 50 U/µl	Affimetrix
Isopropyl β-D-1-thiogalactopyranoside (IPTG)	in H_2O, Sigma
Glutathione Sepharose 4B	GE Healthcare

Antibodies for Western Blot and Immunofluorescence

Antibody	Dilution	Application	Species	Company
RYR (sc-13942)	1:200	WB	rabbit	Santa Cruz
DHPR (sc-103588)	1:100	IF	goat	Santa Cruz
Dysferlin (ab15108)	1:500	WB	rabbit	Abcam
Dysferlin (NCL-Hamlet)	1:500/1:50	WB/IF	mouse	Novocastra
Amphiphysin II (sc-13575)	1:500	WB	mouse	Santa Cruz
Mitsugumin (ab106438)	1:1000	WB	rabbit	Abcam
SERCA (ab2818)	1:2500	WB	mouse	Abcam
Junctophilin 2 (PA5-20640)	1.1000	WB	rabbit	Thermo
STIM1 (610954)	1:250	WB	mouse	BD Biosciences
FKBP12 (ab24373)	1:1000	WB	rabbit	Abcam
TRPC3 (ab51560)	1:1000	WB	rabbit	Abcam
Orai1 (ab59330)	1:200	WB	rabbit	Abcam
PMCA (ab2825)	1.1000	WB	mouse	Abcam
anti HA (sc-7392)	1:50	IF	mouse	Santa Cruz
anti Lamp1 (ab24170)	1:600	IF	rabbit	Abcam

anti Golgi (ab27043)	1:100	IF	mouse	Abcam
anti PDI (ab27092)	1:1000	IF	mouse	Abcam
anti Pex14 (10594-1-AP)	1:100	IF	mouse	Proteintech
anti MYC (sc-789)	1.100	IF	rabbit	Santa Cruz
Cy3 anti rabbit	1:100	IF	goat	Jackson
Cy3 anti mouse	1:100	IF	donkey	Jackson
Cy3 anti goat	1:100	IF	donkey	Jackson
AlexaFluor 488 anti rabbit	1:100	IF	goat	Life technologies
AlexaFluor 488 anti mouse	1:100	IF	donkey	Life technologies
Anti rabbit HRP	1:10000	WB	goat	Dianova
Anti mouse HRP	1:10000	WB	donkey	Dianova

3.1.6 Immunofluorescence

PBS

8 g	NaCl
0.2 g	KCl
1.44 g	Na_2HPO_4 x $2H_2O$
0.24 g	KH_2PO_4

pH 7.4

Fixative for Cos7/HeLa cells

4 % (v/v) Paraformaldehyde (PFA) in PBS Affimetrix

Fixative for cardiomyocytes

100 % (v/v) Ethanol Merck

Blocking Solution for Cos7/HeLa cells

5 %(w/v) BSA (Roth) and 0.5 % (w/v) Triton (Roth) in PBS

Blocking solution for cardiomyocytes

3 % (v/v) Horse serum (Gibco), 0.5 % (v/v) Saponin, in PBS

Mounting medium

Vectashield Mounting Medium with DAPI Vector Laboratories

Vectashield HardSet Mounting Medium with DAPI Vector Laboratories

Chemical compounds

Phalloidin	Santa Cruz
Cytochalasin D in DMSO	Tocris
FM4-64 1 mM in DMSO	MoBiTec
Di8ANEPPS	provided by Viacheslav Nicolaev (UMG)

3.1.7 SDH staining

SDH solution

0.216 mg	Sodium succinate
0.024 M	Na_2HPO_4 x $2H_20$
0.024 M	KH_2PO_4, pH 7.4
8 mg	Nitroblue tetrazolium
10 mM	$MgCl_2$
2.5 mg	Menadione

3.1.8 Electron microscopy and liposome experiments

Phosphotungstic acid hydrate in H_2O	Fluka
Extruder	provided by Tolga Soykan (MPI for Experimental Medicine, Göttingen)
Membranes (100 nm)	Echelon
Lipids	Avanti polar lipids, Echelon
Brain extract from bovine brain, type 1	Sigma
Pip Strips	Echelon
Carbon/formvar coated copper grids	Polysciences

Hydration solution for tubulation experiments

30 mM	Tris pH 7.4
150 mM	NaCl
300 mM	Sucrose
1 mM	EDTA

Hydration solution for flotation experiments

20 mM	Tris pH 7.4
100 mM	NaCl
150 mM	Sucrose
1 mM	EDTA

Sucrose-solution

0.25 - 2 M Sucrose in hydration solution for flotation experiments containing 1 mM $CaCl_2$.

3.1.9 Ca^{2+} imaging

Caffeine	Sigma
Fura-2 (AM)	in DMSO, MoBiTec
Fluo-4 (AM)	in DMSO, Invitrogen
BTS	in DMSO, Sigma
Laminin	Sigma
Pluoronic F-127, 20 % (w/v)	in DMSO, Sigma

Cardiomyocytes

Isolation solution

113 mM	NaCl,
4.7 mM	KCl
0.6 mM	KH_2PO_4
0.6 mM	$MgSO_4 \times 7H_2O$
1.2 mM	$Na_2HPO_4 \times 2H_2O$
0.032 mM	Phenol-red
12 mM	$NaHCO_3$
10 mM	KHCO3
10 mM	HEPES
30 mM	Taurine
5.5 mM	Glucose
10 mM	BDM

pH 7.42

Enzyme solution

0.075 mg/ml Liberase
0.014 % Trypsin
0.013 mM $CaCl_2$
in isolation solution

Stop solution

10 % Bovine calf serum and 0.013 mM $CaCl_2$ in isolation solution

Solution for Ca^{2+} reintroduction

5 % Bovine calf serum containing 0.1 - 1.6 mM $CaCl_2$ in isolation solution

Tyrode's solution with Ca^{2+}

140 mM NaCl
5.4 mM KCl
1 mM MgCl
5 mM Hepes
10 mM Glucose
1 mM $CaCl_2$
pH 7.54

Tyrode's solution without Ca^{2+}

140 mM NaCl
5.4 mM KCl
1 mM $MgCl_2$
5 mM HEPES
10 mM Glucose
pH 7.54

Fluo-4 calibration solution

135 mM	LiCl
2 mM	$MnCl_2$
10 mM	Caffeine
10 mM	BDM
1 mM	Ouabain
10 µM	Ionomycin
10 mM	HEPES

pH 7.54

Caffeine solution

10 mM Caffeine in Tyrode's solution without Ca^{2+}

ASC-Tyrode with isoprenaline

1 l	Tyrode´s solution with Ca^{2+}
50 mg	Ascorbic acid
5 µl	HCl (32 %)
10^{-7} M	Isoprenaline

Fluo-4 staining solution

10 µM Fluo-4 AM and 0.04 % (v/v) Pluronic F-127 in Tyrode's solution without Ca^{2+}

Skeletal Muscle

Ringer's solution with Ca^{2+}

145 mM	NaCl
2.5 mM	KCl
10 mM	HEPES
1 mM	$MgSO_4 \times 7H_2O$
10 mM	Glucose
2 mM	$CaCl_2 \times 2H_2O$

pH 7.4

Ringer's solution without Ca^{2+}

145 mM	NaCl
2.5 mM	KCl
10 mM	HEPES
1 mM	$MgSO_4 \times 7H_2O$
10 mM	Glucose
0.5 mM	EGTA

pH 7.4

Hypotonic solution for spark measurements

Ringer's solution with Ca^{2+} containing 70 mM NaCl (instead of 145 mM)

Collagenase-solution

4 mg/ml Collagenase type 2 (Worthington) in Ringer's solution with Ca^{2+}

Caffeine-solution

30 mM Caffeine in Ringer's solution without Ca^{2+}

Fura-2 staining solution

10 µM Fura-2 AM and 0.04 % Pluronic F-127 in Ringer's solution without Ca^{2+}

3.1.10 Equipment

Epifluorescence microscope

Axioimager M1 (Zeiss) equipped with a Plan Neofluar 100x/1.3 Oil lens.
AxioCam HRm (Zeiss) and Axiovision 4.8 software (Zeiss) were used for acquisition.

Laser scanning confocal microscope for immunofluorescence imaging

LSM 710 (Zeiss); ZEN 2009 software (Zeiss)

Laser scanning confocal microscope for measurement of Ca^{2+} sparks

LSM 5 Pascal, Zeiss; analysis by Image J

Electron microscope

LEO EM912 Omega (Zeiss) with on-axis 2048x2048-CCD camera (Proscan)

Epifluorescence microscope for measurement of Ca^{2+} transients

Microscope, Nikon Eclipse TE300

Optical setup, IonWizard

Analysis of Ca^{2+} transients

IONWizard Analyze Version 5.0 (ION OPTIX)

Analysis of Ca^{2+} sparks

Image J analysis software /Plug In SparkMaster (NIH)

Western Blot detection

Luminescent image reader LAS-4000 mini (Fujifilm)

Sonifier UP 50H (Hielscher)

Tissue Ruptor (Quiagen)

Centrifuges

Beckman coulter CC-GPKR

Eppendorf centrifuge 5424

Optima TL centrifuge, TLA 100.2 rotor

RC-5 centrifuge (Sorvall) Thermo Fisher, GSA rotor

3.2 Methods

3.2.1 Genotyping of mice

Mouse tails were incubated in 350 µl lysis buffer with 60 µg proteinase K (2 mg/ml) over night at 55 °C in a shaker. The DNA was extracted with 400 µl phenol/chloroform at room temperature. The mixture was shaken 60 times and centrifuged 3 min at 10000 rpm at room temperature. The supernatant was transferred into a new e-cup and phenol/chloroform extraction was repeated. The supernatant was again transferred into a new e-cup and DNA was extracted with 300 µl chloroform. The DNA was precipitated by adding 600 µl 100% ethanol and 30 µl 3M sodium acetate pH 6.0 and washed with 70 % ethanol. The pellet was dried and resuspended in 30 µl dH_2O. Genotyping PCR was performed with Precissor Polymerase. Primers P1 and P2 amplify a 3.4 kb fragment from the WT allele and primers P1 and P3 amplify a 3 kb fragment from the KO allele only (Bansal et al., 2003).

3.2.2 Molecular cloning

3.2.2.1 Manipulation of DNA

For restriction digestion 1 µg of DNA was digested with 0.2 to 0.3 µl enzyme at 37 °C for required times. The DNA was purified by High Pure PCR Product Purification Kit (Roche) or was extracted from agarose gel by NucleoSpin Extraction Kit (Macherey-Nagel). Ligation was carried out by mixing 50 ng of vector-DNA with three-fold molar mass of insert-DNA with 1 µl of T4-ligase and 2 µl 10x ligase buffer and added with dH_2O to a final volume of 20 µl. Blunt ligation was carried out at room temperature for 60 min and sticky end ligation at room temperature for 20 min. The ligation mix was directly used for transformation.

3.2.2.2 Transformation

An aliquot of competent cells was thawed on ice and 1 µl of ligation mix was added to 10 µl of competent cells and incubated on ice for 20 min. A short heat pulse at 42°C (70 s) was given and the cells were incubated on ice for another 10 min. The cells were suspended in LB medium without antibiotics and incubated at 37 °C for one hour in a shaker and were then plated on LB plates containing appropriate antibiotics. The plates were incubated over night at 37 °C and single colonies were picked with a sterile pipette tip and incubated over night in 3 ml LB-medium with antibiotics.

3.2.2.3 Plasmid purification

For Mini plasmid purification single colonies were incubated over night in 3 ml LB medium containing appropriate resistance and were then centrifuged for one min at

8000 rpm. The supernatant was discarded, the pellet was resuspended in 200 µl buffer P1 and 300 µl buffer P2 was added and the sample was inverted and incubated for 5 min at room temperature. 300 µl buffer P3 was added, the sample was inverted and centrifuged for 10 min at 14000 rpm. The supernatant was transferred into a new e-cup and the DNA was precipitated with 0.7 volumes of isopropanol and 20 min centrifugation at 14000 rpm. The pellet was washed with 70% ethanol, dried for 10 min at 37 °C and resuspended in 30 µl dH_20.
For Midi plasmid purification 100 ml LB-medium was inoculated with 100 µl of overnight culture. The cells were harvested by 20 min centrifugation at 3000 rpm and preparation of DNA was done according to the manufacturers protocol (Macherey-Nagel) and DNA was eluted from columns with dH_2O.

3.2.2.4 DNA sequencing

DNA sequencing was done with BigDye Terminator v3.1 Cycle Sequencing Kit (Applied Biosystems) according to the manufacturers instructions. For purification of the cycle sequencing product 220 µl 100 % ethanol, 120 µl H_2O and 10 µl 3 M sodium acetate (pH 4.6) was added, the mix was vortexed and incubated for 15 min at room temperature and centrifuged for 20 min at 14000 rpm. The pellet was washed with 70 % ethanol, dried and resuspended in 10 µl formamide. DNA sequencing was done by Andreas Ohlenbusch (Department of Pediatrics, UMG) by sanger sequencing (DNA-sequencer ABI AVANT 3100, Advanced Biolab).

3.2.2.5 Expression constructs

Several dysferlin constructs for mammalian expression have been already available in my group. These included a GFP-dysferlin construct (pcDNA4-GFP-Dysfl) which had been cloned into EcoRI and NotI sites of pcDNA4/TO/myc His B-vector, an N-terminal His6-tagged construct (pcDNA4-His6-Dysfl) and a C-terminal myc-tagged construct (pcDNA4-Dysfl-Myc/His6). For cloning of a bacterial expression construct of dysferlin (pET41aΔN-B-His6-Dysf), the pET41a vector was cleaved by NdeI and BglII and klenow fill-in with following blunt ligation was performed to delete the GST tag from the vector. N-terminal his-tagged dysferlin was then inserted into KpnI and NotI sites of the vector. Furthermore, four dysferlin constructs containing pathogenic mutations have already been available. A further patient mutation, mutation V67D, was introduced into dysferlin-constructs pcDNA4-GFP-Dysfl and pET41aΔNB-His6-Dysfl by DpnI mutagenesis using primers OST907 and 908 (C2A mutant). For degradation of methylated parental DNA the PCR product was cleaved with 8 u DpnI at 37°C for one hour and was then transformed into BIOBlue Chemically Competent Cells. Positive

clones were identified by sequencing. The transmembrane mutant pET41aΔN-B-His6-DysflΔTM was also generated by DpnI mutagenesis with primers OST616 and 617. Three truncated dysferlin constructs were cloned. Two truncated constructs contain only the last two C2 domains with or without (C2FG) the transmembrane domain. They were amplified by primers JH12 and JH3 (with transmembrane domain) or JH10 (without transmembrane domain) and introduced into EcoRI and NotI sites of pcDNA4-GFP-vector. The pcDNA4-GFP-minidys3 was generated by DpnI mutagenesis with primers JH53 and JH 54 using pcDNA4-GFP-dsyfl as template (Azakir et al., 2012) The minidysferlin 3 was then cloned into EcoRI and NotI sites of pGEX6pI vector and pcDNA4-GFP vector. pGEX4T1-C2A to C2G were kindly provided by Michael Sinnreich (University of Montreal, Canada). The C2 domains were cloned into EcoRI and NotI sites of pGEX6p1 vector. pGEX6p1-C2A-V67D was generated by DpnI mutagenesis with pGEX6p1-C2A and primers OST 907 and 908. Bin1 (kindly provided by Pietro de Camilli, University of Yale, USA) was cloned into BamHI and NotI sites of pGEX6p2-vector. All constructs were verified by DNA sequencing.

3.2.3 Western Blotting

For Western Blot of mouse muscle homogenates, the quadriceps femoris muscle was isolated from young (9-11 weeks) and old (50-66 weeks) wild-type and knock-out mice and was frozen in liquid nitrogen and stored at -80°C. Muscle samples were homogenized in homogenization buffer with the tissue ruptor (Quiagen) and protein concentration was determined by BCA assay (Uptima). Samples were mixed with 4x sample buffer and incubated for 5 min at 95°C. 20 µg protein was loaded on 8-12 % SDS gels (depending on protein size) and transferred onto nitrocellulose membranes. Proteins were detected by antibodies listed above. For statistical analysis densitometry levels were determined using Image J analysis software and were normalized to GAPDH.

3.2.4 Protein expression

Proteins were cloned into bacterial expression vectors and transformed into competent BL21-RIL or BL21star/rosetta cells. A 50 ml overnight culture was grown in LB containing antibiotics. This culture was used to inoculate the main culture of 500 ml LB containing antibiotics. At an OD_{600} of 0.5 to 0.6 protein expression was induced by 0.5 mM IPTG and the culture was incubated for 3 h at 30°C and vigorous shaking. The cells were harvested at 5000 rpm in a Sorvall GSM centrifugation rotor for 20 min, washed with cold PBS again centrifuged at 3000 rpm for 20 min and about 1 g of bacteria could be collected from a 500 ml culture. The cells were frozen at -80°C,

thawed on ice and per 1 g of pellet the cells were resuspended in 10 ml lysis buffer containing Complete Protease Inhibitors without EDTA, DNAse and 50 µg/ml lysozyme. The resuspended cells were rotated for 30 min at 4°C and the cell lysate was frozen in 1 ml aliquots at -80°C.The lysate was thawed on ice and sonicated (ultrasonic processor, Hielscher) two times for 10 s with an amplitude setting of 30 %. Total cell lysate was verified by Western Blot and used for further experiments. Expression of Bin1 was done as described above. The cell lysate was then centrifuged at 42000 rpm for 50 min at 4°C and the supernatant was used for protein purification in batch via Glutathione sepharose 4B. Purification was done according to manufacturer's protocol. The glutathione sepharose was washed 3 times with washing buffer and the protein was bound to the column material for 1 hour at room temperature on a rotating platform. The column was washed again 3 times and the protein was eluted with elution buffer. Expression of C2 domains was done as explained above; cells were harvested after 2 h induction at 30 °c. 1 g of cell pellet was resuspended in 10 ml lysis buffer for C2 domains containing Complete Protease Inhibitors without EDTA, DNAse and 50 µg/ml lysozyme and was rotated for 30 min at 4°C and the cell lysate was frozen in 1 ml aliquots at -80°C. Lysates were then thawed on ice, supplemented with 0.1 mM PMSF, 3 mM DTT, 0.4 % Triton X-100 and 0.4 % sodium deoxycholate and sonicated two times 10 s at 30 % amplitude. Inclusion bodies were pelleted for 30 min. at max. speed at 4 °C. The pellet was washed and resuspended in 8 M urea-buffer for 2 hours on a rotating platform at room temperature. Insoluble material was separated by centrifugation for another 30 min at 4 °C at max. speed. The soluble protein in the supernatant was then refolded by adding it drop-wise under constant agitation to 10 times the volume of 1M NDSB201 solution. To remove the urea from refolded protein, the sample was dialyzed two times against lysis buffer without detergents and concentrated afterwards.

3.2.5 Liposome experiments

For preparation of liposomes glass tubes were rinsed with chloroform, 10 µl Folch Fraction lipids (100 mg/ml) with or without 5 % PIP2, PI3P or NBD-labeled PE were added and evaporated with N_2. Lipids were then hydrated with 750 µl hydration solution. The solution was added drop wise to the lipids with vigorous vortexing so that liposomes were formed. Liposomes were stored in the dark at 4°C. For liposome tubulation experiments liposomes were extruded 21 times through 100 nm membranes afterwards.

3.2.5.1 Liposome tubulation and electron microscopy

For liposome tubulation experiments, 2.5 µl of protein lysate (10 µg/µl) and Bin1 protein (2 µg/µl) was added to 7.5 µl of liposomes in presence of 2.5 mM $CaCl_2$ and the liposome protein mixture was incubated at 37°C for 20 min. Negative stain of liposomes was modified from the protocol of Brian Peter (lab of Harvey McMahon). The liposome-protein mixture was diluted 1:10 with hydration solution and 6 µl aliquots were absorbed onto formvar- and carbon-coated copper grids for 45 s, stained for 20 s with PTA, blotted and washed with hydration solution, blotted again, air dried and analyzed by electron microscopy. Binding of C2 domains to liposomes was carried out as described above using liposomes from Folch fraction lipids containing 5 % NBD-labeled PE and analyzing them by fluorescence microscopy.

3.2.5.2 Liposome flotation

Liposome flotation assay was modified from Klopfenstein et al., 2004. 5 µl of Bin1 protein (2 µg/µl) and 40 µl of dysferlin lysates (5 µg/µl) were added to 100 µl of liposomes in presence of 2.5 mM $CaCl_2$ and the liposome protein mixture was incubated at 37°C for 20 min. 2 M sucrose-solution was added to the protein-liposome mixture to bring the final concentration to 1.6 M sucrose and the mixture was overlaid with 300 µl 1.4 M sucrose, 150 µl 0.4 M sucrose and 300 µl 0.25 M sucrose. Gradient centrifugation was carried out using a TLS55 rotor for 60 min at 4°C and 55000 rpm. 200 µl fractions were taken and analyzed by SDS-PAGE and immunoblotting.

3.2.5.3 PIP-strips

PIP-strips were used according to manufacturer's protocol. PIP-strips were incubated with 5 ml PI(4,5)P2 Grip™ protein (positive control, 0.5 µg/ml) or 500 µl Bin1 (0.01 µg/µl) or dysferlin protein lysates (5 µg/µl) in 3 % BSA in TBST and detected by anti-GST (Bin1 and control protein) or anti-dysferlin (Hamlet) antibodies (dysferlin, minidysferlin 3 and C2A mutant) and chemiluminescence.

3.2.6 Immunofluorescence staining

For immunofluorescence staining of cell lines, cells were seeded on cover slips. The cells were washed two times with PBS, fixed with 4% PFA for 15 min and washed again with blocking solution. After incubation with blocking solution for 20 min the cells were incubated with the first antibody diluted in blocking solution for 1 h in a moist chamber at room temperature and washed three times 5 min with PBS. The cells were incubated with the second antibody in blocking solution (3 % horse serum, 0.5 % saponin in PBS) for 1 h in a moist chamber at room temperature, then washed again

three times for 5 min and mounted with Vectashield mounting medium on a microscope slide. Plasma membrane staining with FM4-64 was carried out according to manufacturer's instructions. Cells on cover slips were incubated for 60 s with 1 µM FM4-64 on ice, washed with PBS 1% PFA and imaged by confocal microscopy. For inhibition of actin cytoskeleton cells were incubated with 1 µM cyto D for 30 min at 37°C (Shinozaki-Narikawa et al., 2006).

For immunofluorescence staining of isolated cardiomyocytes cover slips were incubated with laminin mixture (40 µl laminin per 3 ml of PBS) for one hour for better cell adhesion. The cells were seed on the laminin-coated cover slips and incubated for one hour. The cells were fixed with ice-cold 100% ethanol at -20° for 20 min and washed three times 5 min with cold PBS. The cells were incubated with blocking solution (5 % BSA, 0.5 % Trition X-100 in PBS) for 1 h and incubated with the first antibody diluted in blocking solution at 4°C in a moist chamber overnight. The cells were washed with PBS for 10 min three times, incubated with the second antibody diluted in blocking solution for 1.5 h at room chamber in a moist chamber and mounted with Vectashield hard set mounting medium on a microscope slide. Cells were imaged by fluorescence or confocal microscopy.

Di8ANNEPS staining was carried out by Viacheslav Nicolaev (Department of Cardiology, UMG). Isolated cardiomyocytes were seeded on laminin-coated cover slips, washed with PBS, stained with di8ANEPPS for 15 min and analyzed by confocal microscopy.

3.2.7 SDH staining

For SDH staining gastrocnemius muscles were isolated from wild-type and knock-out mice at the age of 8 or 13 to 17 weeks and muscles were embedded in mounting medium (Tissue-Tek), frozen in isopentane cooled in liquid nitrogen and stored at -80°C until later analysis. Sections were cut on a microtome and slices were again stored at -80°C. SDH staining was carried out using the nitroblue tetrazolium technique (Defendi and Pearson, 1955). Slices were pre-warmed at room temperature for 30 min, incubated for 30 min at 37°C in SDH staining solution and washed in H_2O for 2 min. The slices were then fixed in 10 % formalin for 10 min and rinsed in H_2O and mounted with Aquatex.

3.2.8 Ca^{2+} imaging

Ca^{2+} measurements were done in collaboration with the lab of Lars Maier (UMG, Department. of Cardiology).

3.2.8.1 Ca^{2+} imaging in cardiomyocytes

3.2.8.1.1 Preparation of cardiomyocytes

Cardiomyocytes from wild-type and dysferlin-null mice hearts were isolated by Timo Schulte (UMG, Department of Cardiology) as described in Backs et al., 2009. Hearts were excised from mice after isoflurane anesthesia and following cervical dislocation. Hearts were mounted on a Langendorff perfusion apparatus and perfused with isolation solution. Perfusion was then switched to enzyme solution for 7 min and hearts were removed, dissected and dispersed afterwards. Stop solution was added and the tissue was filtered through nylon gauze afterwards. Isolated cardiomyocytes were allowed to settle for 7 min, the supernatant was discarded and the cells were resuspended in isolation Tyrode containing 0.1 mM Ca^{2+} and were settled again. This step was repeated with isolation solution containing 0.2 mM, 0.4 mM, 0.8 mM and 1.6 mM Ca^{2+} for slow Ca^{2+} reintroduction. After the last step the cells were seed on laminin coated chambers with glass bottoms and incubated for 15 min at room temperature for settling of the cardiomyocytes. The cells were then incubated with 10 µM of the acetomethyl ester (AM) form of Fluo-4 in the dark at room temperature for 20 min for Ca^{2+} measurements and for 7 min for spark-measurements.

3.2.8.1.2 Detection of intracellular Ca^{2+} transients and shortening

Detection of Ca^{2+} transients was carried out by epifluorescence microscopy (ION OPTIX) at 37°C. The chamber was mounted on the microscope and cells were provided with a constant flow of 80 ml/h of Tyrode´s solution with Ca^{2+} using a superfusion system. The cells were rinsed with this solution for at least 10 min to remove excess dye from the chambers and to allow cleavage of AM groups from the dye by esterases and for another 10 min with a stimulation of 1 Hz to achieve a steady-state. The image of the cells were detected by a camera (MyoCam) and displayed on a monitor. The Ca^{2+} indicator dye Fluo-4 AM was excited with a wave length of 488 nm using a 75 W xenon arc lamp on the stage of a Nicon Eclipse TE 200-U inverted microscope. Emitted fluorescence at 535 nm was measured using a photomultipier and shortening of the cells was measured using a sarcomere length detection system (Ion Optix Corp, Milton, Mass). Fluo-4 is a non-ratiometric dye; therefore the Ca^{2+} concentration is determined by a relative increase in fluorescence intensity due to elevations of free Ca^{2+} levels in the cytoplasm. Ca^{2+} transient amplitudes and shortening of the cells were measured at 0.5, 1, 2, 3 and 4 Hz. After subtraction of the background fluorescence, F/F_0 was calculated by dividing the raw fluorescence (F) by the baseline fluorescence (F_0). For measurement of stress induced differences in Ca^{2+} release, the cells were provided with a constant flow of Tyrode's solution with

isoprenaline and Ca^{2+} transients and shortening were measured again at 1 Hz. For measurement of SR Ca^{2+} content stimulation was stopped for 30 s and Ca^{2+} transients before and after rest were analyzed (post-rest relation). Furthermore, the Ca^{2+} content was measured by caffeine stimulated Ca^{2+}-release. Stimulation was stopped and addition of Tyrode's solution with caffeine evoked Ca^{2+} release from the SR. Analysis of Ca^{2+} transients and shortening was done with IONWizard Analyze Version 5.0 (ION OPTIX). Non-stimulated events were detected during measurement of Ca^{2+} transients and shortening during steady-state stimulation and when stimulation was paused. Analysis of non-stimulated events was done using the following semi quantitative arrhythmia score: single non-stimulated event: 1 point, bigeminy or trigeminus (coupled non-stimulated event): 2 points, couplet (two following non-stimulated events): 3 points, triplet (three following non-stimulated events): 4 points, salvo (four or more following non-stimulated events): 5 points, tachycardia (non-stimulated events following for more then 10 s): 6 points.

3.2.8.1.3 Detection of Ca^{2+} sparks

Detection of Ca^{2+} sparks was performed at room temperature by laser scanning confocal microscopy (LSM 5 Pascal, Zeiss) using a 40x oil-immersion objective. The chamber was mounted on the microscope and cells were provided with a constant flow of Tyrode's solution with Ca^{2+}. The cells were rinsed with this solution for at least 10 min to remove excess dye from the chambers and to allow de-esterification. The Ca^{2+} indicator dye Fluo-4 AM was excited with an argon laser at 488 nm and emitted fluorescence was collected through a 515 nm long-pass filter. The protocol for spark-measurement was as follows: Cells were measured with 0.25 Hz stimulation and after an unstimulated period of 30 s. Measurements were repeated with Tyrode's solution containing isoprenaline. Measurements were done in "line-scan"-mode with a pixel time of 0.8 µs, a scan time of 960 µs, 510 pixel per line, a pixel size of 0.1 µm, a pixel depth of 12 bit, a scan width of 51 µm (zoom factor 4.5) and 4000 lines. Analysis of spark measurements was done with Image J plug in Sparkmaster (Picht et al., 2007). Ca^{2+} spark frequency (CaSpF) was normalized to cell width and scan time ($\mu m^{-1}*s^{-1}$). Peak of Ca^{2+} sparks was normalized to F/F_0 (the raw fluorescence was divided by the baseline fluorescence after subtraction of the background fluorescence). Duration of the sparks was taken from the full-duration half maximum (FDHM) and width of the sparks from the full-width half maximum (FWHM). The Ca^{2+} spark volume was calculated from duration, width and amplitude of the sparks and the Ca^{2+} leak was calculated from spark volume, scan time and cell width.

3.2.8.1.4 Calibration of Fluo-4

For calibration of Fluo-4 F_{max} was measured by exposing the cells to 10 µM ionomycin in presence of 10 mM $MnCl_2$ to saturate fluorescence (Yao et al., 1997). The cells were rinsed 10 min with Tyrode's solution with Ca^{2+} and fluorescence was measured by line-scan. Tyrode's solution was then changed three times with calibration solution and fluorescence was measured every minute for a period of about 15 min. F_{max} was then calculated as $F_{max}= 5xF_{Mn}$ and F_{min} was calculated as $F_{min}=1/40\ F_{max}$. $[Ca]_i$ was calculated using a Kd value of 864 nm (Merrit et al., 1990) and $[Ca]_i$ was calculated as $[Ca]_i = Kd\ x\ (F-F_{min})/(F_{max}-F)$ (Grynkiewicz et al., 1985).

3.2.8.2 Ca^{2+} imaging in skeletal muscle fibers

3.2.8.2.1 Isolation of single skeletal muscle fibers

Isolation of single skeletal muscle fibers was modified from Capote et al., 2005. FDB muscles were isolated from hind limps of dysferlin-null and wild-type mice after isoflurane anesthesia and following cervical dislocation and were then incubated in collagenase solution for 50 min at 37°C for enzymatic dissociation of muscle fibers. Muscle fibers were then striped of from tendons mechanically and were dissociated mechanically by pipetting up and down. Single skeletal muscle fibers were seed on laminin coated glass chambers and were incubated 30 min at room temperature until fibers were settled. Fibers were then incubated for 15 min in Fura-2 solution (10 µM). For caffeine-experiments Fura-2 solution contained 20 µM N-benzyl-p-toluene sulphonamide (BTS). For spark measurements fibers were incubated for 7 min in Fluo-4 solution (10 µM).

3.2.8.2.2 Detection of intracellular Ca^{2+} transients

Detection of intracellular Ca^{2+} transients was done by epifluorescence microscopy with the same set up as in section 3.2.8.1.2 and measurements were performed at room temperature. The chamber was mounted on the microscope and was provided with a constant flow of 80 ml/h of Ringer's solution with Ca^{2+}. The chamber was rinsed at least 10 min to remove excess dye and to allow cleavage of AM groups from the dye. The cells were incubated for another 10 min at a stimulation of 0.5 Hz to achieve a steady-state. The ratiometric Ca^{2+} indicator dye Fura-2 AM was excited at 340 and 380 nm and emitted fluorescence at 510 nm was detected using a photomultipier. Ratiometric dyes change their excitation or emission spectrum according to the free Ca^{2+} concentration in the cytoplasm. Therefore, the ratio of the emission after excitation at 340 respectively 380 nm directly correlates with the amount of intracellular Ca^{2+} after subtraction of the background fluorescence. Ca^{2+} transients were measured at 0.5, 1, 2

and 4 Hz. For measurement of SR Ca^{2+} content the cells were incubated for 4 min with Ringer's solution without Ca^{2+} containing 20 µM BTS to inhibit contraction of muscle fibers (Pinniger et al., 2005) and SR Ca^{2+} release was evoked by addition of 30 mM caffeine solution containing 20 µM BTS.

To measure the influence of mechanical stress on muscle fibers, wild-type and dysferlin knock-out mice were subjected to treadmill running. The mice were familiarized with the treadmill on 3 consecutive days for 15 min per day at a speed of 15 m per min and a 0 % incline and were then subjected to running until exhaustion for 90 min at a speed of 15 to 20 m per min (Wang et al., 2005). The control group continued to run for 15 min per day. Immediately after the last run the mice were killed and FDB muscles were isolated and Ca^{2+} transients were measured as described above. Analysis of Ca^{2+} transients was done with IONWizard Analyze Version 5.0 (ION OPTIX).

3.2.8.2.3 Detection of Ca^{2+} sparks

Measurement of Ca^{2+} sparks in FDB fibers was done like explained in section 3.2.8.1.3 using the Ca^{2+} indicator Fluo-4. Compared to cardiomyocytes, in skeletal muscle fibers no Ca^{2+} sparks can be detected in healthy wild-type muscle. Therefore, Ca^{2+} sparks were measured after induction of osmotic shock (Wang et al., 2005). Cells were perfused with Ringer's solution containing Ca^{2+} for 10 min and then the cells were shocked by perfusion with hypotonic solution for 100 s and Ca^{2+} sparks were measured for 15 min.

3.2.9 Running wheel experiment

The running wheel experiment was done in collaboration with David Liebetanz (UMG, Deptartment of Clinical Neurophysiology). Wild-type and dysferlin-null mice were housed individually and cages were mounted with a conventional running wheel at the age of 4, 12, 20, 40, 75 and 90 weeks over a period of three weeks. The running wheel was connected to a computer and daily voluntary running activity was monitored. One revolution corresponds to a running distance of 0.38 m. A rotation sensor with a resolution of 16/turn was connected to the wheel axis. Wheel activity was recorded using LabVIEW™-based custom software (National Instruments Corp.). In the first running period the mice reached the maximum running performance at day 12 and in the following running periods at day 8. Average daily distance (m) and average daily running velocity (m/s) was calculated from all values above a threshold of 40 % of the mean running distance started from day 12 or day 8 respectively.

3.2.10 Statistics

Statistical analysis was done with Excel or GraphPad Prism 4 by student's t-test or two-way ANOVA for repeated measurements. P-values less than 0.05 were considered statistically significant.

4. Results

4.1 Heterologous expression of dysferlin induces tubulation in non-muscle cells

Previous unpublished work of my group demonstrated that heterologous expression of dysferlin in non-muscle cells lead to induction of tubular structures. These were shown to be newly induced membrane structures as cholesterol extraction by methyl-β-cyclodextrin treatment resulted in depletion of the tubular structures. Dysferlin and its human homologues myoferlin and otoferlin belong to the family of ferlins and therefore have a very similar domain structure that may suggest a similar protein function. This lead to the question whether all ferlins are able to induce membrane structures after heterologous expression. To compare expression of the three ferlins, they were expressed as green fluorescent protein (GFP) or human influenza hemagglutinin (HA) fusion proteins in Cos 7 cells. As indicated in figure 4.1 expression of dysferlin in non-muscle cells lead to induction of tubular structures which were not seen in cells transfected with the dysferlin homologues otoferlin or myoferlin. The network-like structure of myoferlin and otoferlin suggested ER localization of these two proteins which was corroborated by coimmunofluorescence staining of the ER with protein disulfide isomerase (PDI) (figure 4.1). In contrast, dysferlin-induced tubular structures did not show localization at the ER as indicated in figure 4.1. These results indicate that induction of membrane tubules in non-muscle cells is specific for dysferlin.

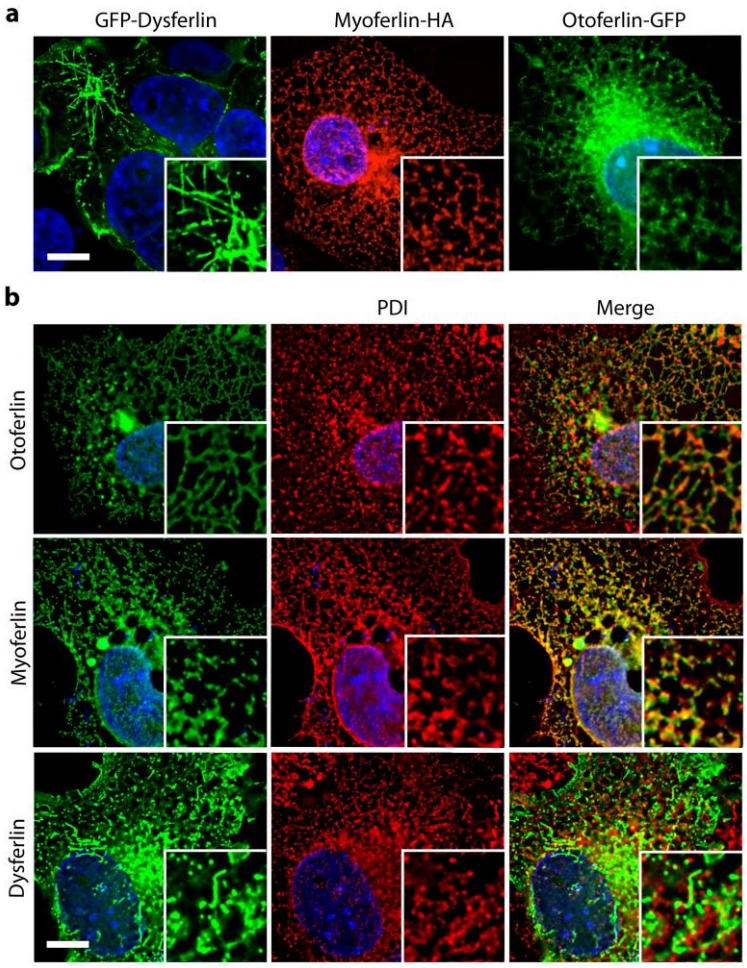

Figure 4.1: In contrast to its homologues oto- and myoferlin, dysferlin induces tubular structures after heterologous expression in Cos 7 cells. a) Cos 7 cells were transfected with GFP-dysferlin, GFP-otoferlin or myoferlin-HA (immunolabelled with anti-HA antibody) and analyzed 48 h after transient transfection. b) Transfected cells were co labeled with anti-PDI antibody as marker for the ER. Cells were analyzed by fluorescence microscopy, and z-stack images were deconvoluted. Scale bar: 10 µm.

4.2 Dysferlin-induced tubules do not colocalize with any organelle of the cell

To further analyze the tubular structures induced by dysferlin expression in Cos 7 cells, dysferlin-transfected cells were colabeled with several markers for cell organelles. As indicated in figure 4.2a, tubules induced by dysferlin did not colocalize with lamp1, Golgi protein 58K, PEX14 or Rab7. Therefore, the tubules were not localized to lysosomes, Golgi apparatus, late endosomes or peroxisomes which emphasizes the hypothesis that these tubules are a newly induced membrane compartment. In previous unpublished results from my group it was demonstrated that the tubules additionally did not colocalize with mitochondria and microtubules. Nevertheless, dysferlin-induced tubules are associated with the microtubule system as they were

disrupted by nocodazole-treatment, an agent interfering with microtubule polymerization (AG Thoms/Klinge, unpublished).

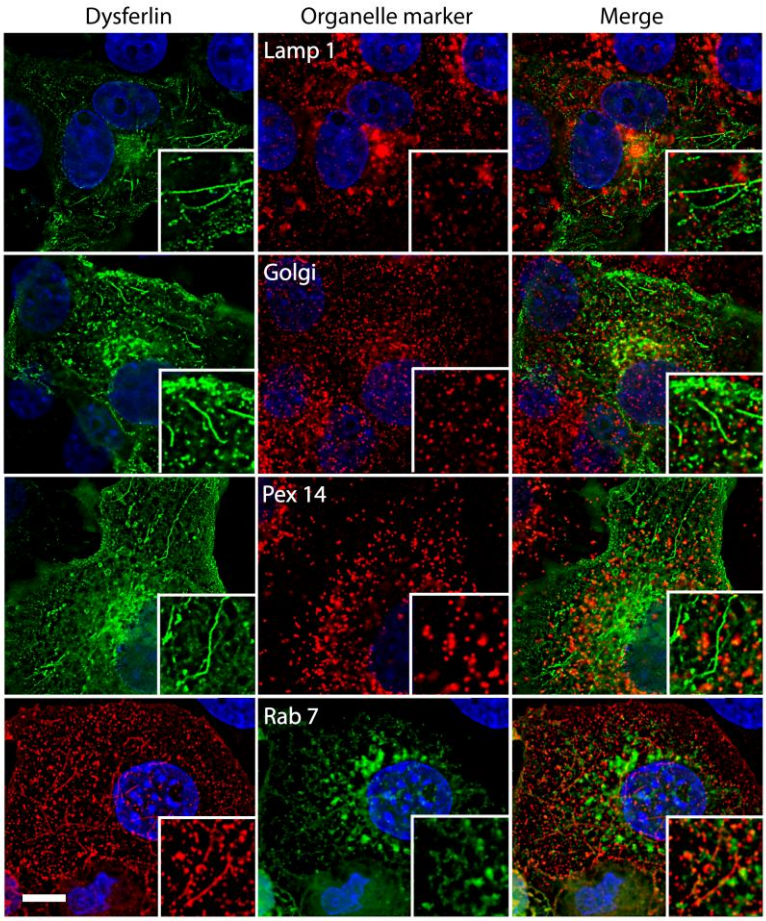

Figure 4.2a: Dysferlin-induced tubules do not colocalize with organelle markers for lysosomes, Golgi-apparatus, peroxisomes and endosomes. Cos 7 cells were transfected with GFP-dysferlin or dysferlin-myc respectively (immunolaneled with anti-myc antibody) and costained with anti-lamp1 (lysosome-marker), anti-Golgi 58K (Golgi-marker) and anti-PEX14 (peroxisome marker) or cotransfected with GFP-Rab7 (endosome marker). Cells were analyzed by fluorescence microscopy, and z-stack images were deconvoluted. Scale bar: 10 µm.

Additionally, dysferlin-induced tubular structures did not colocalize with the actin cytoskeleton of the cell as shown by costaining of GFP-dysferlin-transfected cells with phalloidin (figure 4.2b). Furthermore, induction of tubules by dysferlin was not inhibited by cytochalasin D (cyto D), an agent depolimerizing the actin microfilaments, but cyto D seemed to stabilize the tubules as these structures showed a more pronounced appearance after treatment with cyto D (figure 4.2b). These results further confirm that dysferlin-induced tubules are newly induced membranous structures as they did not colocalize with any cellular organelle, the microtubule system or the cytoskeleton.

Interestingly, the tubules were stabilized by inhibition of depolimerization of the actin microfilaments.

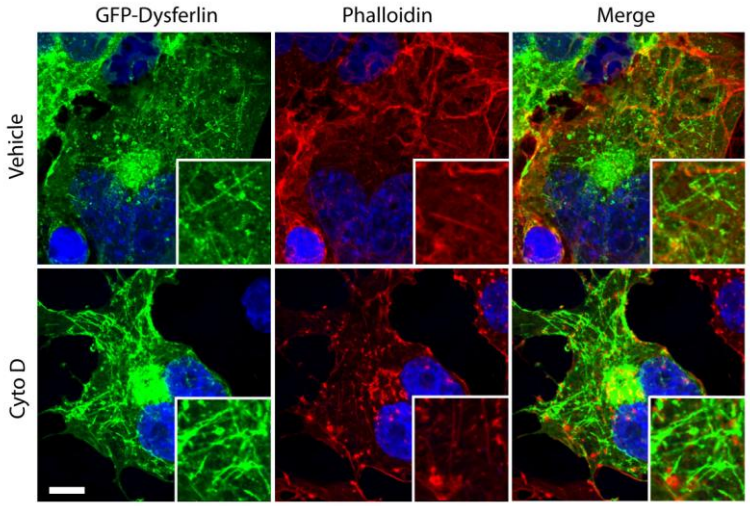

Figure 4.2b: Cytochalasin D stabilizes dysferin-induced tubules. Cos 7 cells were transfected with GFP-dysferlin, stained with phallioidin to visualize the actin cytoskeleton and were vehicle or cyto D treated afterwards. Dysferlin-induced tubules did not colocalize with the actin cytoskeleton but appear more pronounced after cyto D treatment. Cells were analyzed by confocal microscopy. Scale bar: 10 µm.

4.3 Dysferlin-induced tubules are PIP2 and PIP3 containing membranes

Extraction of cholesterol by methyl-β-cyclodextrin treatment lead to disruption of the tubular structures that were induced by heterologous dysferlin expression. Furthermore, the tubules did not colocalize with any cellular organelle, the microtubule system or with the actin cytoskeleton. Therefore, we concluded that these structures are tubular membranes induced by dysferlin expression in non-muscle cells. We further analyzed the dysferlin-induced tubular membranes in terms of its phospholipid composition. As it is known that dysferlin is located at the T-tubule system in skeletal muscle and that dysferlin is involved in formation of the T-tubule system the tubular structures were analyzed with regard to PIP2 and phosphatidiylinositol (3,4,5)-trisphosphate (PIP3) composition, lipids that are found in T-tubule membranes (Milting et al., 1994). Pleckstrin homology domains (PH domains) have high affinity to phospholipids and are therefore often used to detect phospholipids. Recombinant PH domains of the signaling proteins Akt or PLCδ1 respectively were used as sensors for PIP3 and PIP2 and were coexpressed as GFP-fusion proteins with MYC-tagged dysferlin (done by Sven Thoms and Lars Klinge, figure 4.3.a). Dysferlin-induced membrane tubules indeed showed colocalization with both phospholipid sensors as indicated in figure 4.3a. This further substantiated that dysferlin-induced tubules are

membrane systems containing at least PIP2 and PIP3. To further analyze dysferlin with regard to PIP2, dysferlin was cotransfected with the PI(4)P5-kinase (PIP2 kinase) and the PIP2 phospatase synaptojanin 1. PIP2 kinase is a type I kinase that synthesizes PIP2 from PI4P. Expression of PIP2 kinase in Cos 7 cells leads to formation of PIP2-containing vacuolar structures. As shown in figure 4.3.b, coexpression of the PIP2 kinase together with dysferlin lead to recruitment of dysferlin to the PIP2-containing vacuolar structures indicating, that dysferlin bound PIP2 and was recruited to PIP2-containing membranes. PIP2 phospatase synaptojanin 1 dephosphorylates PIP2 thereby destructing PIP2 to PI4P. Interestingly, coexpression of dysferlin with the PIP2 phosphatase lead to partial colocalization of dysferlin and synaptojanin 1, and the dysferlin-induced tubular structures were disrupted (figure 4.3c). When truncated dysferlin constructs or pathogenic mutants were coexpressed with the PIP2 kinase no colocalization of the constructs with the kinase-induced vacuolar structures was detected (figure 4.3b). Additionally, no colocalization of the truncated or mutant dysferlin constructs with PIP2 phosphatase was detected (figure 4.3c). In conclusion, dysferlin was recruited to PIP2 kinase-induced vacuoles and this phenomenon required the full-length dysferlin protein. Furthermore, no tubule induction of the full-length dysferlin was observed after coexpression with the PIP2 phosphatase.

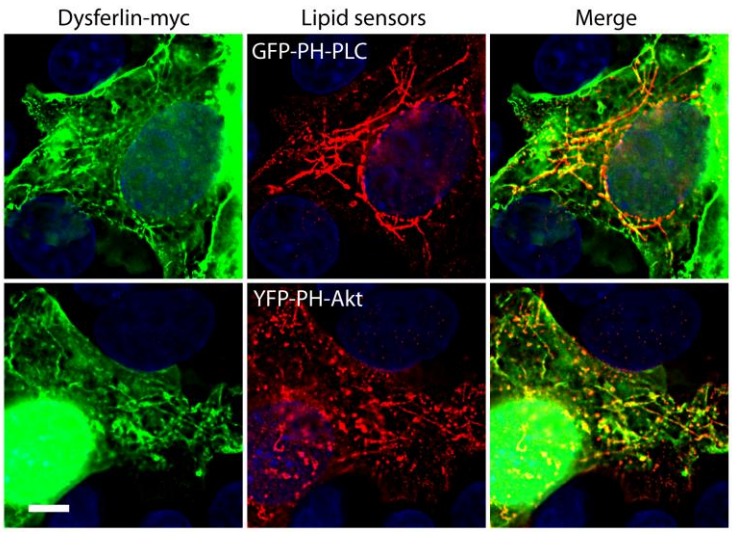

Figure 4.3a: Dysferlin-induced tubules contain PIP2 and PIP3. Cos 7 cells were cotransfected with dysferlin-myc (immunolanelled with anti-MYC antibody) and GFP-PH-PLC (PIP2-sensor) or YFP-PH-Akt (PIP3-sensor) (done by Sven Thoms and Lars Klinge). Tubules induced by dysferlin colocalize with both lipid sensors. Cells were analyzed by fluorescence microscopy and z-stacks were deconvoluted. Scale bar: 10 µm.

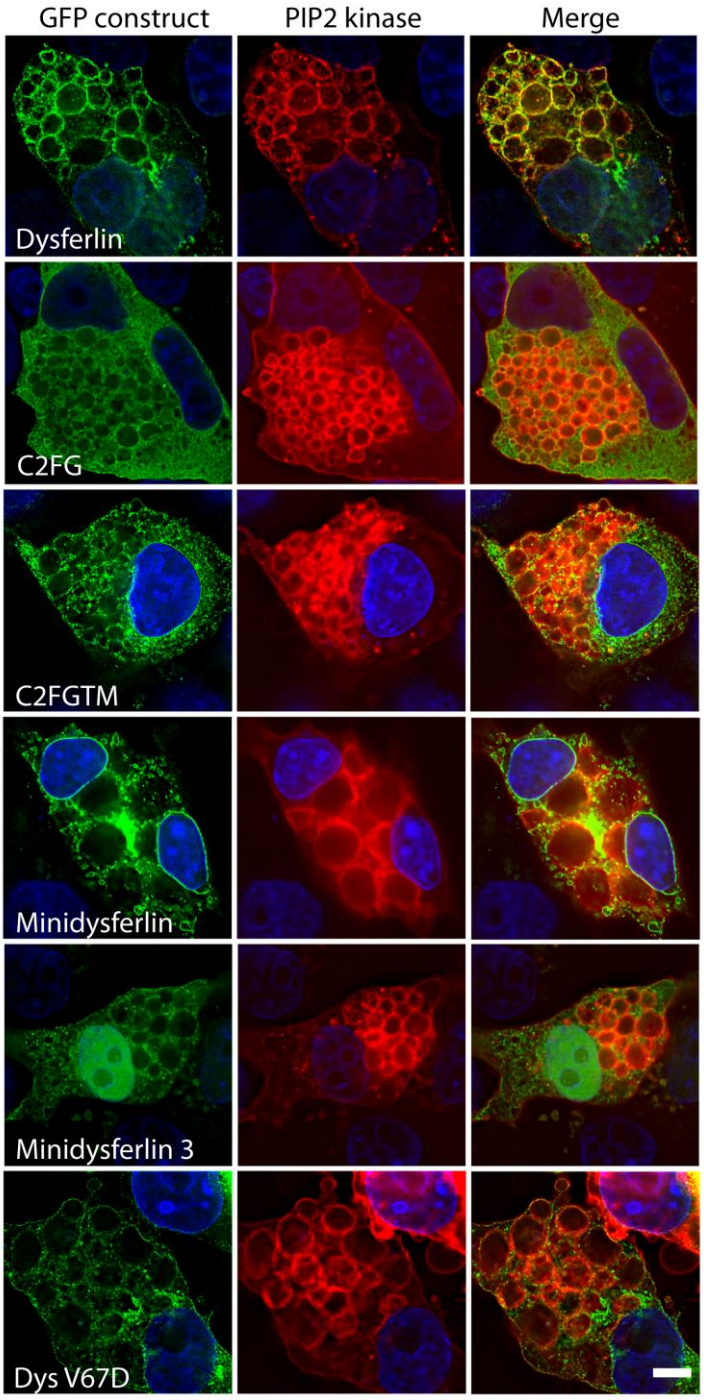

Figure 4.3b: Only the full-length dysferlin is recruited to PIP2-containing vacuolar structures induced by PIP2 kinase. Cos 7 cell were cotransfect with GFP-tagged full-length, truncated or mutant constructs of dysferlin and the RFP-tagged PIP2 kinase. The full-length dysferlin did colocalize with the PIP2 kinase at vacuolar structures which was not detected with any of the truncated or mutant constructs of dysferlin. Cells were analyzed by fluorescence microscopy and z-stacks were deconvoluted. Scale bar: 10 µm.

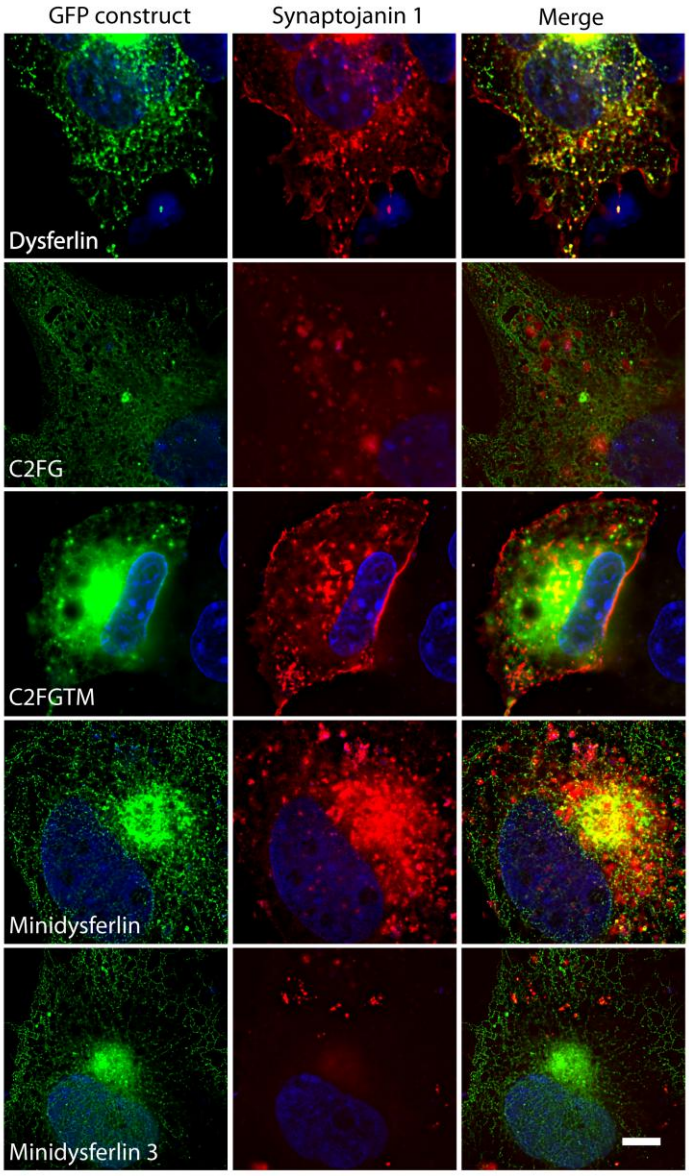

Figure 4.3c: Dysferlin colocalizes with synaptojanin 1 but does not induce tubular structures in presence of synaptojanin 1. Cos 7 cells were transfected with GFP-tagged full length dysferlin, truncated or mutant constructs of dysferlin and RFP-synatojanin 1. The full-length dysferlin colocalized with synaptojanin 1 but did not induce tubular structures in presence of synaptojanin 1. The truncated and mutant dysferlin constructs did not colocalize with synaptojanin 1. Cells were analyzed by fluorescence microscopy and z-stacks were deconvoluted. Scale bar: 10 µm.

4.4 Induction of tubular membranes requires the full-length dysferlin protein

The dysferlin protein has a molecular mass of about 230 kDa and contains two ferlin domains, seven C2 domains, and a transmembrane domain (TM). In order to learn more about the function of the dysferlin protein, it was necessary to identify functional domains of the protein. Four truncated constructs were generated and expressed in

Cos 7 cells (see figure 4.4b). Among them was minidyferlin which was found in a patient with a moderate and late onset dysferlinopathy consisting of the last two C2 domains and a truncated N-terminal part of the protein that resulted from a frame shift mutation and a cryptic startcodon downstream of the natural ATG (Krahn et al. 2010). A second minidysferlin, called minidysferlin 3, was tested, which consisted again of the last two C2 domains and the C2A domain (Azakir et al. 2012). This minidysferlin 3 was claimed to have the same membrane repair capability like the full-length dysferlin protein (Azakir et al. 2012). Two further truncated dysferlin constructs were cloned including the last two C2 domains with (C2FGTM) and without the TM domain (C2FG). These constructs were tested for tubule induction in Cos 7 cells and the results in figure 4.4a indicate that none of the truncated dysferlin versions was able to induce tubular membrane structures like the full-length protein. Instead, all but the construct lacking the TM domain showed a network-like expression pattern which colocalized with the ER marker PDI (not shown). The construct lacking the TM domain was expressed in the entire cytosol of the cell.

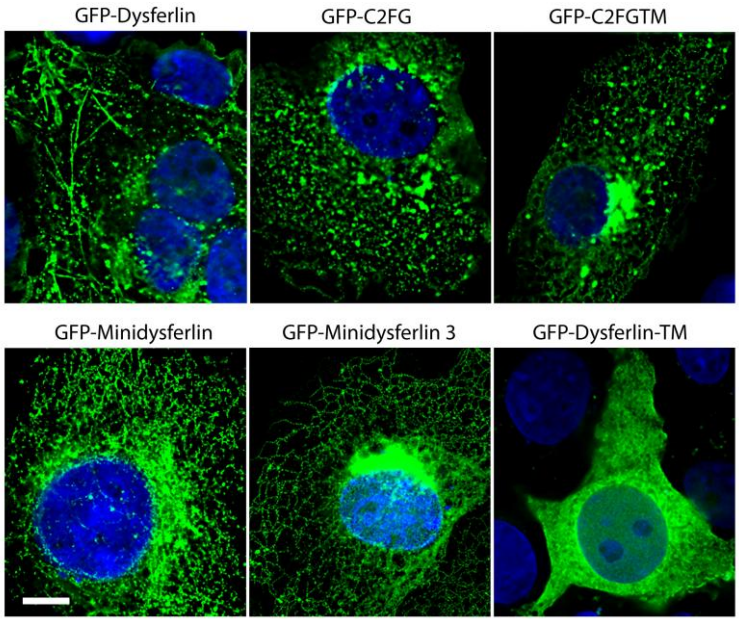

Figure 4.4a: The full-length dysferlin construct is needed for tubule induction. Cos 7 cells were transfected with GFP-tagged wild-type or truncated dysferlin constructs. None of the truncated constructs was able to induce tubulation like the full-length dysferlin. Cells were analyzed by fluorescence microscopy, and z-stack images were deconvoluted. Scale bar: 10 µm.

The truncated constructs were additionally expressed in C2C12 cells, a murine myoblast cell line, in order to examine the localization of the proteins. Dysferlin localized to the T-tubule system in C2C12 cells (Klinge et al., 2007). When the dysferlin full-length protein was expressed in these cells it showed T-tubule localization as it was seen previously (Klinge et al., 2007, figure 4.4b). In contrast, truncated dysferlin constructs did show a punctate expression pattern not suggesting localization at the intracellular network previously identified as T-tubule system (Klinge et al., 2007). With the minidysferlin construct we already analyzed a mutant version of dysferlin that derived from a patient. As most of the disease-causing variants are point mutations (Krahn et al., 2009) four pathogenic mutants of dysferlin were tested with regard to their tubule formation capacity. Three pathogenic mutants contain mutations in one of the C2 domains (mutation pG2999W in C2B, mutation pV398X in C2C or mutation pL1341P in C2E) and none of these mutants induced tubule formation in Cos 7 cells (experiment done by Sven Thoms and Lars Klinge, not shown) and none of these mutants did show localization at tubular structures in C2C12 cells (figure 4.4b). One mutant containing the point mutation between the C2D and C2E domains (mutation pR1333L) did induce tubular structures in about 20 % of Cos 7 cells. Furthermore, this mutant also partially showed a tubular expression pattern in C2C12 cells suggesting partial T-tubule localization. This indicates that pathogenic mutants of dysferlin were not able to induce or showed an impaired tubulation in Cos 7 cells and probably did not localize to the T-tubule system in C2C12 cells.

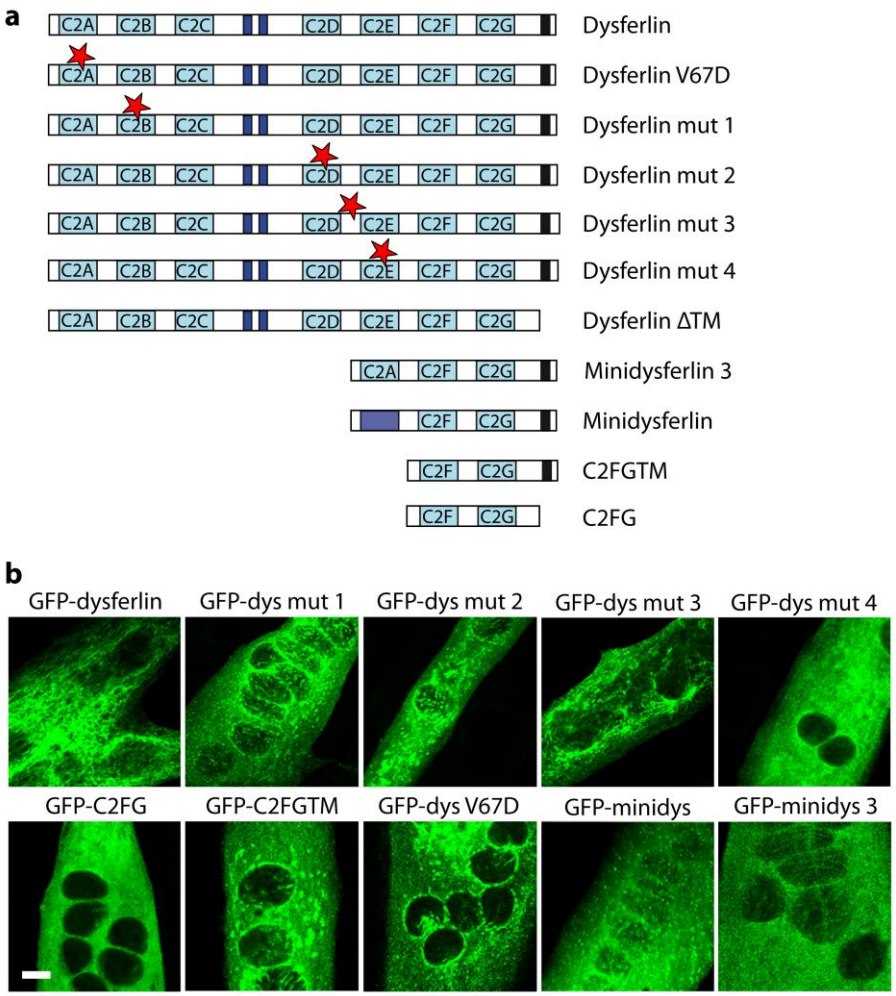

Figure 4.4b: In contrast to full-length dysferlin, most mutant and truncated dysferlins do not show tubular expression patterns in C2C12 cells. a) Domain diagram of dysferlin constructs used for transfection in Cos 7 and C2C12 cells. b) C2C12 cells were transfected with GFP-tagged dysferlin full-length construct, pathogenic mutants of dysferlin or truncated dysferlin constructs and analyzed by confocal microscopy. Only the full-length dysferlin localized to tubular network structures previously identified as the T-tubule system in C2C12 cells. Scale bar: 10 µm.

4.5 Dysferlin-induced tubules are continuous with the plasma membrane

It was already shown that dysferlin induced tubules in Cos 7 cells are newly build membrane structures that contain high amounts of the phospholipid PIP2 which is also found in membranes of the T-tubule system. The T-tubule system partly develops from invaginations of the plasma membrane. Therefore we analyzed whether dysferlin-induced membranes in Cos 7 cells are continuous with the plasma membrane and possibly develop by invagination from the plasma membrane. FM4-64 is a fluorescent lipophilic dye that is often used to stain the plasma membrane of cells. GFP-dysferlin transfected Cos 7 and HeLa cells were costained with the membrane dye FM4-64.

Interestingly membrane tubules showed colabeling with the membrane dye in Hela (figure 4.5) and Cos 7 cells (not shown). After cyto D treatment the dysferlin-induced tubules appeared more pronounced as detected before and show colocalization with FM4-64 (figure 4.5).

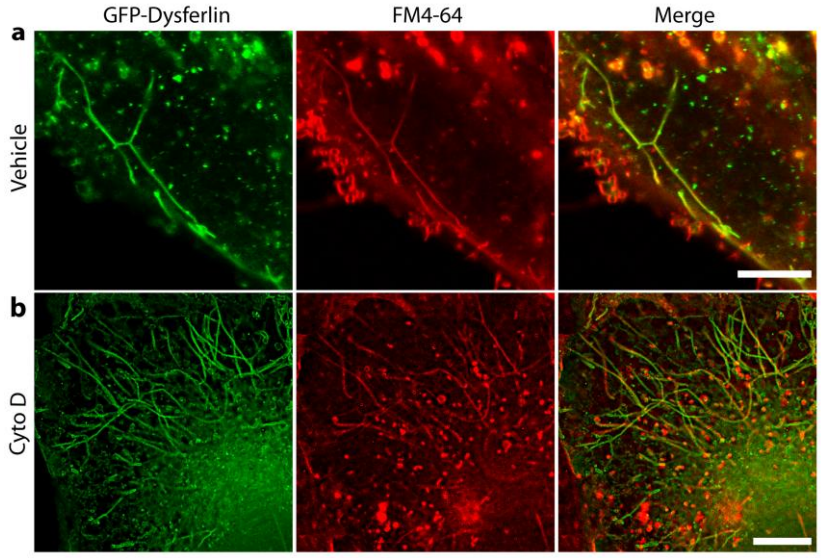

Figure 4.5: Dysferlin-induced tubules are continuous with the plasma membrane. Hela (a) or Cos 7 (b) cells were transfected with GFP-dysferlin, vehicle or cytochalasin D treated and costained with the plasma membrane dye FM4-64. Dysferlin-induced tubules colocalize with FM4-64 staining in vehicle and cyto D treated cells. Cells were analyzed by confocal microscopy (a) or fluorescence microscopy and deconvoluted afterwards (b). Scale bar: 10 µm.

4.6 Full-length dysferlin binds to phospholipids in vitro

The previous experiments demonstrated that dysferlin colocalized with the phospholipids PIP2 and PIP3 and that dysferlin is recruited to PIP2-containing structures. This indicates that dysferlin binds to phospholipids, and especially to PIP2. Therrien et al. showed in vitro that the C2A domain of dysferlin binds to phospholipids in a Ca^{2+}-dependent manner, but so far in vitro lipid binding studies with the full-length dysferlin protein have not been published. To test the lipid binding ability of dysferlin, full-length dysferlin protein, minidysferlin 3 and a pathogenic mutant of dysferlin (mutant pV67D in C2A) were expressed as His6-tagged proteins by an E.coli expression system. Commercially available PIP strips blotted with several phospholipids found in mammalian membranes were used to detect dysferlin binding. Bin1, a BAR-domain protein localizing to the T-tubule system in skeletal muscle (Butler et al. 1997), is known to bind phospholipids, especially PIP2 and was therefore used as positive control. The results corroborated the expected binding of Bin1 to PIP2 which

furthermore binds to phosphatidylinositol (3)-phosphate (PI3P) (figure 4.6a). Like Bin1, the dysferlin full-length protein and minidysferlin 3 showed binding to PIP2 and PI3P. Interestingly, the dysferlin mutant V67D which contains a mutation in the C2A domain did only show binding affinity to PI3P but not PIP2. Bin1 and full-length dysferlin did also bind to phosphatidic acid. The results show that the full-length dysferlin bound to PIP2 and that the C2A domain was necessary for PIP2 interaction.

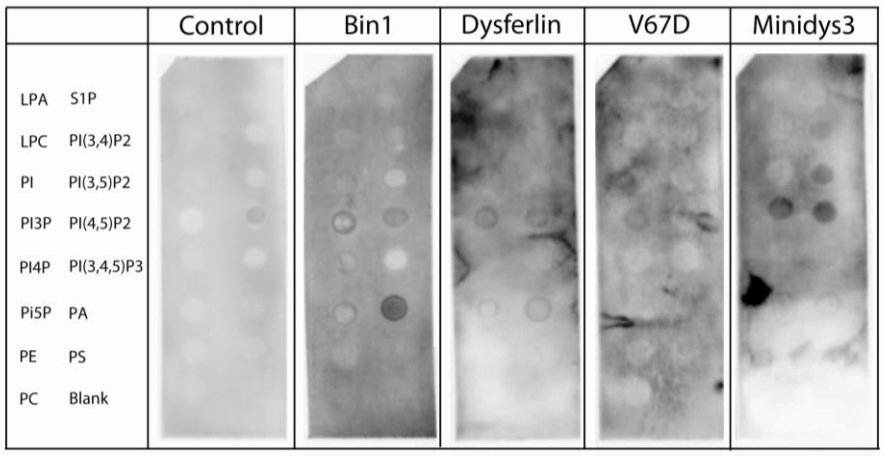

Figure 4.6a: Full-length dysferlin binds to PIP2 and the C2A domain is necessary for this binding. Bin1, full-length dysferlin, minidysferlin 3 and a dysferlin mutant (V67D) were expressed in E.coli expression systems as His6-tagged (full-length dysferlin and mutant V67D) or GST-fusion proteins (Bin1 and minidysferlin 3). PIP strips (Echelon) were incubated with protein lysates and the proteins were detected by primary antibodies against dysferlin, Bin1, or GST, secondary HRP-coupled antibodies and chemiluminescence.

PIP strips are usually used as a first screening of protein lipid binding. To further support observations by the PIP-strip experiments, liposome flotation experiments were performed. Liposomes were prepared from Folch fraction lipids containing additional 5 % PIP2 or PI3P or Folch fraction lipids only and were incubated in presence of Ca^{2+} with dysferlin or Bin1 which was used as positive control. Sucrose gradient centrifugation was carried out and fractions were analyzed by Western blotting to detect flotation of proteins. Membranes were recovered from the top fraction and unbound protein remained in the lower fractions. As shown in figure 4.6b Bin1 was detected in the top fraction in presence of Folch fraction liposomes as well as Folch fraction liposomes with 5 % added PIP2. In absence of liposomes, no Bin1 protein was detected in the top fraction. Dysferlin protein was detected in the top fraction only in presence of Folch fraction lipids containing 5 % PIP2. In absence of liposomes or liposomes made of Folch fraction lipids containing 5 % PI3P or Folch fraction lipids only, no flotation of protein was detected. These results confirm the binding affinity of

the dysferlin full-length protein to the phospholipid PIP2. In contrast, no binding of dysferlin to PI3P was detected by the membrane flotation assay.

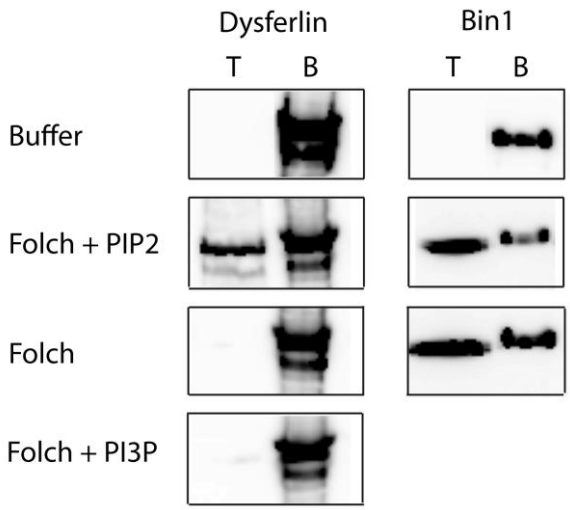

Figure 4.6b: Dysferlin is able to bind to PIP2. Liposomes were made of Folch fraction lipids containing 5 % PIP2 or PI3P or Folch lipids only and extruded through a 100 nm filter. Liposomes or buffer (as negative control) were incubated with dysferlin or Bin1, overlayed with a sucrose gradient and ultracentrifugation was carried out followed by fractionation and Western blot. T = top fraction, B = bottom fraction.

4.7 Dysferlin tubulates membranes in vitro

Dysferlin is able to induce a tubular membrane network continuous with the plasma membrane when expressed in non-muscle cells. These membranes contain high amounts of PIP2, a phospholipid found in the T-tubule system of skeletal muscle. Furthermore, it was demonstrated that dysferlin was able to bind phospholipids in vitro. These findings suggest that dysferlin is able to mediate membrane tubulation. To determine the ability of dysferlin to tubulate or deform biological membranes in vitro, a liposome tubulation assay with recombinant dysferlin full-length protein was performed. As Bin1 is able to induce tubulation of liposomes (Lee et. el., 2002) this protein was used as positive control. Liposomes made of Folch fraction 1 lipids were incubated with the recombinant proteins in presence of Ca^{2+} and analyzed by electron microscopy. As indicated in figure 4.7a, Bin1 as expected induced tubulation of liposomes. Interestingly, also the dysferlin full-length protein did induce liposome tubulation in this cell-free system. The pathogenic C2A mutant of dysferlin and minidysferlin 3 did not induce tubulation. When 5 % PIP2 was added to Folch fraction lipids, tubulation of liposomes by dysferlin was increased and tubulation appeared more pronounced compared to tubulation of Folch liposomes. These results gave evidence that dysferlin exhibits a powerful membrane deformation capacity and that presence of PIP2 lipids in

biological membranes increases tubulation properties of dysferlin. Minidysferlin 3 failed to tubulate membranes in vitro which indicates that the full-length protein is necessary for tubulation. Further, the C2A mutant of dysferlin also failed to induce tubulation therefore, the C2A domain is not only necessary for PIP2 binding but is also required for liposome tubulation.

The important role of the C2A domain was further confirmed by a liposome binding experiment using the single C2 domains of dysferlin. The recombinant C2 domain proteins of dysferlin were incubated with liposomes made from Folch fraction lipids containing 5 % NBD-PE (7-nitro-2-1,3-benzoxadiazole-4-yl phosphatidylethanolamine) in presence of Ca^{2+} and were analyzed by fluorescence microscopy (figure 4.7b). The results demonstrate that the C2A domain of dysferlin induced aggregation of liposomes which was not detected with the other C2 domains. This further indicates the crucial role of the C2A domain in membrane binding properties of dysferlin.

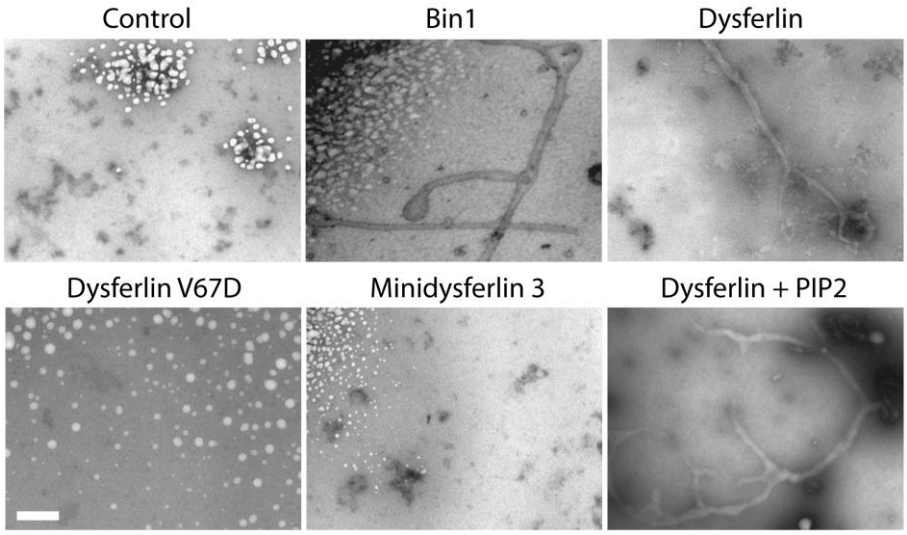

Figure 4.7a: Dysferlin induces tubulation of membranes in vitro. Dysferlin full-length protein, dysferlin mutant V67D, minidysferlin 3 and Bin1 were expressed in E.coli expression systems, incubated with liposomes made from Folch fraction 1 lipids and extruded through a 100 nm filter afterwards, absorbed onto formvar coated copper grids, stained with 2 % PTA and analyzed by EM. Bin1 and dysferlin were able to induce tubulation of liposomes in presence of Ca^{2+} whereas the minidysferlin 3 and the C2A mutant of dysferlin were not. Tubulation efficiency of dysferlin increased when 5 % PIP2 were present in liposomes. Scale bar: 0.2µm.

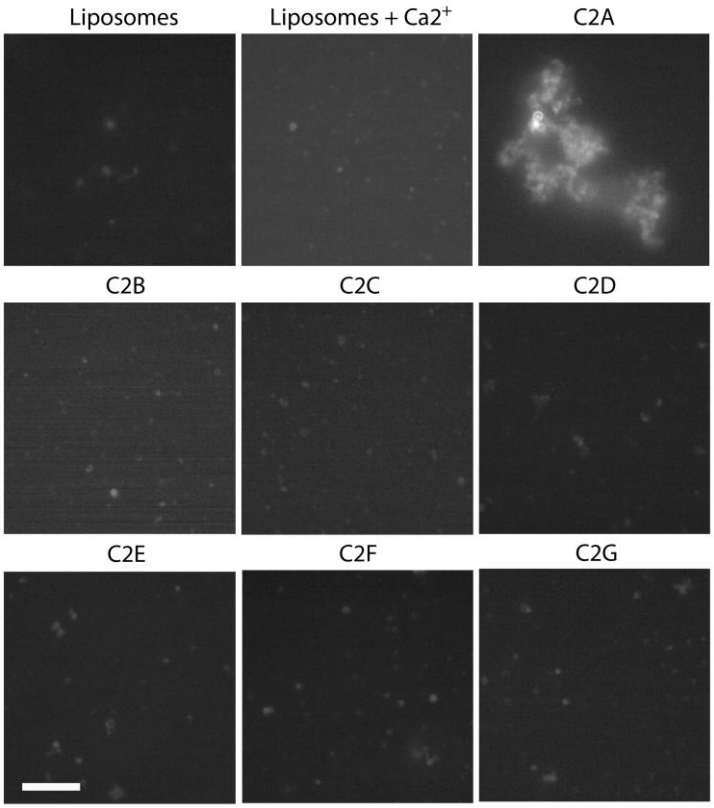

Figure 4.7b: The C2A domain of dysferlin aggregates liposomes in vitro. The seven C2 domains were expressed as GST-tagged proteins in e.coli expression systems, refolded after urea denaturation and incubated with liposomes prepared from Folch fraction lipids and 5 % NBD-PE and Ca^{2+} and analyzed by fluorescence microscopy. Only the C2A domain lead to aggregation of liposomes in presence of Ca^{2+}. Scale bar 20 µm.

4.8 Dysferlin is localized at the T-tubule system in cardiomyozytes

In heart muscle dysferlin protein is expressed twice as high as in skeletal muscle (Anderson et al., 1999). Furthermore, it was shown that dysferlin knock-out mice develop a cardiomyopathy after stress exercise (Han et al., 2007) and in some patients with dysferlin-deficiency a cardiomyopathy was also described (Kuru et al., 2004; Wenzel et al., 2007; Guglieri et al., 2008) although this appears not a regular feature of dysferlin-deficiency. These are indications of a possible physiological function of dysferlin not only in skeletal but also in heart muscle which made further analysis of dysferlin in cardiomyocytes necessary. In order to analyze the localization of dysferlin coimmunofluorescence labeling with the DHPR as a T-tubule marker was performed. As shown in figure 4.8, dysferlin localized to the T-tubule system also in cardiomyocytes.

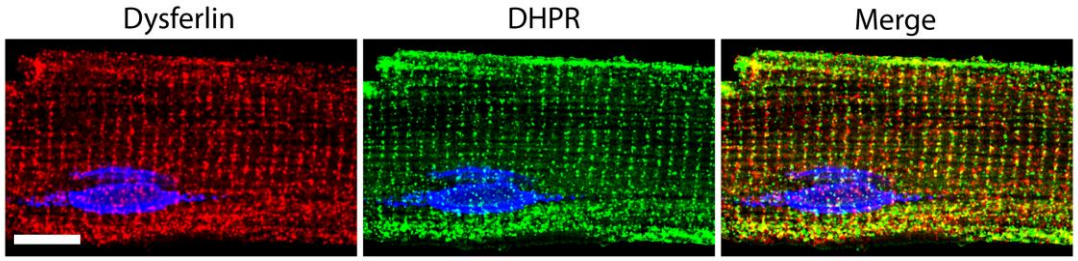

Figure 4.8: Dysferlin localizes to the T-tubule system in dysferlin-deficient cardiomyocytes. Cardiomyocytes were isolated from hearts of wild-type mice (20 weeks old) and stained with antibodies against dysferlin and DHPR. Cells were analyzed by fluorescence microscopy and z-stacks were deconvoluted. Scale bar: 10 µm.

4.9 Dysferlin-deficient cardiomyocytes show an abnormal T-tubule system

It was previously shown that dysferlin localizes to the T-tubule system in skeletal muscle and that the T-tubule system in dysferlin-deficient skeletal muscle is of abnormal morphology (Klinge et al., 2010). As dysferlin also localizes to the T-tubule system in heart muscle, dysferlin-deficiency may have an influence on the morphology of the T-tubule system in cardiomyocytes. Di-8-butyl-aminonaphthyl-ethylene-pyridinium-proply-sulfonate (Di8ANEPPS) is a membrane dye that can be applied to detect the T-tubule system in living cardiomyocytes (Nishimura et al., 2006). Staining of isolated wild-type cardiomyocytes showed the regular staining pattern of the T-tubule system with mainly transversal orientation (figure 4.9). In contrast, staining of dysferlin knock-out cardiomyocytes revealed an irregular, dilated and predominantly longitudinal orientated T-tubule system (figure 4.9, done by Viacheslav Nikolaev). This indicates that dysferlin is crucial not only for maintenance of normal T-tubule structure in skeletal muscle, but also of heart muscle.

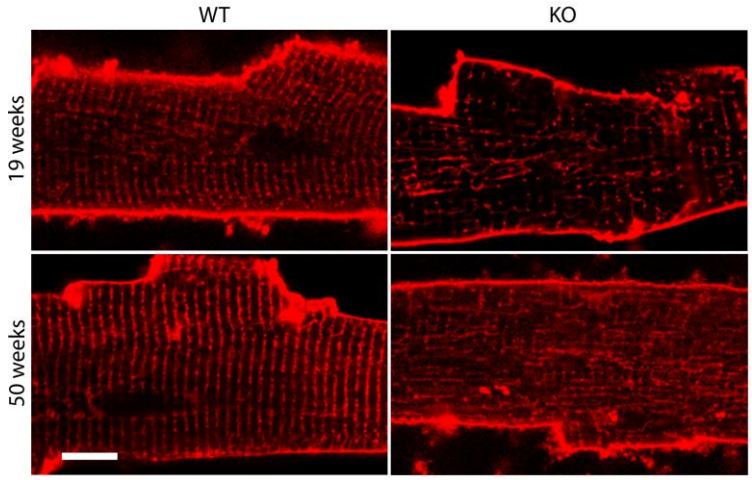

Figure 4.9: The T-tubule system in dysferlin-deficient cardiomyocytes shows an abnormal configuration. Cardiomyocytes from young (19 weeks) and aged (50 weeks) dysferlin-null and wild-type mice were isolated, stained with the membrane dye Di8ANEPPS and analyzed by confocal microscopy (done by Viacheslav Nikolaev). Scale bar 10 µm.

4.10 Dysferlin is upregulated after myocardial infarction

We have now demonstrated that dysferlin localizes to the T-tubule system in cardiomyocytes and that in the T-tubule system of heart muscle is irregularly configured when dysferlin is absent. Furthermore, it was shown in previous experiments that dysferlin binds to phospholipids and is able to mediate membrane tubulation. This lead to the hypothesis, that dysferlin may also play a role in the process of T-tubule biogenesis in heart muscle and furthermore in T-tubule remodelling, a process that is implicated in hearts after myocardial infarction (MI). Therefore, a dysferlin Western blot was carried out with samples from rat heart homogenates after MI and sham-treated hearts (provided by Viacheslav Nikolaev). As indicated in figure 4.10, protein levels of dysferlin were significantly upregulated in rat hearts after MI when compared to sham-treated hearts. This indicates a role of dysferlin in the process of T-tubule remodelling after MI.

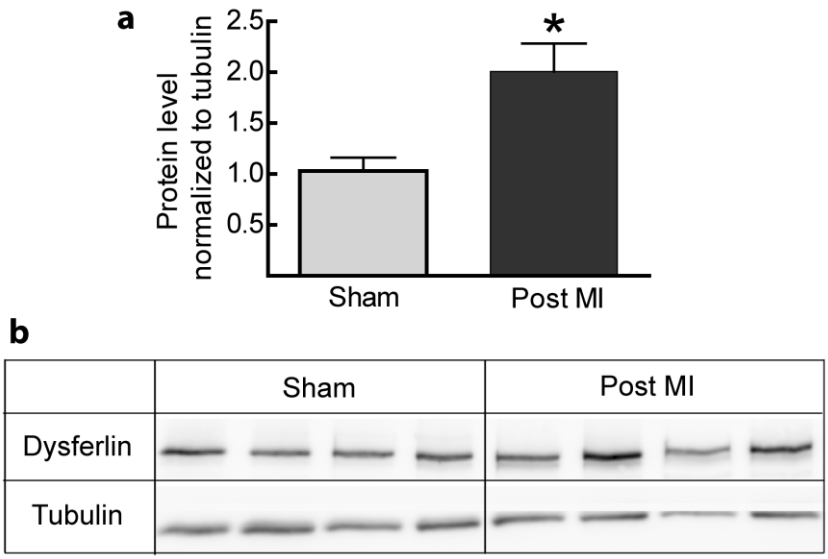

Figure 4.10: Dysferlin is upregulated after myocardial infarction. Myocardial infarction (MI) was induced in rat hearts by ligation of the left coronary artery (samples provided by Viacheslav Nicolaev). Homogenates of rat hearts after induction of MI or sham treatment were separated by SDS gel electrophoresis, blotted onto nitrocellulose membranes, incubated with a dysferlin antibody and detected by chemiluminescence (b). Protein levels were determined by densitometry using Image J analysis software and were normalized to tubulin to ensure equal protein loading. Protein levels of KO hearts were then normalized to WT hearts (a). *$p<0.05$, N = 4 per group.

4.11 Analysis of Ca^{2+} release and shortening in cardiomyocytes

4.11.1 Ca^{2+} release and shortening are not altered in dysferlin-deficient cardiomyocytes

It was shown that dysferlin localizes to the T-tubule system in cardiomyocytes and that dysferlin-deficiency leads to an irregular conformation of the T-tubule system. The T-tubule system is required for propagation of the action potential into the interior of the cardiomyocyte where the process of excitation-contraction coupling (EC-coupling) is initiated. To investigate possible functional consequences of an abnormal T-tubule morphology in dysferlin-deficiency on the process of EC-coupling Ca^{2+} measurements in isolated cardiomyocytes were carried out in cooperation with the lab of Lars Maier (Department of Cardiology, UMG). Single cardiomyocytes were isolated from wild-type and dysferlin-deficient mice (50 weeks of age) and loaded with the Ca^{2+}-sensitive dye Fluo-4. Cells were electrically stimulated at 0.5 to 4 Hz and Ca^{2+} release and fractional shortening of the cardiomyocytes was detected by epifluorescence microscopy. Increasing the stimulation frequency modifies the amplitude and contraction kinetics as well as relaxation kinetics which depend on sarcoplasmatic reticulum (SR) Ca^{2+} load, SR Ca^{2+} uptake and ryanodine receptor 2 (RYR2) inactivation. As shown in

figure 4.11.1, the Ca^{2+} transient amplitudes of wild-type and knock-out cardiomyocytes showed a negative force-frequency relationship. Fractional shortening of both groups decreased from 0.5 to 1 Hz and increased again with higher frequency. The results showed no significant differences in Ca^{2+} release and fractional shortening of knock-out and wild-type cardiomyocytes. Additional parameters like relaxation time and time to peak of both, the Ca^{2+} transient amplitudes and the fractional shortening of the cells did not show significant differences between knock-out and control group. The relaxation time is the time needed to transport the released Ca^{2+} back into the SR (by SR Ca^{2+}-ATPase (SERCA)) and out of the cell (by Na^{+}/Ca^{2+}-exchanger (NCX) or sarcolemmal Ca^{2+} pump). The parameter 50 % relaxation time describes the time that is needed to decrease the Ca^{2+} transient and the contraction to 50 % of its peak value. As in mouse cardiomyocytes 92 % of Ca^{2+} is transported back into the SR (Maier et al., 2000) and only 7 % are transported out of the cell by NCX and 1 % by the sarcolemmal Ca^{2+} pump, the relaxation time depends mainly on SERCA and therefore can be considered as an indicator for SERCA function. At higher heart-rates a process called frequency-dependent acceleration of relaxation (FDAR) leads to rapid refilling of the SR Ca^{2+} store (Maier and Bers, 2002). As indicated in figure 4.11.1, FDAR occurred in all cells for both, Ca^{2+} transient amplitudes and shortening. The time to peak is the time from electrical stimulation of the cell until the peak of Ca^{2+} release, respectively contraction, is reached witch includes activation of dihydropyridine receptor (DHPR), coupled gating of DHPR and RyR and Ca^{2+} release of RyR. The time to peak is therefore a measure for the contractility process of the cell. Both, SERCA function and contractility were not altered in dysferlin-deficient cardiomyocytes. These results point out that under normal physiological conditions Ca^{2+} homeostasis is not altered in dysferlin-deficient cardiomyocytes.

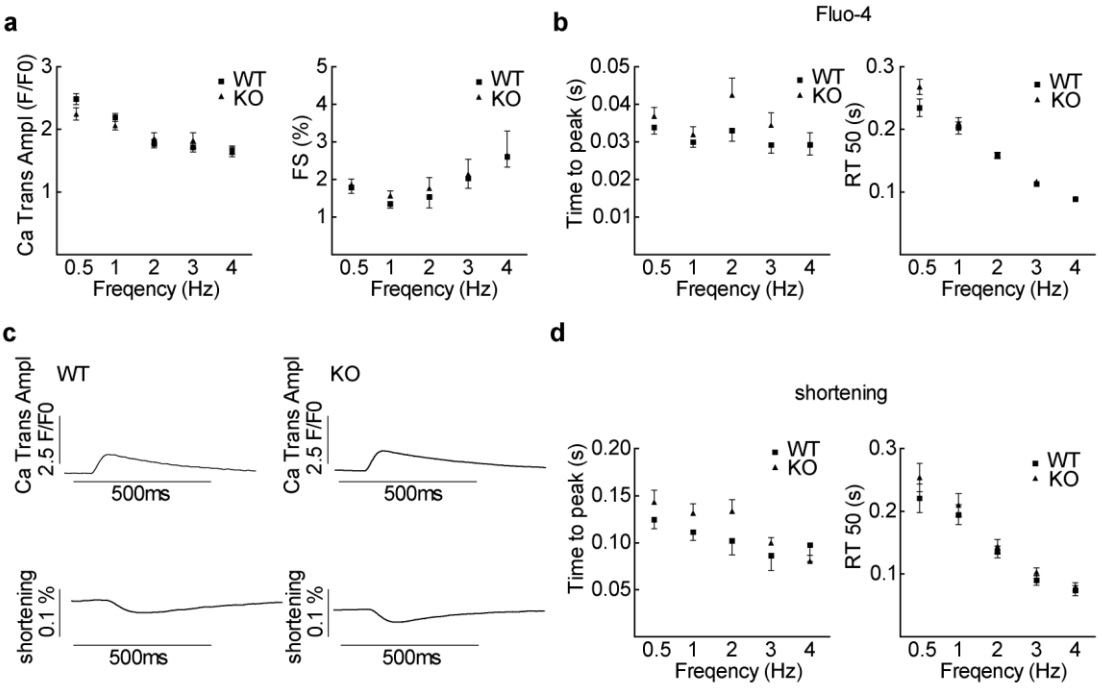

Figure 4.11.1: Ca^{2+} release and fractional shortening of dysferlin-deficient cardiomyocytes are not altered under normal conditions. Isolated cardiomyocytes were loaded with Fluo-4 and Ca^{2+} release and shortening were detected after stimulation with 0.5 to 4 Hz. (a) Average Ca^{2+} transient amplitudes (left) and fractional shortening (right). (b) Average time to peak and 50 % relaxation time of Ca^{2+} transient amplitudes (c) Representative steady-state (1 Hz) Ca^{2+} transient amplitudes and fractional shortening of WT and KO cardiomyocytes (d) Average time to peak and 50 % relaxation time of fractional shortening. Data presented as mean +/- SEM, N = 7 mice and ≥ 8 fibers.

4.11.2 Isoprenaline treatment unmasks deficits of dysferlin-deficient cardiomyocytes

Isoprenaline as a $ß_1$ and $ß_2$-receptor agonist has positive ionotropic effects on hearts (Schwinger et. al., 1993) by activating cAMP-dependent pathways which increase intracellular Ca^{2+} transients (Pieske et al., 1997). Therefore, isoprenaline is often used to induce a stress situation in cardiomyocytes. As indicated in figure 4.11.2, isoprenaline treatment lead to significantly increased Ca^{2+} release and significantly increased contraction in both, dysferlin-deficient and wild-type cardiomyocytes. Interestingly, the dysferlin-deficient cardiomyocytes showed significantly decreased Ca^{2+} release compared to wild-type cells after isoprenaline treatment indicating significant deficits of dysferlin-deficient cardiomyocytes after isoprenaline treatment. Furthermore, isoprenaline treatment significantly increased the time to peak and the relaxation time of Ca^{2+} release and shortening of the cells but no differences were observed between knock-out and wild-type cardiomyocytes.

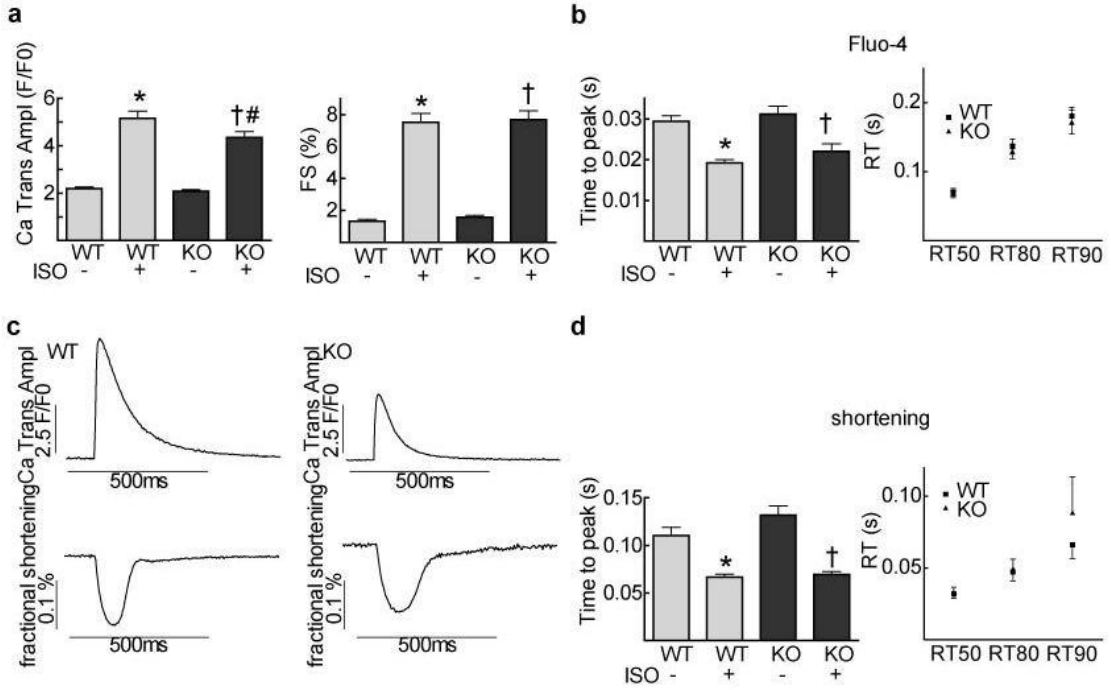

Figure 4.11.2: Ca^{2+} release of dysferlin-deficient cardiomyocytes is significantly decreased after induction of stress by isoprenaline. Isolated cardiomyocytes were loaded with Fuo-4 and treated with the ß-receptor agonist isoprenaline (10^{-7}M). a) Average Ca^{2+} transient amplitudes (left) and fractional shortening (right) at 1 Hz. (b) Average time to peak and relaxation times of Ca^{2+} transient amplitudes at 1 Hz (c) Representative steady-state (1 Hz) Ca^{2+} transient amplitudes and fractional shortening of WT and KO cardiomyocytes (d) Average time to peak and relaxation times of fractional shortening at 1 Hz. Data presented as mean +/- SEM (*p<0.05 vs. WT, #p<0.05 vs.WT+ISO, †p<0.05 vs. KO), N = 7 mice and ≥ 24 fibers per group.

4.11.3 Significantly decreased SR Ca^{2+} content in dysferlin-deficient cardiomyocytes

Rapid application of caffeine leads to reversible opening of RyR channels thereby releasing all Ca^{2+} from the SR. This is a very efficient experimental method often used to determine the SR Ca^{2+} load of cardiomyocytes. The caffeine-induced Ca^{2+} transient can be directly used to calculate the Ca^{2+} content of the SR. The results shown in figure 4.11.3a indicate that the SR Ca^{2+} content of the dysferlin-deficient cardiomyocytes was significantly decreased compared to wild-type cells. The decreased SR Ca^{2+} content was already seen in the vehicle-treated cells and became even more obvious after isoprenaline treatment. In presence of caffeine, the Ca^{2+} ions that are transported back into the SR by SERCA are directly released again by the opened RyR channel. Therefore, the relaxation time of the caffeine-induced transient is an indicator for the NCX function. As shown in figure 4.11.3a the NCX function of the

dysferlin-deficient cardiomyocytes was significantly decreased. A further indicator of the Ca^{2+} content of the SR is the post-rest relation (Bers et al., 2001). The results indicate that Ca^{2+} release and shortening of vehicle-treated wild-type and dysferlin-deficient cells after an unstimulated pause of 30 s was significantly increased compared to the steady-state Ca^{2+} release (figure 4.11.3b). No differences between knock-out and wild-type cells were detected. Isoprenaline treatment lead to a significantly decreased post-rest Ca^{2+} release of dysferlin-deficient cardiomyocytes compared to the wild-type Ca^{2+} release. This also indicates a decreased SR Ca^{2+} content in dysferlin-deficient cardiomyocytes.

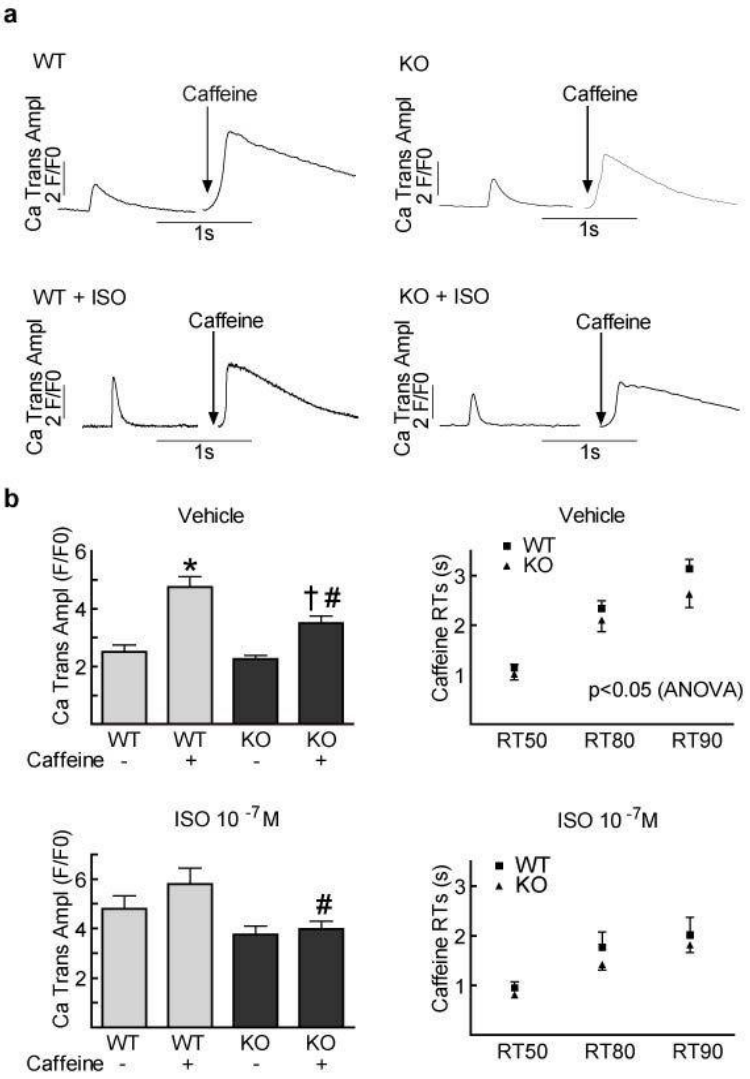

Figure 4.11.3a: Significantly decreased SR Ca^{2+} content and increased NCX function in dysferlin-deficient cardiomyocytes. 10 mM caffeine was rapidly applied to isolated vehicle- or isoprenaline- (10^{-7} M) treated cardiomyocytes. a) Representative steady-state (1 Hz) and caffeine-induced Ca^{2+} transient amplitudes of vehicle- or isoprenaline-treated cells b) Average steady-state and caffeine-induced Ca^{2+} transient amplitudes of vehicle- and isoprenaline-treated cells (left) and average relaxation times of the caffeine-induced Ca^{2+} transients of vehicle- and isoprenaline-treated cells (right). Data presented as mean +/- SEM (*p<0.05 vs. WT, #p<0.05 vs.WT+ISO, †p<0.05 vs. KO), N = 7 mice and ≥ 11 fibers per group.

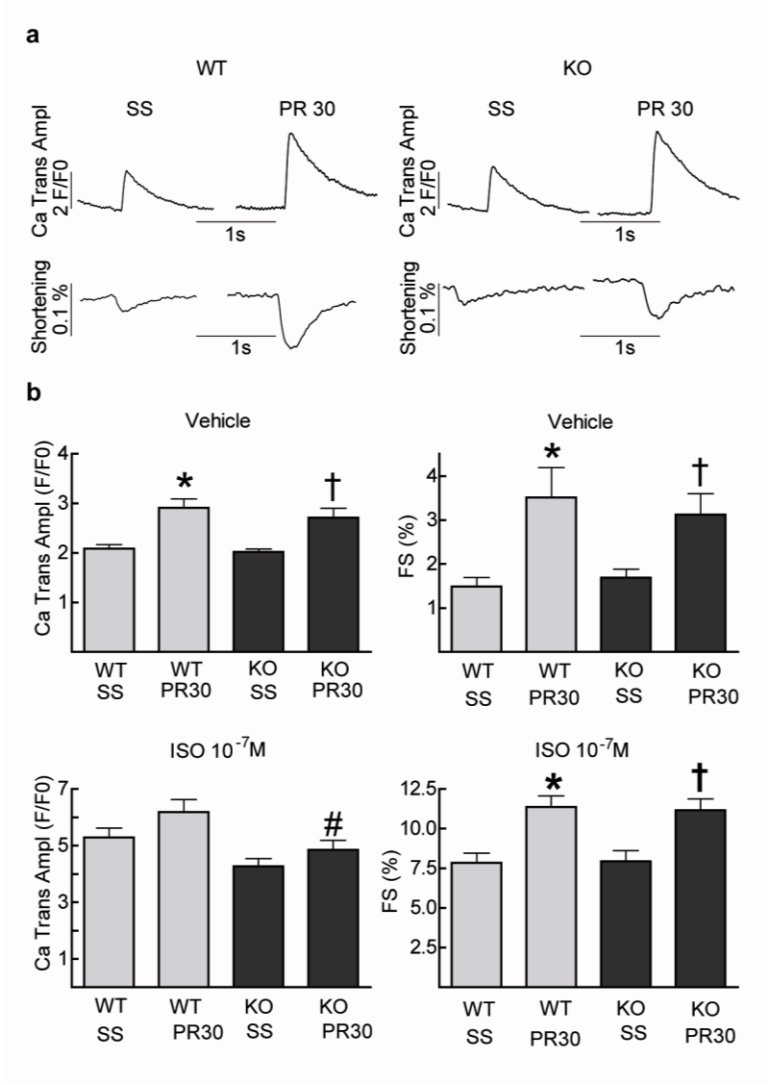

Figure 4.11.3b: Isoprenaline-induced stress leads to significantly reduced post-rest Ca^{2+} release in dysferlin-deficient cardiomyocytes. a) Representative steady-state and post-rest Ca^{2+} transients and fractional shortening of vehicle-treated wild-type and knock-out cells b) Average steady-state (1 Hz) and post-rest (30 s) Ca^{2+} transient amplitudes and fractional shortening of vehicle- and isoprenaline-treated cells. Data presented as mean +/- SEM (*p<0.05 vs. WT, #p<0.05 vs.WT+ISO, †p<0.05 vs. KO), N = 7 mice and ≥ 17 fibers per group.

4.12 Spark measurements revealed a significantly increased SR Ca^{2+} leak in dysferlin-deficient cardiomyocytes

The previous experiments revealed a significantly decreased SR Ca^{2+} content and a significantly decreased post-rest Ca^{2+} release after isoprenaline treatment of dysferlin-deficient cardiomyocytes. Both results lead to the hypothesis that the SR of dysferlin-deficient cardiomyocytes loses Ca^{2+} probably during diastole, the resting period, of the cell. This hypothesis was further analyzed by spark-measurements. Ca^{2+} sparks are local events of Ca^{2+} release through the RyR2 channel which occur during EC-coupling but also during diastole of the cells. Frequency, duration, amplitude and width of the

single sparks contribute to the SR Ca^{2+} leak. Spark measurements were performed by confocal microscopy using Fluo-4 loaded single isolated cardiomyocytes. The results shown in figure 4.12a revealed a significantly increased diastolic SR Ca^{2+} leak in dysferlin-deficient cardiomyocytes. This was due to a significantly increased spark frequency of the knock-out cells. All other parameters were not altered compared to wild-type cardiomyocytes. Isoprenaline treatment increased the SR Ca^{2+} leak in wild-type as well as in dyferlin-deficient cardiomyocytes compared to the vehicle-treated cells. Isoprenaline-treated dysferlin-deficient cardiomyocytes revealed a significantly increased spark width and duration, suggesting a prolonged opening of RyR2, but no alterated spark amplitude compared to the isoprenaline-treated wild-type cells. The significantly increased SR Ca^{2+} leak with prolonged opening of RYR2 especially after induction of stress suggested an increased probability of arrhythmias due to delayed afterdepolarizations in dysferlin-deficient heart muscle. A further indication for an increased probability of arrhythmias was the occurrence of nonstimulated events in electrically paced cardiomyocytes. These were detected during the measurement of Ca^{2+} transients and shortening by epifluorescece microscopy and these proarrythmogenic events occurred during steady-state stimulation and when stimulation was paused to measure the post-rest relation (figure 4.12b). The results in figure 4.12b indicate that proarrhythmogenic events occurred in both, wild-type and dysferlin-deficient cardiomyocytes, but were more frequent in dysferlin-deficient cardiomyocytes. Especially after treatment with isoprenaline nonstimulated events were significantly more frequent in dysferlin-deficient cells relative to wild-type cells. In dysferlin-deficient cardiomyocytes isoprenaline treatment lead to induction of sustained cellular tachycardia, which was not observed in wild-type cells or in vehicle-treated dysferlin-deficient cardiomyocytes. This indicates that dysferlin-deficient cardiomyocytes are prone to arrhythmia especially after induction of stress.

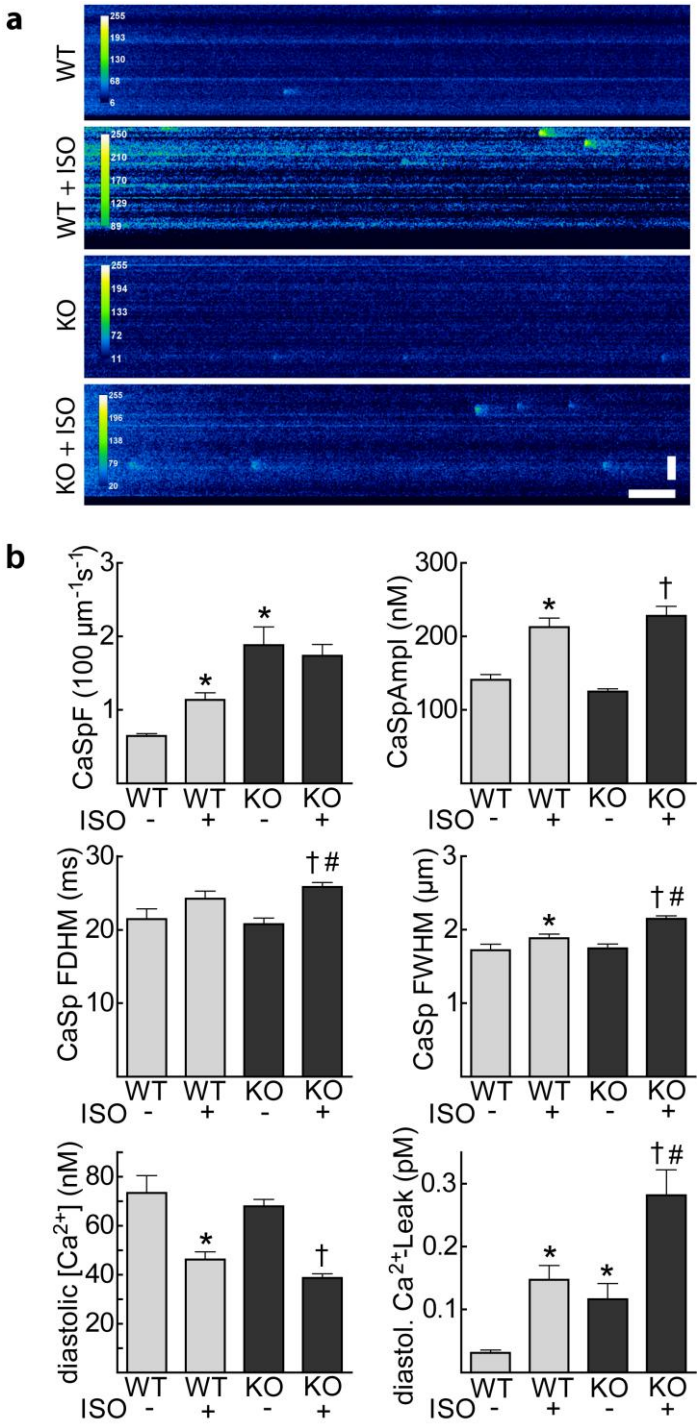

Figure 4.12a: Ca^{2+} spark measurements reveale a significantly increased SR Ca^{2+} leak. Significantly increased spark frequency of dysferlin-deficient cardiomyocytes lead to a significantly increased diastolic Ca^{2+} leak. (a) Representative line scan images (ΔF/F0, 0.96 ms/line) of vehicle- and isoprenaline-treated KO and WT cardiomyocytes. (b) Average spark frequency, diastolic [Ca^{2+}], diastolic SR Ca^{2+} leak and spatiotemporal properties of Ca^{2+} sparks, such as amplitude, full duration at half maximum and spatial spread (full width at half maximum). Data presented as mean+/- SEM. *P<0.05 vs. WT, †P<0.05 vs. KO #P<0.05 vs. WT+ISO. Horizontal scale bar: 200ms, vertical scale bar: 10 µm, N ≥ 4 mice and ≥ 40 fibers per group.

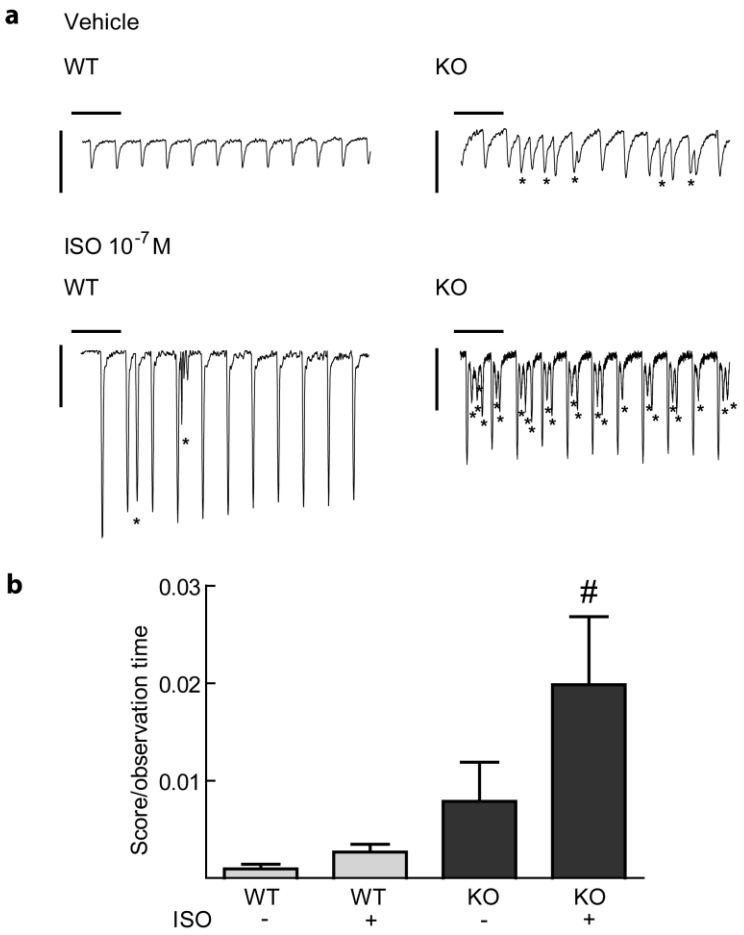

Figure 4.12b: Significantly increased proarrhythmogenic events in isoprenaline-treated dysferlin-deficient cardiomyocytes. a) Original traces of fractional shortening after vehicle or isoprenaline treatment (10^{-7} M) at 1 Hz showing spontaneous cellular arrhythmias (*). b) Average arrhythmia score per observation time. Data presented as mean +/- SEM. #P<0.05 vs. WT+ISO, vertical scale bars: 0.05 %, horizontal scale bars: 2 s.

4.13 Biometric data

Biometric data like age, heart weight and body weight were determined of mice that were used for Ca^{2+} measurements. Mice were 50 to 60 weeks old and dysferlin-deficient mice had a significantly decreased body weight but did not show any differences in their heart weight/body weight ratio. Therefore, aged dysferlin-deficient mice did not show signs of overt cardiac hypertrophy (figure 4.13).

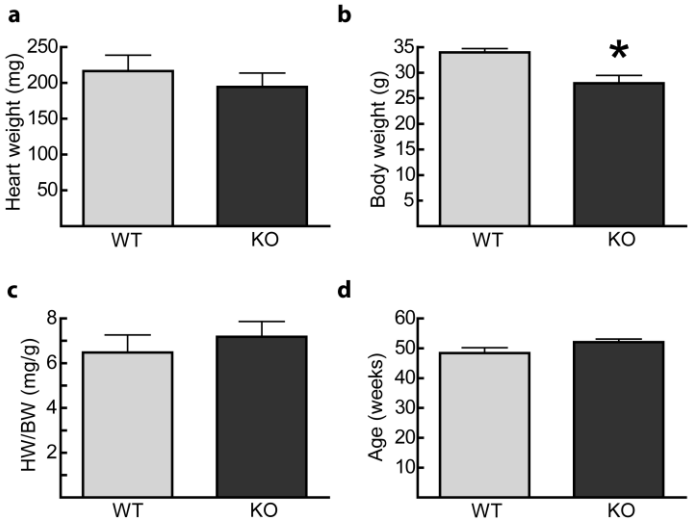

Figure 4.13: Dysferlin-deficient mice do not show signs of hypertrophy. Biometric data were determined from mice used for Ca^{2+}-measurements. a) heart weight, b) body weight, c) heart weight/body weight ratio as indicator for hypertrophy, d) age. Data presented as mean +/- SEM, *p< 0.05 versus WT, N = 10 mice per group.

4.14 Analysis of Ca^{2+} release in skeletal muscle fibers

4.14.1 Increased Ca^{2+} release in dysferlin-deficient muscle fibers

Dysferlin localizes to the T-tubule system (Klinge et al., 2008) and dysferlin-deficient skeletal muscle fibers of mice have a structurally irregular, longitudinally oriented and dilated T-tubule system. As the T-tubule system is a key player in the process of EC-coupling it was necessary to further investigate functional consequences of the aberrant T-tubule system regarding the EC-coupling process also in skeletal muscle fibers. Ca^{2+} release in isolated single skeletal muscle fibers was measured by epifluorescence microscopy in cooperation with Lars Maier (Department of Cardiology, UMG). Single skeletal muscle fibers were isolated from flexor digitorm brevis (FDB) muscles from young (6-20 weeks) and aged (>50 weeks) wild-type and dysferlin knock-out mice and loaded with the Ca^{2+} sensor Fura-2. Ca^{2+} transient amplitudes were measured at 0.5 to 4 Hz stimulation to analyze whether a force-frequency relationship like it was seen in cardiomyocytes exists in skeletal muscle fibers and if it shows any differences between wild-type and dysferlin-deficient cells. As shown in figure 4.14.1a, Ca^{2+} release was significantly increased in muscle fibers from young dysferlin-deficient mice. Ca^{2+} release was also increased in aged dysferlin-deficient mice but this increase was not statistically significant at the single frequencies. Baseline Ca^{2+} fluorescence as indicator for the resting Ca^{2+} concentration was not altered in knock-out compared to wild-type mice.

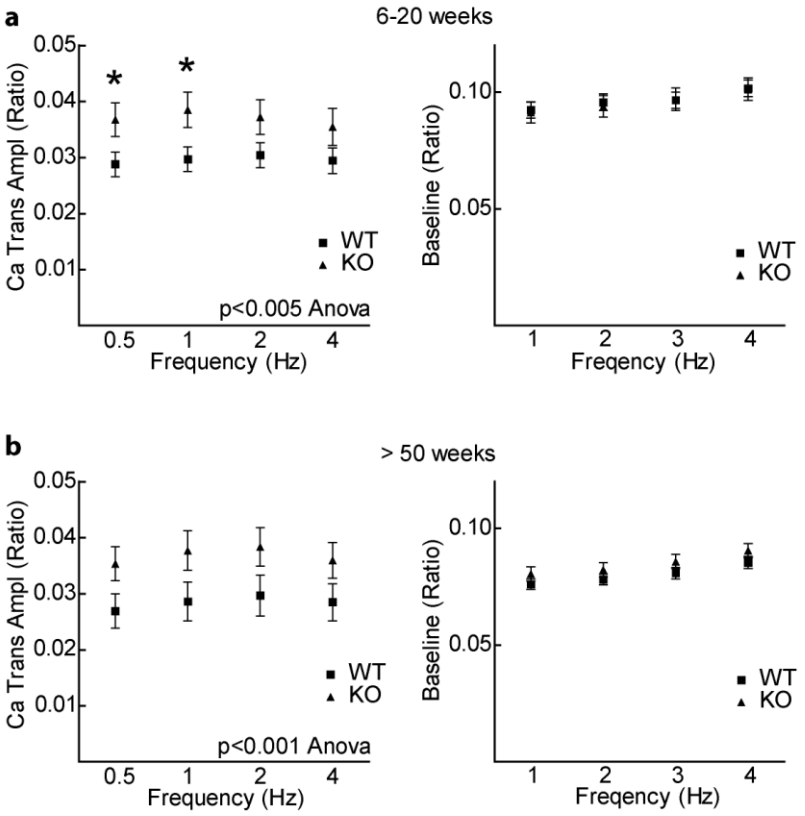

Figure 4.14.1a: Ca^{2+} release of dysferlin-deficient skeletal muscle fibers is significantly increased. Single skeletal muscle fibers were loaded with Fura-2 and Ca^{2+} transient amplitudes (left) and baseline Ca^{2+} fluorescence (right) of skeletal muscle fibers from (a) 6-20 weeks old mice and (b) >50 weeks old mice were detected. Baseline Ca^{2+} fluorescence was not altered but Ca^{2+} release was significantly increased in young and aged mice. Data presented as mean +/-SEM, *p<0.05, N ≥ 3 mice and ≥ 36 fibers per group.

As in cardiomyocytes the relaxation time in skeletal muscle fibers serves as indicator for SERCA function, as most of the Ca^{2+} is transported back into the SR by SERCA and only small parts of Ca^{2+} are transported out of the cell by NCX and the plasma membrane Ca^{2+} ATPase (PMCA). The time to peak can be considered as an indicator for the contractility of the cell as it involves processes like activation of DHPR, coupling of DHPR and RYR and Ca^{2+} release from the SR by RyR1. As indicated in figure 4.14.1b, both parameters, relaxation time and time to peak were not altered in skeletal muscle fibers from young dysferlin-deficient mice. In contrast, skeletal muscle fibers from aged dysferlin-deficient mice revealed significantly increased relaxation times and therefore a decreased SERCA function. Furthermore, also the time to peak was significantly increased, indicating a decreased contractility process in skeletal muscle fibers from aged dysferlin knock-out mice. These results revealed an altered Ca^{2+} homeostasis in dysferlin-deficient skeletal muscle.

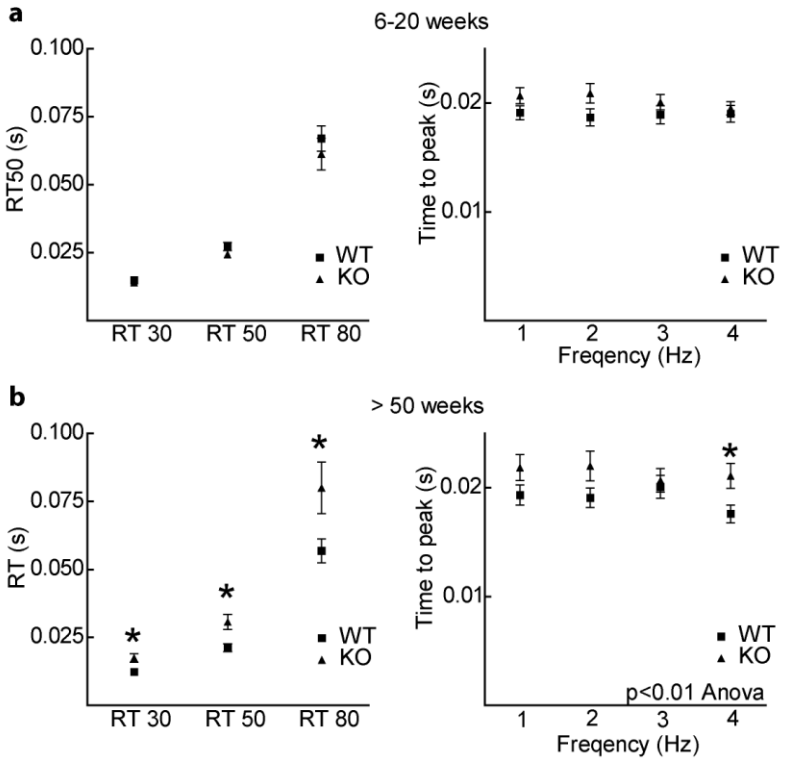

Figure 4.14.1b: Relaxation time and time to peak are significantly increased in skeletal muscle fibers of aged dysferlin-deficient mice. Average relaxation time at 0.5 Hz (left) and time to peak (right) of Ca^{2+} transient amplitudes of skeletal muscle fibers from (a) young and (b) aged mice. Both parameters were not altered in young dysferlin-deficient mice but significantly decreased in aged dysferlin-deficient mice. Data presented as mean +/- SEM, *p<0.05, N ≥ 3 x mice and ≥ 36 fibers per group.

4.14.2 Increased Ca^{2+} release is specific for dysferlin-deficient muscular dystrophy

To analyze whether increased Ca^{2+} amplitudes are specific for dysferlin-deficient skeletal muscle fibers and are not secondary due to the dystrophic process, Ca^{2+} release was also measured in muscle fibers from dystrophin-deficient mdx mice. Mdx mice are a model for dystrophin-deficient muscular dystrophy and the best-studied muscular dystrophy mouse model. As indicated in figure 4.14.2, the dystrohin-deficient skeletal muscle fibers revealed significantly decreased Ca^{2+} release related to wild-type and dysferlin-deficient mice and furthermore showed a significantly prolonged relaxation time indicating a decreased SERCA function. Resting Ca^{2+} concentration was not significantly altered in mdx mice compared to wild-type and dysferlin-deficient mice. These results were consistent with previously published results that demonstrated decreased Ca^{2+} transient amplitudes and decreased SERCA function in mdx mice.

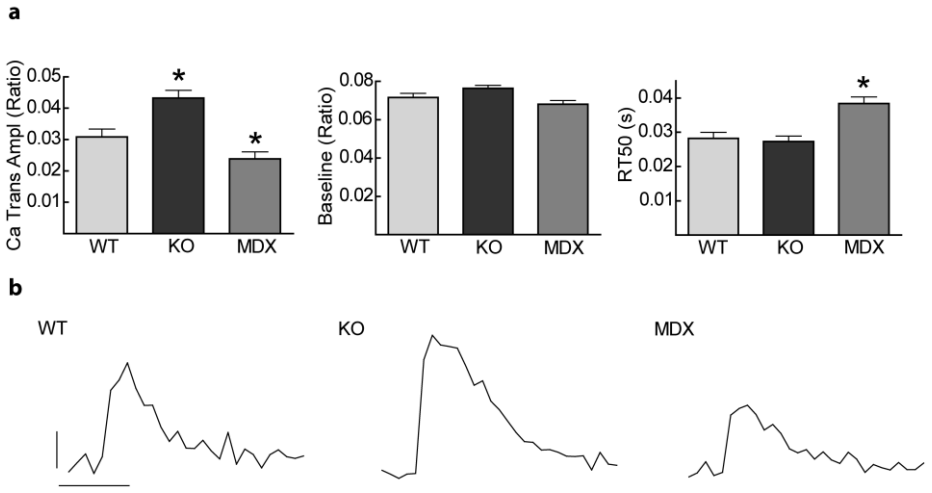

Figure 4.14.2: Increased Ca^{2+} release is specific for dysferlin-deficient skeletal muscle fibers and not due to the dystrophic muscle. (a) Average Ca^{2+} transient amplitudes, baseline fluorescence and 50 % relaxation time at 0.5 Hz stimulation of wild-type, dysferlin-deficient and mdx skeletal muscle fibers. (b) Representative steady-state Ca^{2+} transient amplitudes at 0.5 Hz stimulation. Data presented as mean +/- SEM, *p<0.05, N ≥ 3 mice and ≥ 40 fibers per group, vertical scale bar: 0.01 Ratio, horizontal scale bar: 0.05 s.

4.14.3 Influence of mechanical stress on Ca^{2+} homeostasis skeletal muscle fibers

To determine the influence of mechanical stress on Ca^{2+} release of young dysferlin-deficient skeletal muscle mice were subjected to fatigue exercise treadmill running and Ca^{2+} release was measured directly after the last exercise session. The results revealed a significantly increased baseline Ca^{2+} fluorescence which indicated a significantly increased resting Ca^{2+} concentration after exercise in both, dysferlin-null and wild-type mice. Furthermore, no significant changes of Ca^{2+} release and time to peak between exercised and non-exercised muscle fibers of dysferlin-deficient and wild-type mice could be observed. The relaxation time of wild-type muscle fibers increased significantly after stress exercise but the relaxation time of knock-out muscle fibers was not altered after stress exercise. In summary, myofibers of wild-type mice showed an increased resting Ca^{2+} concentration and increased SERCA function after stress exercise compared to non-exercised muscle fibers and dysferlin-deficient muscle fibers only revealed an increased resting Ca^{2+} concentration without alteration of further parameters.

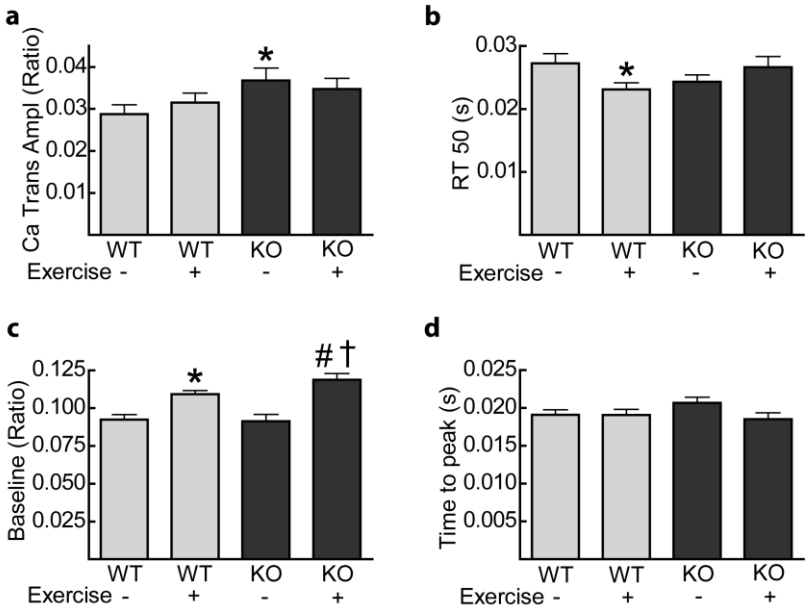

Figure 4.14.3: Stress exercise does not significantly alter Ca^{2+} release. Ca^{2+} release was measured in wild-type and knock-out muscle fibers after mild and fatiguing exercise treadmill running. Fatiguing exercise did not lead to significant changes of Ca^{2+} release in wild-type and knock-out mice related to Ca^{2+} release after mild exercise but resting Ca^{2+} was significantly increased in both groups after exercise. Average a) Ca^{2+} transient amplitudes, b) 50 % relaxation time, c) baseline fluorescence and d) time to peak at 0.5 Hz. Data presented as mean +/- SEM. *P<0.05 vs. WT, †P<0.05 vs. KO, #P<0.05 vs. WT + exercise, N ≥ 5 mice and ≥ 41 fibers per group.

4.14.4 SR Ca^{2+} content is not significantly altered in young dysferlin-deficient mice

To determine whether the altered Ca^{2+} homeostasis of young dysferlin-deficient skeletal muscle fibers is due to an increased Ca^{2+} content of the SR, caffeine-induced Ca^{2+} release was measured. As in cardiomyocytes, rapid application of caffeine leads to opening of RyR1 receptors and therefore to release of all Ca^{2+} ions stored in the SR. As shown in figure 4.14.4, the SR Ca^{2+} content was not significantly altered in dysferlin-deficient skeletal muscle fibers related to wild-type fibers. Furthermore, relaxation time of the caffeine-induced Ca^{2+} transients did not show significant differences compared to wild-type fibers. The relaxation time of the caffeine-induced Ca^{2+} transient is due to the transport of Ca^{2+} out of the cell. Ca^{2+} that is transported back into the SR, is immediately released again through the opened RyR, therefore the relaxation time is an indicator for PMCA and NCX function in skeletal muscle fibers. Caffeine-experiments revealed no alteration in PMCA and NCX function in young dysferlin-deficient muscle fibers.

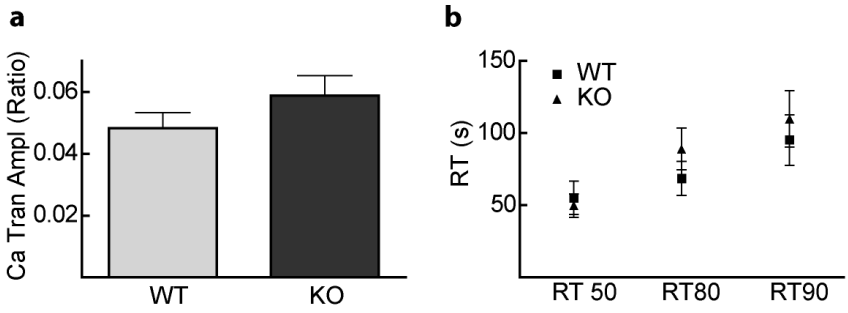

Figure 4.14.4: No alteration of SR Ca^{2+} content and PMCA/NCX function in dysferlin-deficient skeletal muscle fibers. 30 mM caffeine was rapidly applied to isolated skeletal muscle fibers. a) Average caffeine-induced Ca^{2+} transient amplitudes. b) Average relaxation times of the caffeine induced Ca^{2+} transients. Data presented as mean +/- SEM, N = 4 mice and ≥ 17 fibers per group.

4.14.5 Increased Ca^{2+} transients depend on external Ca^{2+}

Young dysferlin-deficient mice reveal increased Ca^{2+} transient amplitudes but do not contain an increased SR Ca^{2+} content. Therefore we addressed the question whether the processes of excitation-coupled Ca^{2+} entry (ECCE) or store-operated Ca^{2+} entry (SOCE) are altered in these mice. To test this, Ca^{2+} depletion was carried out. Ca^{2+} transient amplitudes from wild-type and dysferlin-deficient skeletal muscle fibers were analyzed after changing perfusion of cells from medium containing Ca^{2+} to Ca^{2+}-free medium. The results showed that Ca^{2+} transient amplitudes were significantly increased in dysferlin-deficient fibers from 0 to 4 min after changing to Ca^{2+}-free medium, the time when remaining Ca^{2+} was still present in the external medium. Transients decreased with time and from 6 to 12 min, when Ca^{2+} was no longer present in the external medium no differences between knock-out and dysferlin-deficient fibers could be detected. This indicates that the increased Ca^{2+} transients are dependent on external Ca^{2+}.

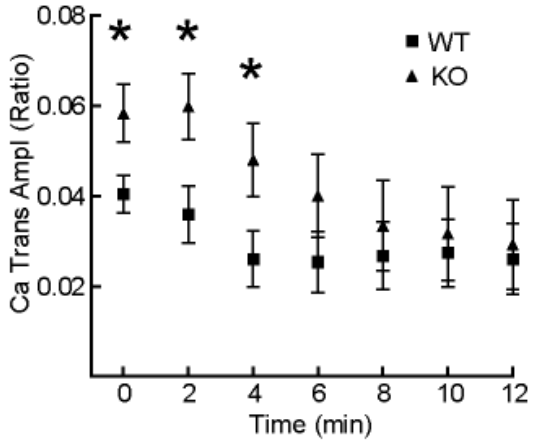

Figure 4.14.5 Increased Ca^{2+} release of dysferlin-deficient fibers depends on external Ca^{2+}. Ca^{2+} transient amplitudes were measured after changing perfusion from Ca^{2+}-containing to Ca^{2+}-free solution. Ca^{2+} transient amplitudes of dysferlin-deficient muscle fibers decrease with decreasing external Ca^{2+} concentration and adapt to wild-type Ca^{2+} transients when Ca^{2+} is depleted from the external medium. Data presented as mean +/- SEM. *P<0.05 vs. WT, N ≥ 3 mice and 12 fibers per group.

4.14.6 Post shock spark measurements reveal a significantly increased Ca^{2+} leak without increased spark frequency in dysferlin-deficient skeletal muscle fibers

It was claimed that alterations of the T-tubule structure can have severe effects on Ca^{2+} homeostasis in skeletal muscle fibers due to increasing spark frequency (Wang et al., 2005). As dysferlin-deficiency leads to T-tubule alterations, we examined Ca^{2+} sparks in dysferlin-deficient skeletal muscle fibers. Ca^{2+} sparks can not be detected in healthy murine skeletal muscle fibers. Therefore, Ca^{2+} sparks were measured after osmotic shock in dysferlin-deficient, wild-type and mdx (as disease control) skeletal muscle fibers. The results indicated that Ca^{2+} spark frequency was significantly increased in mdx fibers which lead to a significantly increased SR Ca^{2+} leak. These results were in line with previously published results (Wang et al., 2005). In contrast, dysferlin-deficient fibers did not show increased Ca^{2+} spark frequency related to wild-type fibers but nevertheless revealed an increased Ca^{2+} leak that was due to increased Ca^{2+} amplitude and increased Ca^{2+} spark duration. These results indicate that despite the altered T-tubule morphology in young dysferlin-defcient mouse muscle no increase in Ca^{2+} spark frequency was observed. Nevertheless, osmotic shock induced a significantly increased Ca^{2+} leak in dysferlin-defcient muscle fibers due to increased amplitude and duration of Ca^{2+} sparks.

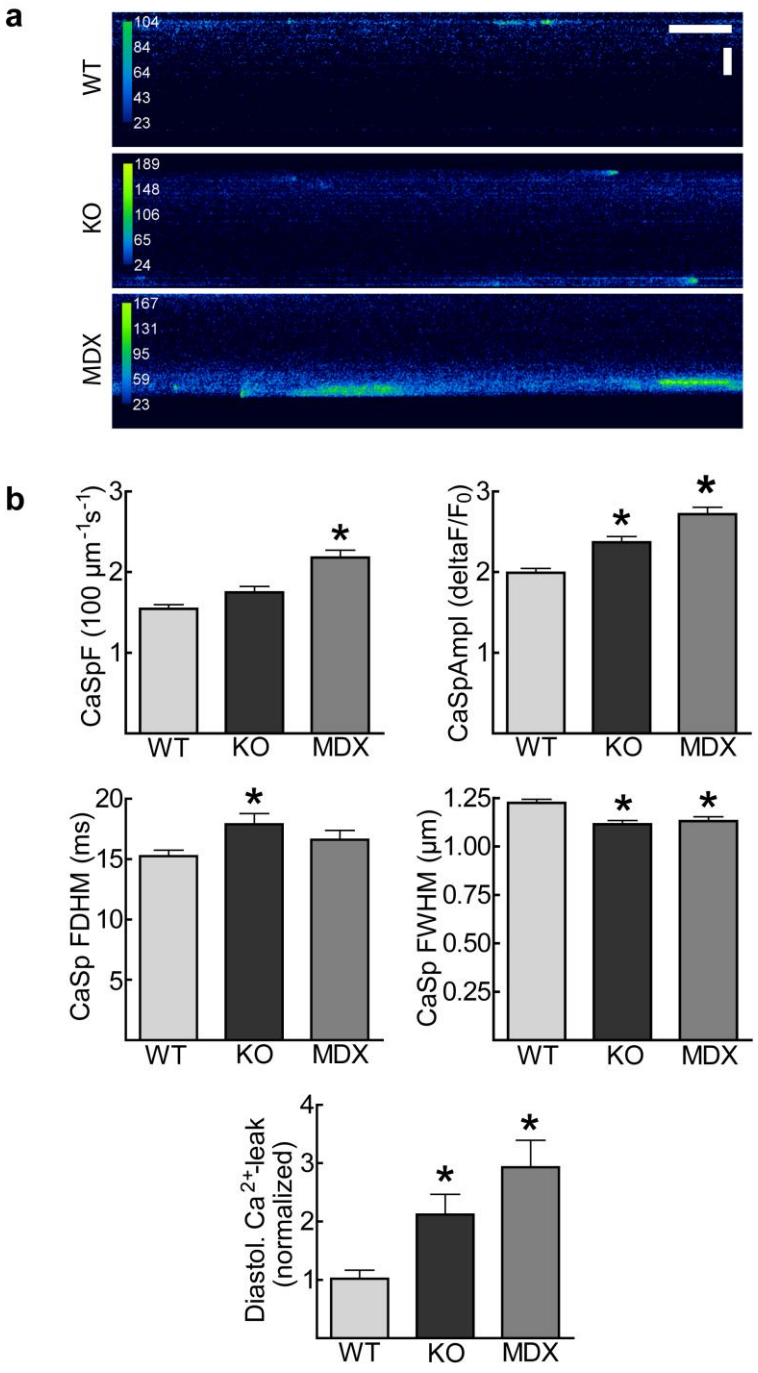

Figure 4.14.6 Ca^{2+} spark frequency is not altered in dysferlin-deficient muscle fibers. Ca^{2+} sparks were measured in wild-type, mdx and dysferlin-deficient muscle fibers after induction of osmotic shock. (a) Representative line scan images (ΔF/F0, 0.96 ms/line) of WT, KO and mdx skeletal muscle fibers (b) Average spark frequency, normalized SR Ca^{2+} leak and spatiotemporal properties of Ca^{2+} sparks, such as amplitude, full duration at half maximum and spatial spread (full width at half maximum). Data presented as mean +/- SEM. *P<0.05 vs. WT, N = 4 mice and ≥ 112 fibers per group, horizontal scale bar: 200 ms, vertical scale bar: 10 µm.

4.15 Analysis of triad proteins in dysferlin-deficient mice

It was demonstrated that dysferlin is located at the T-tubule system and is involved in biogenesis of this membrane system. Furthermore, it is known that the structure of the T-tubule system is significantly altered in dysferlin-deficient skeletal muscle fibers. These abnormalities of the T-tubule structure have influences on the process of EC-coupling. All of these findings made it necessary to analyze the expression of T-tubule- and triad-associated proteins in dysferlin-deficient mouse muscle. Western blot analysis of dysferlin knock-out and wild-type muscle revealed no significantly altered expression levels in young dysferlin-deficient mice (9-11 weeks) as compared to wild-type mice (figure 4.15). In aged dysferlin-deficient mice (50-66 weeks) expression of FKBP12 also known as calstabin 1 and junctophilin 1 was significantly decreased. Junctophilin connects the T-tubule system to the SR membrane and therefore is required for normal triad structure. Calstabin 1 is a protein binding to RyR and maintaining the closed state of the RyR after each contraction to prevent leakage of Ca^{2+} from the SR (Jayaraman et al., 1992, Brillantes et al., 1994). Furthermore, expression of Bin1, a protein involved in T-tubule biogenesis and T-tubule remodeling, was significantly increased in aged dysferlin-deficient mice, indicating an increased turnover of T-tubule membranes in aged dysferlin-deficient mice.

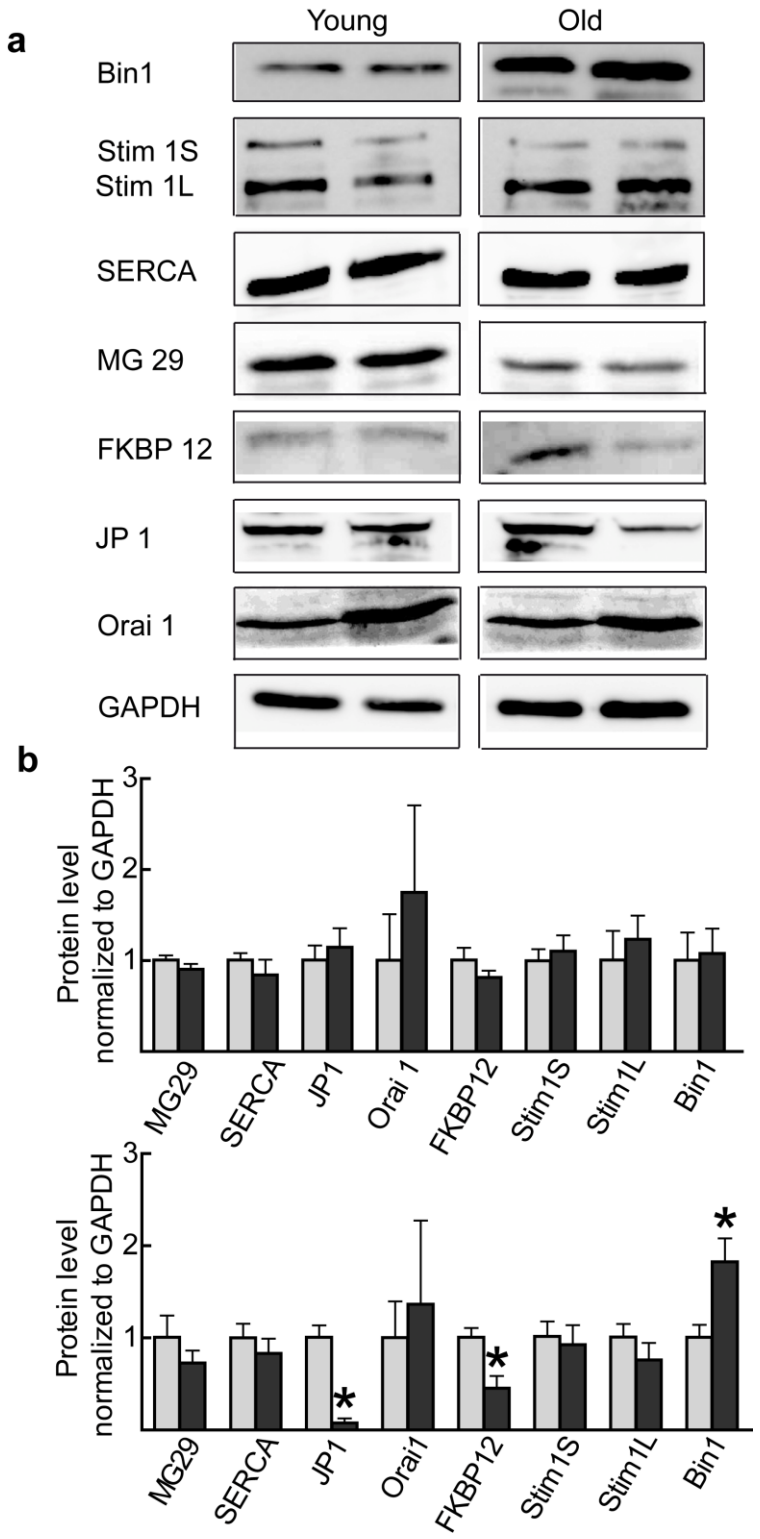

Figure 4.15 No alteration of triad- or T-tubule-associated proteins in dysferlin-deficient muscle. Western blot was carried out using quadriceps femoris muscle homogenates from young (9-11 weeks) and aged (50-66 weeks) wild-type and dysferlin-deficient mice, incubated with antibodies for triad or T-tubule proteins and detected by chemiluminescence. a) Representative original bots b) Average protein level of young (upper panel) and aged (lower panel) mouse muscle normalized to GAPDH. Wild-type protein levels were normalized to 1. Data presented as mean +/- SEM. *P<0.05 vs. WT, N = 3-6 mice per group.

4.16 Significantly increased fatigue resistance of dysferlin-deficient mice.

More than 50 % of patients with dysferlin-deficient muscular dystrophy show above-average motor performance prior to onset of muscle weakness. This is a feature not observed in any other form of muscular dystrophy. Most patients with other types of muscular dystrophy show decreased exercise capacity and the dystrophic muscle is characterized by decreased Ca^{2+} transients which is contrary to the increased Ca^{2+} release observed in dysferlin-deficient muscle fibers. Therefore, we measured exercise capacity of dysferlin-deficient mice at different stages of life. Ca^{2+} measurements of dysferlin-deficient skeletal muscle fibers revealed a significantly altered Ca^{2+} homeostasis with increased Ca^{2+} release. It is already known that dysferlin-deficient skeletal muscle fibers do not have significantly increased muscular strength (Chiu et al., 2009), therefore we had to address the question, whether these mice have increased endurance. At different time points between 4 and 90 weeks of age the running behavior of dysferlin-deficient and wild-type mice was recorded continuously. Over a period of three weeks the mean running velocity per day and the average running distance per day were recorded at each time point. As shown in figure 4.16b the mean weight of young and aged mice was not different. The results shown in figure 4.16.a revealed a significantly increased mean running velocity and running distance per day of young dysferlin-deficient mice related to wild-type mice. In contrast, old dysferlin-deficient mice showed significantly decreased running distances and a decreased mean running velocity most likely as a consequence of the dystrophic process. The running wheel experiment revealed a significantly increased resistance to fatigue of young dysferlin-deficient mice.

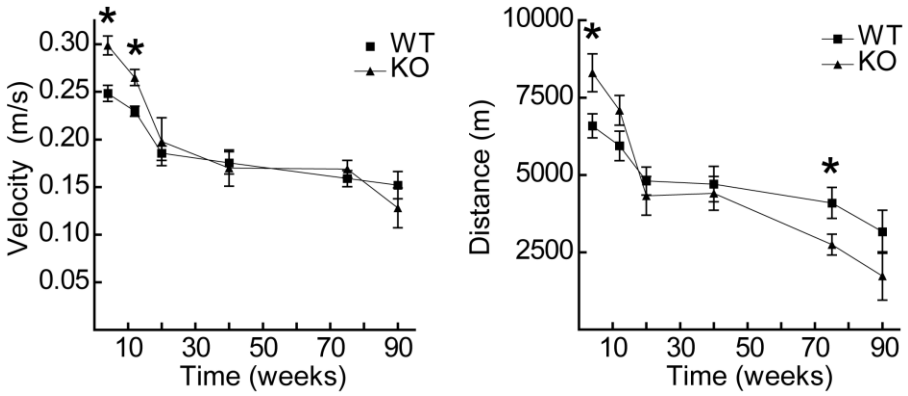

Figure 4.16a: Young dysferlin-deficient mice show a significantly increased resistance to fatigue. At the age of 4, 12, 20, 40, 75 and 90 weeks the running wheel performance of wild-type and dysferlin-deficient mice was tested over a period of three weeks. The mean running velocity per day (left) and the running distance per day (right) were recorded. Data presented as mean +/- SEM, *p>0.05, N ≥ 8 mice per group.

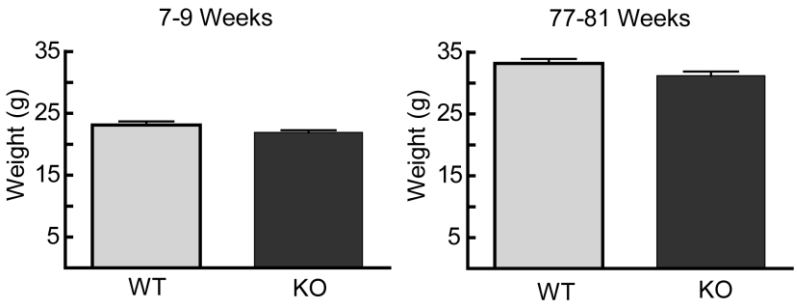

Figure 4.16b: No significant differences in body weight of young and aged dysferlin-deficient mice. Average weight of 7-9 (left) and 77-81(right) weeks old wild-type and dysferlin-deficient mice. Data presented as mean +/- SEM, N ≥ 17 mice per group.

4.17 Increased fatigue resistance of knock-out mice is not due to a shift in fiber types.

Generally, two main fiber types can be distinguished in the muscle, slow twitch type I fibers with low glycolytic high oxidative capacity, slow contraction time but high resistance to fatigue and fast twitch type II fibers which have high glycolytic but low oxidative capacity, fast contraction time but are also fast fatiguing. To examine whether the increased running distance and running velocity of young dysferlin-deficient mice is due to a shift in muscle fiber types, staining of succinate dehydrogenase (SDH) in isolated gastrocnemicus muscles was performed. SDH staining distinguishes between high and low oxidative muscle fibers as SDH is an enzyme located at mitochondria. As shown in figure 4.17, no differences in SDH positive, therefore type I fibers could be observed. Increased fatigue resistance of dysferlin-null mice is therefore not due to a shift in fiber type ratio.

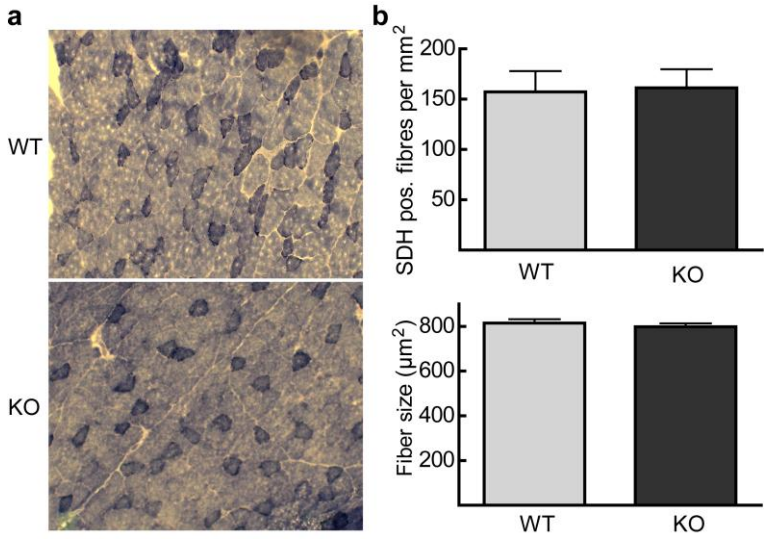

Figure 4.17: No significant difference in muscle fibre type ratio of dysferlin-deficient and wild-type mouse muscles. Gastrocnemius muscles were isolated from 11 week old wild-type and dysferlin-null mice and SDH staining was carried out (succinate dehydrogenase; marker for fast muscle fibre type). a) Representative staining of wild-type and knock-out muscles. Scale bar: 50 µm. b) Average SDH positive type I fibres per mm^2 and average fiber size in mm^2, N = 3 mice per group.

5. Discussion

5.1 Dysferlin induces tubular membrane structures in non-muscle cells

Mutations of dysferlin lead to muscular dystrophy but the pathomechanisms underlying the disease are so far unknown. The cell biological role of dysferlin was claimed to be membrane repair of skeletal muscle fibers as dysferlin-deficient fibers are not able to reseal their plasma membrane after injury. Nevertheless, this can not be the only physiological role of dysferlin, as dysferlin-deficient patients are initially without symptoms and even have a high level of fitness before onset of overt weakness that is not seen in any other form of muscular dystrophy. Membrane repair deficits should have influences on patients right after birth and therefore, this can not explain the pathology underlying the disease sufficiently and further physiological functions of dysferlin had to be analyzed.

In previous experiments, it was detected that dysferlin induces tubular structures after heterologous expression in non-muscle cells. This was the first hint towards a new physiological function of dysferlin and lead to the hypothesis that dysferlin is involved in membrane tubulation and membrane organization. Therefore, these tubular structures needed to be further characterized. The dysferlin protein domain structure resembles that of its paralogues, myoferlin and otoferlin. All of them belong to the ferlin family, are type II membrane proteins and consist of several C2 domains. The structural similarity between the ferlin proteins suggests a similar protein function but expression in Cos 7 cells indicated that only dysferlin was able to induce tubular structures. Myoferlin and otoferlin proteins localized at the ER as demonstrated by PDI costaining. This result indicates that among the ferlins dysferlin possibly is the only protein able to induce tubular structures after heterologous expression. This suggests a physiological role in membrane organization which is specific for dysferlin and probably will not be found for other ferlins. Previous experiments revealed that the tubules induced by dysferlin are membranous structures as they could be depleted by cholesterol extraction. This was further supported by the finding that the tubules do not colocalize with any cellular organelle. In contrast to that, the tubules seem to be in contact with the microtubule system as detected by disruption of the tubules by nocodazole. Phalloidin costaining indicated that the tubules are not in contact with the actin cytoskeleton which was confirmed by inhibition of the actin cytoskeleton by cyto D that did not disrupt the tubular structures but instead led to stabilization of the tubules. Van Deurs et al. demonstrated that treatment of cells with cyto D alone results in tubular invaginations from the plasma membrane. They claim that destruction of the actin cytoskeleton leads to destabilization of the plasma membrane and therefore tubular invaginations

mediated by microtubules (Van Deurs et al., 1996). The dysferlin induced tubules are continuous with the plasma membrane as shown by FM4-64 costaining. Cyto D treatment therefore probably increases tubulation induced by dysferlin by destructing the actin cytoskeleton and promoting the interaction with the microtubule system resulting in sustained invagination of the plasma membrane. The effect of cyto D can probably be further explained by the fact that the tubules are not static but are, like all membrane systems, dynamic structures. Only recently this was shown by our group by live microscopy experiments with dysferlin-transfected cells (Drzymalski, not published). Cyto D not only leads to inhibition of the actin cytoskeleton but further results in a cell cycle arrest which possibly leads to inhibition of tubule movement and thereby stabilization and pronounced appearance of these structures.

Dysferlin is a large protein of about 230 kDa containing several protein domains. To determine which domains are essential for tubulation and to analyze the minimal required number of C2 domains, several truncated dysferlin constructs were cloned, expressed in Cos 7 cells and analyzed for tubule induction. Two constructs containing only the last two C2 domains with or without the transmembrane (TM) domain (see figure 4.3.2) were analyzed. These were not able to induce tubular structures. A minidysferlin found in a patient with a moderate late onset dysferlinopathy that contains the last two C2 domains with the TM domain and an N-terminal part resulting from a frame shift mutation was suggested to be a good candidate for gene transfer studies. In our experiments this minidysferlin did not induce membrane tubulation which indicates that it does not contain all functionally relevant properties of the full-length dysferlin. Minidysferlin 3 containing the last two C2 domains, the TM domain and additionally the C2A domain was demonstrated to efficiently mediate membrane repair like the full-length protein (Azakir et al. 2012). Also this truncated version of dysferlin was not able to induce membrane tubulation after heterologous expression. None of the tested truncated dysferlin constructs did induce membrane tubules. This indicates that all C2 domains are necessary for proper function of dysferlin. Also the TM mutant of dysferlin did not induce membrane tubulation suggesting that also the TM domain is required for proper dysferlin function. In addition to the truncated dysferlin proteins pathogenic mutants were tested for membrane tubulation. Five different mutants were tested, four of them harboring point mutations in one of the C2 domains (C2A, C2C, C2D or C2E) and one containing a point mutation in between two C2 domains (see figure 4.3.2). Again, none of these mutated dysferlin constructs induced membrane tubulation. Interestingly, the mutant containing the mutation in between the C2 domains did show membrane tubulation, although in a lesser proportion of cells compared to the full-length dysferlin which further supports a crucial role of the C2 domains in tubule

formation. It is known that dysferlin localizes to the developing T-tubule system in C2C12 cells, a murine myoblast cell line. All of the constructs mentioned above were additionally expressed in these cells to analyze their subcellular localization. In line with the results obtained from the Cos 7 experiments, none of the truncated dysferlin constructs and pathogenic dysferlin mutants did show a tubular expression pattern like the full-length dysferlin. This suggests no localization of these constructs at the tubular structures previously identified as T-tubule membranes in C2C12 cells (Klinge et al., 2007). Interestingly, only the dysferlin mutant containing the mutation not in the C2 domains did show a partial tubular expression pattern indicating partial T-tubule localization. These results further indicate that the full-length protein is required for protein function and emphasize the crucial role of the dysferlin C2 domains.

Further investigation of the dysferlin-induced tubules revealed that these structures contain high amounts of the phospholipids PIP2 and PIP3 an important component of T-tubular membranes. Furthermore, dysferlin is recruited to PIP2-containing vesicles that are induced by expression of PIP2 kinase. In contrast, truncated dysferlin constructs and pathogenic mutants were not recruited to these structures. When dysferlin was expressed together with the PIP2 phosphatase synaptojanin 1, which dephosphorylates PIP2, dysferlin did not induce membrane tubulation most likely due to PIP2 depletion. These results support that dysferlin-induced tubules are membranous structures containing high amounts of the phospholipids PIP2 and PIP3 and further suggest that dysferlin is able to bind to phospholipids, especially PIP2. As these lipids that are found in T-tubule membranes are present in dysferlin-induced tubules these structures show biochemical similarities with the T-tubule system of skeletal muscle.

The T-tubule system is a highly organized membrane system that invaginates from the plasma membrane into the muscle fiber. Therefore it was further investigated whether dysferlin-induced tubules also invaginate from the plasma membrane. Staining of the tubules with the membrane dye FM4-64 indicated that the tubules are continuous with the plasma membrane as after 1 min of staining, the dye will not be endocytosed and can only reach the tubules by lateral diffusion through the plasma membrane. This indicates that these tubules are continuous with the plasma membrane suggesting dysferlin-mediated plasma membrane invagination, a morphological similarity to skeletal muscle T-tubule system.

5.2 Dysferlin binds to phopholipids and induces membrane curvature in vitro

Coexpression of dysferlin with the PIP2 kinase revealed that dysferlin is recruited to PIP2-containing vesicles. This indicates ability of dysferlin to bind to phospholipids, especially PIP2. The dysferlin C2A domain binds to PIP2 in a Ca^{2+}-dependent manner and all other C2 domains are able to bind negatively charges phospholipids although with weaker binding affinity compared to the C2A domain (Therrien et al., 2009). This, however, was not analyzed for the full-length dysferlin protein. Our PIP-strip experiments indicated binding of the full-length dysferlin protein to PIP2 which was further supported by the results of the flotation assay. This shows that not only the C2A domain, but also the dysferlin full-length protein is able to bind phospholipids, especially PIP2 in presence of Ca^{2+}. Binding of dysferlin to PIP2 was abolished by a pathogenic mutation of the dysferlin C2A domain which highlights the crucial role of this domain in dysferlin function. This specific function was further substantiated by a liposome binding experiment which was carried out with single C2 domains of dysferlin. Only the C2A domain of dysferlin was able to induce aggregation of liposomes in presence of Ca^{2+}. The C2 domains were expressed as GST-tagged proteins. GST is known to cluster with other GST molecules. The liposome aggregation potential of the C2A domain was therefore possibly mediated by clustering of GST and thereby clustering of liposomes that were bound to the C2A domain. As this effect was not observed with the other C2 domains, these domains seem to play only a minor role in lipid binding but nevertheless are crucial for dysferlin function. Minidysferlin 3 was able to bind PIP2 probably due to the presence of a functional C2A domain in this protein.

Dysferlin is localized at the T-tubule system, is involved in its biogenesis and is able to induce T-tubule like structures in non-muscle cells containing phospholipids that are normally present in T-tubule membranes. These findings indicate that dysferlin plays a role in organization of biological membranes which was further supported by the fact that dysferlin is able to bind to phospholipids in vitro. Unpublished experiments demonstrated that dysferlin-induced tubules in Cos 7 cells colocalize with Bin1-induced tubules. As Bin1 is already known to mediate membrane tubulation, this observation further supported the hypothesis that dysferlin is also involved in membrane organization. Liposome tubulation experiments were carried out to investigate the membrane tubulation properties of dysferlin. Indeed, dysferlin was able to induce tubulation of liposomes from Folch fraction lipids in vitro which was further enhanced by addition of PIP2. The C2A mutant of dysferlin and minidysferlin 3 were not able to induce membrane tubulation which indicates that full-length dysferlin is required for correct function in vitro. Minidysferlin 3 seems to be able to bind to PIP2 but is not able to induce membrane tubulation. The C2A mutant additionally was not able to tubulate

membranes like the full-length protein which again highlights the crucial role of the C2A domain in proper dysferlin function. These results are consistent with the findings from the Cos 7 experiments where it was shown that the full-length dysferlin protein is needed for its correct function.

As dysferlin is involved in T-tubule biogenesis the membrane tubulating function of dysferlin that we observed in in vitro experiments leads to the suggestion that dysferlin plays a role in formation of the T-tubule system during its development. This would also explain the abnormal conformation of the T-tubule system that was detected in dysferlin-deficient murine muscle. This hypothesis is also consistent with results from studies using an in vivo model of muscle regeneration. Mouse muscle was treated with notexin to break down the muscle fiber and to induce regeneration. In normal muscle the T-tubule system regenerates normally after notexin treatment but in dysferlin-deficient mouse muscle the T-tubule system did not regenerate properly but revealed an abnormal configured structure (Klinge, not published). These findings provide evidence that the membrane tubulation capacity obtained in vitro is also relevant in vivo.

The abnormal T-tubule system due to dysferlin-deficiency further explains the defective membrane repair mechanism and defective regeneration process detected in dysferlin-deficient mouse muscle. The T-tubule system provides a membrane reservoir for the plasma membrane in muscle fiber regeneration and is involved in transport of membranes (Engel and Franzini-Armstrong, 2004). Furthermore, it was shown that dysferlin translocates from the T-tubule system towards the membrane lesions (Klinge et al., 2007). This indicates that the T-tubule system also provides proteins and possibly membranes needed for the muscle membrane repair mechanism. This suggests that abnormal T-tubule development due to absence of dysferlin leads to deficits in muscle fiber regeneration and repair.

McMahon et al. suggested that C2 domains mediate membrane curvature by inserting their amphiphatic helices into one monolayer of a biological membrane to the level of the glycerol backbones of the lipids (McMahon et al., 2010). This is enough to induce local curvature of both lipid bilayers. Further they hypothesize that large scale deformation of membranes, like tubulation of liposomes can only be mediated by high density of C2 domains as the curvature effects of these domains are additive. This can be achieved by several single C2 domains but would be much more effective when the C2 domains are coupled in a dimer. This suggests that all of the seven C2 domains present in the dysferlin protein mediate local curvature of the T-tubule membrane, but the additive effect of the multi C2 domains is needed for induction of membrane tubulation, which is consistent with our observations in the tubulation experiments.

The Cos 7 experiments indicate that the TM mutant of dysferlin was not able to induce tubular structures and we hypothesize that this observation is due to incorrect localization of the protein. Therefore, we suggest that the TM domain of the dysferlin protein is needed for proper membrane localization of dysferlin but is probably not involved in membrane deformation. This is further highlighted by the fact that the dysferlin protein structure is reminiscent of the structure of a tail-anchored protein. Tail-anchored proteins consist of a single TM domain which is close to the C-terminus and anchors the protein in the membrane the entire N-terminal portion of the protein facing the cytosol. The TM domain of tail-anchored proteins is crucial for proper localization of the whole protein as it contains a signal sequence for its posttranslational membrane insertion. So far it was not determined whether dysferlin belongs to the group of tail-anchored proteins but its protein structure is suggesting this.

5.3 Dysferlin-deficiency influences Ca^{2+} homeostasis

Dysferlin-deficient murine muscle is characterized by an abnormal morphology of the T-tubule system. The T-tubule system is necessary for propagation of the action potential into the interior of the muscle fiber thereby initiating the mechanism of excitation-contraction coupling (EC-coupling) and allowing highly synchronized contraction of the whole muscle fiber at the same time. Therefore we investigated probable functional influences of the altered T-tubule morphology on EC-coupling by Ca^{2+} measurements. Interestingly, Ca^{2+} release was significantly increased in young dysferlin-deficient muscle fibers related to wild-type fibers. The relaxation time as a measure for SR Ca^{2+}-ATPase (SERCA) activity and the time to peak as a measure of the contractility of the cell were not altered and the resting Ca^{2+} concentration was also not different in knock-out compared to wild-type fibers. These results indicate that Ca^{2+} homeostasis is significantly altered in dysferlin-deficient skeletal muscle leading to increased Ca^{2+} release. As mentioned above, muscular dystrophy can have severe influences on Ca^{2+} homeostasis and leads to reduction of Ca^{2+} release for example in mdx mouse muscle. Therefore, Ca^{2+} measurements were additionally carried out in mdx muscle fibers and results were compared to wild-type and dysferlin knock-out fibers. As published previously, Ca^{2+} release was significantly decreased in mdx muscle fibers and SERCA function was significantly decreased related to wild-type fibers. Resting Ca^{2+} concentration was not altered in mdx fibers. Contrary to that, many studies on Ca^{2+} homeostasis in mdx muscle demonstrate that the resting Ca^{2+} concentration is significantly increased in these muscles but still other studies exist, that do not find an altered resting Ca^{2+} concentration (Pressmar et al., 1994). Nevertheless, the results indicate an altered Ca^{2+} homeostasis in mdx mice that is

consistent with previous published results. These results are completely contrary to the alterations found in dysferlin-deficient skeletal muscle. Therefore, alteration in Ca^{2+} homeostasis with increased Ca^{2+} release in young dysferlin-deficient skeletal muscle is due to the absence of the dysferlin protein and not due to the process of muscular dystrophy.

The increased Ca^{2+} release would suggest an increased SR Ca^{2+} content, as this is the main contributor to Ca^{2+} release in skeletal muscle fibers. Caffeine experiments demonstrated that the SR Ca^{2+} content was not significantly altered in dysferlin knock-out muscle fibers. This finding is in line with the normal SERCA function but does not explain the increased Ca^{2+} release. Two further Ca^{2+} entry mechanisms are known so far in skeletal muscle. Store-operated Ca^{2+} entry (SOCE) is a mechanism that comes into action when the Ca^{2+} content of the SR decreases and is necessary to counteract appearance of fatigue. Excitation-coupled Ca^{2+} entry (ECCE) is a mechanism of Ca^{2+} entry independent of SR Ca^{2+} content but dependent on stimulation of the muscle fiber and interaction of DHPR and RyR. The Ca^{2+} depletion experiment indicates, that Ca^{2+} transient amplitudes of knock-out muscle fibers decrease with time when the Ca^{2+} concentration in the surrounding medium decreases but are still significantly increased compared to wild-type fibers. Only when Ca^{2+} is completely absent from the surrounding medium no difference in Ca^{2+} transient amplitudes can be observed any more. This indicates that the increased Ca^{2+} release is dependent on external Ca^{2+}, probably through the mechanism of ECCE. The transients of the knock-out fibers decrease during the first minutes after changing to Ca^{2+}-free perfusion when the Ca^{2+} content in the external medium decreases and SOCE does not play a role yet as the SR still contains normal levels of Ca^{2+}. These experiments point out that increased Ca^{2+} release in dysferlin-deficient skeletal muscle fibers is due to increased Ca^{2+} entry into the muscle fiber, probably by the mechanism of ECCE, but not SOCE. Only recently it was confirmed in our lab that SOCE is not increased in dysferlin-deficient skeletal muscle fibers. Re-addition of Ca^{2+} into the external medium after store depletion did not lead to increased Ca^{2+} entry in dysferlin-null muscle fibers related to wild-type fibers (Büssenschütt, not published). So far it is known that the mechanism of ECCE involves coupling of DHPR and RyR and Bannister et al., claimed that Ca^{2+} enters the muscle fiber through the DHPR itself. In further experiments Ca^{2+} entry through the DHPR has to be analyzed to prove our hypothesis that increased ECCE accounts for the increased Ca^{2+} release.

Wang et. al. suggested that subtle membrane alterations induce Ca^{2+} sparks due to uncoupling of DHPR and RyR. The DHPR is not only needed to activate Ca^{2+} release from the RyR, but also mediates inactivation of the same channel. Altered coupling of

the SR and T-tubule membranes due to osmotic stress or fatigue exercise prevents the inhibitory function of DHPR on the RyR channel so that Ca^{2+} sparks occur. Membrane fragility for example due to dystrophin-deficiency further increases osmotic shock or exercise-induced frequency of Ca^{2+} sparks as the membrane is more susceptible to stress. Our experiments reveal no increased Ca^{2+} spark frequency in dysferlin-deficient muscle fibers after induction of osmotic shock. In contrast to that, Ca^{2+} spark frequency was significantly increased in mdx fibers which is consistent with previously published results. This again indicates a different pathophysiology underlying dysferlin-deficiency as compared to dystrophin-deficiency. Further this suggests that coupling of DHPR and RyR is not altered in young dysferlin-deficient mice. This was additionally supported by the observation that fatigue exercise did not significantly change Ca^{2+} release in dysferlin-null muscle fibers. It was demonstrated that eccentric exercise induces morphological changes of the T-tubule system (Takekura et al., 2001b, Wang et. al., 2005) which leads to increased Ca^{2+} leak from the SR and therefore changes in EC-coupling (Wang et al., 2005, Bellinger et al., 2008). Our data indicate an increased resting Ca^{2+} level in both wild-type and knock-out mice after stress exercise. This is probably due to an increased Ca^{2+} leak from the SR induced by morphological changes of the T-tubule membrane, however, no significant influences on Ca^{2+} release could be observed in dysferlin knock-out or wild-type mouse muscle fibers. In mdx mice it was demonstrated that exercise stress leads to uncoupling of DHPR and RyR which results in induction of muscular dystrophy (Wang et al., 2005). As Ca^{2+} release is not significantly influenced in dysferlin knock-out muscle fibers by stress exercise, this suggests again that coupling of DHPR and RyR is not altered.

In conclusion, Ca^{2+} imaging in young dysferlin-deficient mouse muscle fibers revealed a significantly altered Ca^{2+} homeostasis with increased Ca^{2+} release. Despite the fact that the T-tubule system is abnormally configured in dysferlin-deficincy this has probably no influence on coupling of DHPR and RyR. This suggests that the altered Ca^{2+} homeostasis in young dysferlin-deficient mice does not lead to induction of muscle degeneration but on the contrary may explain increased exercise capacity patients before onset of symptoms.

Ca^{2+} measurements in dysferlin-deficient skeletal muscle fibers from aged mice revealed increased Ca^{2+} transient amplitudes like in the young mice, but the difference was not statistically significant at single frequencies. Furthermore, decreased SERCA activity and decreased contractility were observed in the muscle fibers from old dysferlin knock-out mice. This indicates that dysferlin-deficiency also leads to an altered Ca^{2+} homeostasis in muscle fibers of aged mice with differences related to fibers from young dysferlin knock-out mice. These differences possibly are due to

secondary alterations and not primary effects underlying the dysferlin deficiency. One possible explanation is that ECCE is still increased in aged dysferlin-deficient mice but SR Ca^{2+} content is decreased due to the decreased SERCA-function.

5.3.1 Alteration in Ca^{2+} homeostasis is specifically due to dysferlin-deficiency

Dysferlin-deficiency leads to an abnormal morphology of the T-tubule system and to an alteration in Ca^{2+} homeostasis which shows different characteristics in young compared to aged mice. These alterations could be a direct effect mediated by the absence of the dysferlin protein itself or could be indirect effects due to secondary alterations of triad or T-tubule-associated proteins. Western blots of mouse muscle homogenates from dysferlin-deficient mice did not reveal alterations in expression of any T-tubule or triad-associated protein that was tested. This suggests that alterations in T-tubule system and Ca^{2+} homeostasis are direct effects due to the deficiency of the dysferlin protein. In contrast to that, muscle homogenates from aged mice indicated significant lower amounts of calstabin 1 and junctophilin 1 protein expression in knock-out related to wild-type mice. Junctophilin stabilizes the connection of the T-tubule system with the SR membrane. The protein is therefore necessary for maintenance of the triad structure and absence of this protein leads to a disrupted triad and T-tubule structure. In dysferlin-deficient skeletal muscle where the T-tubule system is already altered this probably leads to secondary alterations of T-tubule or triad proteins. The altered T-tubule structure may lead to loss of proper localization of junctophilin 1 and therefore depletion of the protein. This observation may explain differences in Ca^{2+} release that had been detected in muscle fibers from aged dysferlin-deficient mice compared to young mice. The decreased contractility observed in these muscle fibers could be due to an additional defect mediated by the absence of the junctophilin 1 protein. Calstabin 1 was also found to be less expressed in aged dysferlin-deficient muscle. The protein stabilizes RyR1 in its closed state therefore, absence of calstabin 1 leads to increased open probability of the receptor which might result in a Ca^{2+} leak from the SR due to increased frequency of Ca^{2+} sparks. In addition to the decreased SERCA function this would result in decreased SR Ca^{2+} content which has to be analyzed in further experiments. Interestingly, SERCA protein was not observed to be less expressed in aged dysferlin-deficient muscle indicating that the decreased SERCA function has to be explained by decreased activity and not decreased expression.

Bin1 protein was observed to be expressed at higher levels in muscle from aged knock-out compared to wild-type mice. The protein is known to play a role in regeneration of the T-tubule system. Loss of Bin1 as well as dysferlin lead to an abnormal T-tubule structure, but the T-tubule system in both cases is still present. This

indicates that both proteins are not alone involved in development and maintenance of T-tubule structure and probably take over each other's function in absence of one of the proteins. Therefore Bin1 expression is increased in aged dysferlin-deficient mouse muscle witch further indicates an increased membrane turnover. This highlights further that in aged dysferlin-deficient muscle alteration of the T-tubule structure seems to be present at higher degrees as compared to young muscle, where Bin1 expression is not increased.

In conclusion, the abnormal T-tubule system in dysferlin-deficient mice is a consequence of the loss of the dysferlin protein. In aged muscle this defect is further impaired by secondary alterations probably as a consequence of the dystrophic process. In aged dysferlin-deficient muscle, secondary alterations of junctophilin 1 and calstabin 1 expression may account for differences in Ca^{2+} release compared to young dysferlin-deficient mouse muscle.

5.4 Dysferlin-deficiency leads to increased resistance to fatigue

Increased Ca^{2+} release was observed in dysferlin-deficient skeletal muscle fibers from young mice. The question remains now, whether this alteration in Ca^{2+} homeostasis influences muscle physiology and exercise properties of dysferlin-deficient mice. It was already demonstrated that dysferlin-deficient mice do not reveal increased muscle strength (Chiu et al., 2009). A running wheel experiment to test longitudinally the motor performance of wild-type and dysferlin knock-out mice was carried out and dysferlin-deficient mice indeed run significantly longer distances per day and showed significantly higher running velocity compared to wild-type mice of the same age. Two main muscle fiber types exist in skeletal muscle. Type I fibers are specialized in long duration contractile activities and type II fibers are specialized in short duration anaerobic activities and are fast fatiguing. Interestingly, type I fibers are found to a higher extent in endurance athletes and type II fibers in power athletes and it was proposed that endurance training may lead to a shift in fiber types which increases motor performance. The increased running behavior of the young dysferlin-deficient mice could therefore be due to an increased level of type I fibers. However, this was not the fact as the ratio of type I to type II fibers was not different in young dysferlin knock-out mice compared to wild-type mice. Furthermore, no difference in weight of wild-type and knock-out mice was observed that could have influenced motor performance. The results from the running wheel experiment indicate therefore that young dysferlin-deficient mice have a significantly increased resistance to fatigue which is probably due to the altered Ca^{2+} homeostasis and the increased ECCE mechanism observed in muscle fibers of these mice. Motor performance of dysferlin-deficient mice

declines with age so that with the age of 20 weeks no differences between dysferlin-deficient and wild-type mice were observed any more. This is probably due to secondary alterations due to onset of muscular dystrophy. Due to ongoing and increasing muscular dystrophy, dysferlin-deficient mice at the age of 70 weeks show significantly decreased motor performance related to wild-type mice. Interestingly, this time course of running behavior can be compared to motor performance of dysferlinopathy patients which have a high level of fitness in childhood, before onset of muscular dystrophy symptoms and only reveal decline of motor performance in the 2nd decade of life, after onset of symptoms. These results highly indicate that absence of dysferlin leads to changes in Ca^{2+} homeostasis which increases motor performance in mice and human and only in older age secondary mechanisms lead to damage of muscle fibers and therefore to muscular dystrophy.

5.5 Dysferlin localizes to the T-tubule system in cardiomyocytes

Besides its expression in skeletal muscle, dysferlin is expressed even in higher amounts in heart muscle but the role of dysferlin in the heart was not studied intensively so far. By colocaization of dysferlin with DHPR we demonstrated for the first time that also in heart muscle dysferlin is localized at the T-tubule system. Dysferlin is involved in T-tubule biogenesis in skeletal muscle by mediating tubulation of the T-tubule membrane system. This suggests that dysferlin-deficiency possibly influences the T-tubule structure in cardiomyocytes like it was observed in skeletal muscle. The presence of cardiomyopathies in some patients and in animal models further highlights that dysferlin plays an important role in heart muscle. Staining of the T-tubule system with the membrane dye and T-tubule marker di8ANEPPS indicated that the T-tubule system in dysferlin-deficient heart muscle is irregularly configured and more longitudinally oriented compared to wild-type mice which proved that dysferlin is necessary for proper T-tubule structures in heart as well as in skeletal muscle. Interestingly, the observed phenotype resembles the phenotype of cardiomyocytes after induction of myocardial infarction (MI) which shows dilated and longitudinal oriented T-tubules that are undergoing a process of T-tubule regeneration (Wagner et al., 2012). Furthermore, Bin1, a protein that is like dysferlin involved in membrane tubulation and T-tubule development in skeletal muscle was recently implicated in the process of T-tubule remodeling in the heart (Lyon et al., 2012). Therefore, we analyzed dysferlin expression in heart muscle from rats after induction of MI and compared it to sham-treated rat muscle. Dysferlin expression was significantly upregulated in heart muscle after MI which indicated a possible role of dysferlin in the process of T-tubule remodeling after MI. This further suggests that dysferlin is not only involved in T-tubule

development and maintenance of proper T-tubule structure in skeletal but also in heart muscle and that dysferlin-deficiency not only leads to defects in skeletal but also in heart muscle. Therefore dysferlin-deficiency may have additional influences on cardiac health.

5.6 Dysferlin-deficiency influences Ca^{2+} homeostasis in cardiomyocytes

Analysis of dysferlin in heart muscle revealed that the protein is located at the T-tubule system and is involved in maintenance and probably development of normal T-tubular structures in cardiomyocytes. Like in skeletal muscle this may have influences on the process of EC-coupling and therefore Ca^{2+} homeostasis of the heart. Ca^{2+} imaging in cardiomyocytes indicated that dysferlin-deficiency leads to significantly decreased SR Ca^{2+} stores. Under normal physiological conditions this deficit can be adjusted by other mechanisms so that no differences in Ca^{2+} release can be observed between wild-type and knock-out cardiomyocytes. SERCA function and contractility of the cells are also not influenced by dysferlin-deficiency under normal conditions. The decreased SR Ca^{2+} content is probably balanced by Ca^{2+} entry through the DHPR in dysferlin-deficient cardiomyocytes. This would result in additionally increased Na^{+}/Ca^{2+}-exchanger (NCX) function as the increased amount of Ca^{2+} entering the cell has to be exported again out of the cell by the NCX. NCX function can be measured by the decline of the caffeine-induced Ca^{2+} transient which is indeed faster by trend in dysferlin-deficient cardiomyocytes. These results are in line with biometric data of the mice which showed no signs of hypertrophy as they had a normal heart/body weight ratio. When stress was induced in dysferlin-null cardiomyocytes, here done by isoprenaline treatment, Ca^{2+} release was observed to be significantly decreased compared to wild-type cells. This indicates that in stress situations the decreased Ca^{2+} content of the SR can no longer be balanced and deficits of the dysferlin-deficient cardiomyocytes are unmasked. Therefore, dysferlin-deficiency probably has no effect on cardiomyocytes under normal physiologic conditions but may have severe influences on the heart in stress situations. Ca^{2+} release in dysferlin-deficient cardiomyocytes was significantly decreased after an unstimulated period of 30 s during isoprenaline treatment. This indicates that the cells loose Ca^{2+} from the SR during diastole, which would explain the decreased Ca^{2+} content in these cells. This was further analyzed by spark measurements that demonstrated a significantly increased Ca^{2+} spark frequency and therefore a significantly increased SR Ca^{2+} leak in dysferlin-deficient cardiomyocytes which was further increased by isoprenaline-induced stress. The appearance of Ca^{2+} sparks during diastole of the heart is to a certain level normal but if the spark frequency increases, this may have severe influences on heart physiology as an increased Ca^{2+}

leak may trigger arrhythmia and therefore heart failure. Increased Ca^{2+} leak from the SR during diastole leads to increased Ca^{2+} export by the NCX and therefore import of Na^{+} into the cell which may result in membrane depolarization and arrhythmogenic events during diastole. The presence of an increased SR Ca^{2+} leak in dysferlin-deficient cardiomyocytes was further supported by the observation of a significantly increased number of proarrhythmogenic events during detection of Ca^{2+} transients. These nonstimulated events occurred during steady-state stimulation as well as in situations when stimulation was paused and their number was significantly increased when cells were treated with isoprenaline. These results clearly point out that dysferlin-deficiency has severe effects on cardiomyocyte function which can be compensated under normal physiological situations but may lead to heart failure in stress situations.

In heart failure, T-tubule remodeling is observed which leads to unorganized T-tubule structures and repositioning of the DHPRs away from the Z-line resulting in some orphaned RyRs (Song et. al., 2006). It was claimed that these orphaned RyRs are physically separated from the DHPRs and therefore do not respond to normal physiological stimulation. However, these receptors can be activated later with variable latencies through nearby Ca^{2+} elevations. These are due to RyRs that are normally triggered to release Ca^{2+}. This delayed reaction results in Ca^{2+} sparks that occur during diastole of the heart. The abnormal T-tubule structure in dysferlin-deficient cardiomyocytes may lead to some orphaned RyRs that increase Ca^{2+} spark frequency under normal physiological conditions. Under basal conditions this increase is probably not high enough to trigger severe arrhythmias and the resulting decreased Ca^{2+} content is probably balanced by increased Ca^{2+} entry through the DHPR so that the dysferlin-deficiency does not have severe influences on the heart under normal physiological conditions. These observations are reminiscent of a disease called catecholaminergic polymorphic ventricular tachycardia (CPVT), an arrhythmogenic disorder of the heart. No structural heart disease or electrocardiogram abnormalities are present in these patients but emotional or physical stress may lead to severe arrhythmias and sudden cardiac death (Wehrens et al., 2003). CPVT patients reveal mutations of the RyR2 that are leading to decreased binding affinity of calstabin 2 to the receptor despite the fact that under basal conditions calstabin 2 is able to bind to RyR2 normally. Physical or emotional stress leads to activation of the sympathetic nervous system and release of catecholamines and hence activation of ß-adrenal receptors. This induces RyR2 phsophorylation by protein kinase A and thereby dissociation of calstabin 2 from RyR2 leading to increased open probability of the receptor (Marx et al., 2002). This is part of the normal fight or flight response but in these patients decreased binding affinity of calstabin 2 to RyR2 leads to a severe RyR2 leak in stress situations which results in

arrhythmias and sudden cardiac death. As compared to the CPVT patients dysferlin-deficiency leads to an increased Ca^{2+} leak that is also present in basal conditions, but which can be balanced under normal conditions. In stress situations the effect of catecholamines possibly is added to the basal Ca^{2+} leak and Ca^{2+} sparks are further increased due to calstabin dissociation form the RyR. This results in fatal membrane depolarization during diastole and therefore occurrence of arrhythmias.

In conclusion, the disorganized T-tubule structure in cardiomyocytes due to dysferlin-deficiency probably leads to basal alterations in Ca^{2+} homeostasis which can be compensated under normal physiological conditions but in combination with emotional or physical stress this has severe influences on heart physiology. In stress situations, dysferlin-deficiency in heart may induce fatal arrhythmias which may also result in sudden cardiac death. This observation is of high clinical relevance to patients affected by dysferlin-deficiency. Therefore, alteration of Ca^{2+} homeostasis in dysferlin-deficient muscular dystrophy should be further investigated as a possible translational therapeutic approach.

6. Conclusion

Dysferlin is localized to the T-tubule system of the skeletal muscle and is involved in the biogenesis of this membrane system. The dysferlin protein structure and its homology to Fer1 suggested a function of the protein in membrane binding. Preliminary results revealed a membrane tubulating function of dysferlin after heterologous expression in non-muscle cells. We were now able to reveal that these structures are membranes containing biochemical and morphological properties of the T-tubule system in skeletal muscle with high amounts of PIP2 and continuity with the plasma membrane. Further we were able to show for the first time that the full-length dysferlin is able to bind to PIP2 and to mediate membrane tubulation in vitro. These observations suggest that dysferlin is involved in tubulation of the T-tubule system during its development, which explains the unorganized T-tubule system in dysferlin-deficient muscle. This tubulating function of dysferlin is specific for the protein among the ferlins and for the full-length protein. The minidysferlins tested in this study were not able to functionally replace the full-length protein. The abnormal T-tubule development due to dysferlin-deficiency explains the defective membrane repair mechanism and the defective regeneration process detected in dysferlin-deficient mouse muscle. The abnormal T-tubule system further leads to an altered Ca^{2+} homeostasis in young dysferlin-deficient mice which results in increased resistance to fatigue. This alteration was found to be a direct effect of dysferlin-deficiency and was not due to secondary alterations of triad or T-tubule proteins. This additionally explains the increased exercise capacity in dysferlinopathy patients which can be observed before onset of symptoms. When dysferlin-deficient mice age, secondary alterations due to the onset and increase of muscular dystrophy lead to further structural alterations of the T-tubule system and therefore deficiencies in Ca^{2+} homeostasis that are not observed in young mice.

Further we analyzed the role of dysferlin in the heart. As in skeletal muscle dysferlin was detected at the T-tubule system in heart muscle and dysferlin-deficiency resulted in abnormal configuration of the T-tubule system in cardiomyocytes. We were able to detect an increase of the dysferlin protein after MI indicating a role of the protein in T-tubule remodeling. Further the aberrant T-tubule system in dysferlin-deficiency leads to a defective Ca^{2+} homeostasis which can be compensated under normal physiological conditions but which may lead to severe arrhythmias in stress situations. This indicates that dysferlin-deficiency does not only lead to alterations in skeletal muscle of patients but additionally may have severe influences on heart physiology which is of high clinical relevance for patients affected by dysferlin deficiency.

7. Bibliography

Achanzar WE, Ward S. (1997). A nematode gene required for sperm vesicle fusion. J Cell Sci. *110*, 1073-1081.

Al-Qusairi L, Laporte J. (2011). T-tubule biogenesis and triad formation in skeletal muscle and implication in human diseases. Skelet Muscle *1*, 26.

Al-Qusairi L, Weiss N, Toussaint A, Berbey C, Messaddeq N, Kretz C, Sanoudou D, Beggs AH, Allard B, Mandel JL, Laporte J, Jacquemond V, Buj-Bello A. (2009). T-tubule disorganization and defective excitation-contraction coupling in muscle fibers lacking myotubularin lipid phosphatase. Proc Natl Acad Sci *106*, 18763-18768.

Ampong BN, Imamura M, Matsumiya T, Yoshida M, Takeda S. (2005). Intracellular localization of dysferlin and its association with the dihydropyridine receptor. Acta Myol *24*, 134-144.

Anderson LV, Davison K, Moss JA, Young C, Cullen MJ, Walsh J, Johnson MA, Bashir R, Britton S, Keers S, Argov Z, Mahjneh I, Fougerousse F, Beckmann JS, Bushby KM. (1999). Dysferlin is a plasma membrane protein and is expressed early in human development. Hum Mol Genet *8*, 855-861.

Anderson LV, Harrison RM, Pogue R, Vafiadaki E, Pollitt C, Davison K, Moss JA, Keers S, Pyle A, Shaw PJ, Mahjneh I, Argov Z, Greenberg CR, Wrogemann K, Bertorini T, Goebel HH, Beckmann JS, Bashir R, Bushby KM. (2000). Secondary reduction in calpain 3 expression in patients with limb girdle muscular dystrophy type 2B and Miyoshi myopathy (primary dysferlinopathies). Neuromuscul Disord *10*, 553-559.

Andersson DC, Meli AC, Reiken S, Betzenhauser MJ, Umanskaya A, Shiomi T, D'Armiento J, Marks AR. (2012). Leaky ryanodine receptors in β-sarcoglycan deficient mice: a potential common defect in muscular dystrophy. Skelet Muscle *2*, 9.

Aoki M, Liu J, Richard I, Bashir R, Britton S, Keers SM, Oeltjen J, Brown HE, Marchand S, Bourg N, Beley C, McKenna-Yasek D, Arahata K, Bohlega S, Cupler E, Illa I, Majneh I, Barohn RJ, Urtizberea JA, Fardeau M, Amato A, Angelini C, Bushby K, Beckmann JS, Brown RH Jr. (2001). Genomic organization of the dysferlin gene and novel mutations in Miyoshi myopathy. Neurology *57*, 271-278.

Azakir BA, Di Fulvio S, Salomon S, Brockhoff M, Therrien C, Sinnreich M. (2012). Modular dispensability of dysferlin C2 domains reveals rational design for mini-dysferlin molecules. J Biol Chem *10*, 287, 27629-27636.

Backs J, Backs T, Neef S, Kreusser MM, Lehmann LH, Patrick DM, Grueter CE, Qi X, Richardson JA, Hill JA, Katus HA, Bassel-Duby R, Maier LS, Olson EN. (2009). The delta isoform of CaM kinase II is required for pathological cardiac hypertrophy and remodeling after pressure overload. Proc Natl Acad Sci USA *106*, 2342-2347.

Bannister RA, Pessah IN, Beam KG. (2009). The skeletal L-type Ca^{2+} current is a major contributor to excitation-coupled Ca^{2+} entry. J Gen Physiol *133*, 79-91.

Bansal D, Miyake K, Vogel SS, Groh S, Chen CC, Williamson R, McNeil PL, Campbell KP. (2003). Defective membrane repair in dysferlin-deficient muscular dystrophy. Nature *423*, 168-172.

Bashir R, Britton S, Strachan T, Keers S, Vafiadaki E, Lako M, Richard I, Marchand S, Bourg N, Argov Z. (1998). A gene related to caenorhabditis elegans spermatogenesis factor fer-1 is mutated in limb-girdle muscular dystrophy type 2B. Nat Genet *20*, 37-42.

Bellinger AM, Reiken S, Dura M, Murphy PW, Deng SX, Landry DW, Nieman D, Lehnart SE, Samaru M, LaCampagne A, Marks AR. (2008). Remodeling of ryanodine receptor complex causes "leaky" channels: a molecular mechanism for decreased exercise capacity. Proc Natl Acad Sci USA *105*, 2198-2202.

Bers DM. (2001). Excitation-contraction coupling and cardiac contractil force. 2nd edition. Kluwer Academic Publishers.

Bers DM. (2002) Cardiac excitation-contraction coupling. Nature *415*, 198-205.

Bers DM, Guo T. (2005). Calcium signaling in cardiac ventricular myocytes. Ann N Y Acad Sci *1047*, 86-98.

Bittner RE, Anderson LV, Burkhardt E, Bashir R, Vafiadaki E, Ivanova S, Raffelsberger T, Maerk I, Höger H, Jung M, Karbasiyan M, Storch M, Lassmann H, Moss JA, Davison K, Harrison R, Bushby KM, Reis A. (1999). Dysferlin deletion in SJL mice (SJL-Dysf) defines a natural model for limb girdle muscular dystrophy 2B. Nat Genet *23*, 141-142.

Borgonovo B, Cocucci E, Racchetti G, Podini P, Bachi B, Meldolesi J. (2002). Regulated exocytosis: a novel, widely expressed system. Nat Cell Biol *4*, 955-962.

Brillantes AB, Ondrias K, Scott A, Kobrinsky E, Ondriasová E, Moschella MC, Jayaraman T, Landers M, Ehrlich BE, Marks AR. (1994). Stabilization of calcium release channel (ryanodine receptor) function by FK506-binding protein. Cell *77*, 513-523.

Butler MH, David C, Ochoa GC, Freyberg Z, Daniell L, Grabs D, Cremona O, De Camilli P. (1997). Amphiphysin II (SH3P9; BIN1), a member of the amphiphysin/Rvs family, is concentrated in the cortical cytomatrix of axon initial segments and nodes of ranvier in brain and around T tubules in skeletal muscle. J Cell Biol *137*, 1355-1367.

Cai C, Weisleder N, Ko JK, Komazaki S, Sunada Y, Nishi M, Takeshima H, Ma J. (2009). Membrane repair defects in muscular dystrophy are linked to altered interaction between MG53, caveolin-3, and dysferlin. J Biol Chem *284*, 15894-15902.

Capote J, Bolaños P, Schuhmeier RP, Melzer W, Caputo C. (2005). Calcium transients in developing mouse skeletal muscle fibres. J Physiol *564*, 451-464.

Cenacchi G, Fanin M, De Giorgi LB, Angelini C. (2005). Ultrastructural changes in dysferlinopathy support defective membrane repair mechanism. J Clin Pathol *58*, 190-195.

Cherednichenko G, Hurne AM, Fessenden JD, Lee EH, Allen PD, Beam KG, Pessah IN. (2004). Conformational activation of Ca^{2+} entry by depolarization of skeletal myotubes. Proc Natl Acad Sci USA *101*, 15793-15798.

Chiu YH, Hornsey MA, Klinge L, Jørgensen LH, Laval SH, Charlton R, Barresi R, Straub V, Lochmüller H, Bushby K. (2009). Attenuated muscle regeneration is a key factor in dysferlin-deficient muscular dystrophy. Hum Mol Genet *18*, 1976-1989.

Cho, W., Stahelin, R.V. (2006). Membrane binding and subcellular targeting of C2 domains. Biochim Biophys Acta *1761*, 838-49.

Couchoux H, Allard B, Legrand C, Jacquemond V, Berthier C. (2007). Loss of caveolin-3 induced by the dystrophy-associated P104L mutation impairs L-type calcium channel function in mouse skeletal muscle cells. J Physiol *580*, 745-754.

Davis DB, Delmonte AJ, Ly CT, McNally EM. (2000). Myoferlin, a candidate gene and potential modifier of muscular dystrophy. Hum Mol Genet *9*, 217-226.

Davis DB, Doherty KR, Delmonte AJ, McNally EM. (2002). Calcium-sensitive phospholipid binding properties of normal and mutant ferlin C2 domains. J Biol Chem *277*, 22883-22888.

Defendi V, Pearson B. (1955). Quantitative estimation of succinic dehydrogenase activity in a single microscopic tissue section. J Histochem Cytochem *3*, 61-69.

De Luna N, Freixas A, Gallano P, Caselles L, Rojas-García R, Paradas C, Nogales G, Dominguez-Perles R, Gonzalez-Quereda L, Vílchez JJ, Márquez C, Bautista J, Guerrero A, Salazar JA, Pou A, Illa I, Gallardo E. (2006). Dysferlin expression in monocytes: a source of mRNA for mutation analysis. Neuromuscul Disord *17*, 69-76.

Dirksen RT. (2009). Checking your SOCCs and feet: the molecular mechanisms of Ca2+ entry in skeletal muscle. J Physiol *587*, 3139-3147.

Doherty KR, Cave A, Davis DB, Delmonte AJ, Posey A, Earley JU, Hadhazy M, McNally EM. (2005). Normal myoblast fusion requires myoferlin. Development *132*: 5565-75.

Doherty KR, Demonbreun AR, Wallace GQ, Cave A, Posey AD, Heretis K, Pytel P, McNally EM. (2008). The endocytic recycling protein EHD2 interacts with myoferlin to regulate myoblast fusion. J Biol Chem *283*, 20252-20260.

Duguez S, Bartoli M, Richard I. (2006) Calpain 3: a key regulator of the sarcomere? FEBS J *273*, 3427-3436.

Dulhunty AF. Excitation-contraction coupling from the 1950s into the new millennium. (2006). Clin Exp Pharmacol Physiol *33*, 763-772.

Edwards JN, Friedrich O, Cully TR, von Wegner F, Murphy RM, Launikonis BS. (2010). Upregulation of store-operated Ca^{2+} entry in dystrophic mdx mouse muscle. Am J Physiol Cell Physiol *299*, C42-50.

Engel AG, Franzini-Armstrong C. (2004). Myology Third ed. McGraw-Hill, New York.

Flucher BE, Takekura H, Franzini-Armstrang C. (1993). Development of the excitation-contraction coupling apparatus in skeletal muscle: association of sarcoplasmatic reticulum and transverse tubules with myofibrils. Dev Biol *160*, 135-147.

Fong PY, Turner PR, Denetclaw WF, Steinhardt RA. (1990). Increased activity of calcium leak channels in myotubes of Duchenne human and mdx mouse origin. Science *250*, 673-676.

Franco A Jr, Lansman JB. (1990). Calcium entry through stretch-inactivated ion channels in mdx myotubes. Nature *344*, 670-673.

Franzini-Armstrong C. (1991). Simultaneous maturation of transverse tubules and sarcoplasmic reticulum during muscle differentiation in the mouse. Dev Biol *146*, 353-363.

Frost A, Perera R, Roux A, Spasov K, Destaing O, Egelman EH, De Camilli P, Unger VM. (2008). Structural basis of membrane invagination by F-BAR domains. Cell *132*, 807-817.

Fujita E, Kouroku Y, Isoai A, Kumagai H, Misutani A, Matsuda C, Hayashi YK, Momoi T. (2007). Two endoplasmic reticulum-associated degradation (ERAD) systems for the novel variant of the mutant dysferlin: ubiquitin/proteasome ERAD(I) and autophagy/lysosome ERAD(II). Hum Mol Genet *16*, 618-629.

Galbiati F, Engelman JA, Volonte D, Zhang XL, Minetti C, Li M, Hou H, Jr Kneitz B, Edelmann W, Lisanti MP. (2001). Caveolin-3 null mice show a loss of caveolae, changes in the microdomain distribution of the dystrophin-glycoprotein complex, and t-tubule abnormalities. J Biol Chem *276*, 21425-21433.

Gallardo E, Rojas-García R, de Luna N, Pou A, Brown RH Jr, Illa I. (2001). Inflammation in dysferlin myopathy: immunohistochemical characterization of 13 patients. Neurology *57*, 2136-2138.

Goonasekera SA, Lam CK, Millay DP, Sargent MA, Hajjar RJ, Kranias EG, Molkentin JD. (2011). Mitigation of muscular dystrophy in mice by SERCA overexpression in skeletal muscle. J Clin Invest *121*, 1044-1052.

Grynkiewicz G, Poenie M, Tsien RY. (1985). A new generation of Ca2+ indicators with greatly improved fluorescence properties. J Biol Chem *260*, 3440-3450.

Guglieri M, Magri F, D'Angelo MG, Prelle A, Morandi L, Rodolico C, Cagliani R, Mora M, Fortunato F, Bordoni A, Del Bo R, Ghezzi S, Pagliarani S, Lucchiari S, Salani S, Zecca C, Lamperti C, Ronchi D, Aguennouz M, Ciscato P, Di Blasi C, Ruggieri A, Moroni I, Turconi A, Toscano A, Moggio M, Bresolin N, Comi GP. (2008). Clinical, molecular, and protein correlations in a large sample of genetically diagnosed Italian limb girdle muscular dystrophy patients. Hum Mutat *29*, 258-66.

Haase H, Podzuweit T, Lutsch G, Hohaus A, Kostka S, Lindschau C, Kott M, Kraft R, Morano I. (1999). Signaling from beta-adrenoceptor to L-type calcium channel: identification of a novel cardiac protein kinase A target possessing similarities to AHNAK. FASEB J *13*, 2161-2172.

Han R, Bansal D, Miyake K, Muniz VP, Weiss RM, McNeil PL, Campbell KP. (2007) Dysferlin-mediated membrane repair protects the heart from stress-induced left ventricular injury. J Clin Invest *117*, 1805-1813.

Han R, Campbell KP. (2007). Dysferlin and muscle membrane repair. Curr Opin Cell Biol *19*, 409-416.

Hattori H, Nagata E, Oya Y, Takahashi T, Aoki M, Ito D, Suzuki N. (2007). A novel compound heterozygous dysferlin mutation in Miyoshi myopathy siblings responding to dantrolene. Eur J Neurol *14*, 1288-1291.

Hernandez-Deviez DJ, Martin S, Laval SH, Lo HP, Cooper ST, North KN, Bushby K, Parton RG. (2006). Aberrant dysferlin trafficking in cells lacking caveolin or expressing dystrophy mutants of caveolin-3. Hum Mol Genet *15*, 129-142.

Ho M, Gallardo E, McKenna-Yasek D, De Luna N, Illa I, Brown Jr RH. (2002). A novel, blood-based diagnostic assay for limb girdle muscular dystrophy 2B and Miyoshi myopathy. Ann Neurol *51*, 129-133.

Ho M, Post CM, Donahue LR, Lidov HG, Bronson RT, Goolsby H, Watkins SC, Cox GA, Brown RH Jr. (2004). Disruption of muscle membrane and phenotype divergence in two novel mouse models of dysferlin deficiency. Hum Mol Genet *13*, 1999-2010.

Hong TT, Smyth JW, Gao D, Chu KY, Vogan JM, Fong TS, Jensen BC, Colecraft HM, Shaw RM. (2010). BIN1 localizes the L-type calcium channel to cardiac T-tubules. PLoS Biol *8*, 1000312.

Hong TT, Smyth JW, Chu KY, Vogan JM, Fong TS, Jensen BC, Fang K, Halushka MK, Russell SD, Colecraft H, Hoopes CW, Ocorr K, Chi NC, Shaw RM. (2012). BIN1 is reduced and Cav1.2 trafficking is impaired in human failing cardiomyocytes. Heart Rhythm *9*, 812-820.

Huang Y, Laval SH, van Remoortere A, Baudier J, Benaud C, Anderson LV, Straub V, Deelder A, Frants RR, den Dunnen JT, Bushby K, van der Maarel SM. (2007) AHNAK, a novel component of the dysferlin protein complex, redistributes to the cytoplasm with dysferlin during skeletal muscle regeneration. Faseb J *21*, 732-742.

Huang Y, de Morree A, van Remoortere A, Bushby K, Frants RR, Dunnen JT, van der Maarel SM. (2008) Calpain 3 is a modulator of the dysferlin protein complex in skeletal muscle. Hum Mol Genet *17*, 1855–1866.

Illa I, Serrano-Munuera C, Gallardo E, Lasa A, Rojas-Garcia R, Palmer J, Gallano P, Baiget M, Matsuda C, Brown RH. (2001) Distal anterior compartment myopathy: a dysferlin mutation causing a new muscular dystrophy phenotype. Ann Nerol *49*, 130-134.

Ishikawa H. (1968). Formation of elaborate networks of T-system tubules in cultured skeletal muscle with special reference to the T-system formation. J Cell Biol *38*, 51-66.

Ito K, Komazaki S, Sasamoto K, Yoshida M, Nishi M, Kitamura K, Takeshima H. (2001). Deficiency of triad junction and contraction in mutant skeletal muscle lacking junctophilin type 1. J Cell Biol *154*, 1059-1067.

Jayaraman T, Brillantes AM, Timerman AP, Fleischer S, Erdjument-Bromage H, Tempst P, Marks AR. (1992). FK506 binding protein associated with the calcium release channel (ryanodine receptor). J Biol Chem *267*, 9474-9477.

Kargacin ME, Kargacin GJ. (1996). The sarcoplasmic reticulum calcium pump is functionally altered in dystrophic muscle. Biochim Biophys Acta *1290*, 4-8.

Kelly AM. (1980). T tubules in neonatal rat soleus and extensor digitorum longus muscles. Dev Biol *80*, 501-505.

Kho C, Lee A, Jeong D, Hajjar RJ. (2010). Refilling Intracellular Calcium Stores. Drug Discov Today Dis Mech *7*, 145-150.

Klinge L, Laval S, Keers S, Haldane F, Straub V, Barresi R, Bushby K. (2007). From T-tubule to sarcolemma: damage-induced dysferlin translocation in early myogenesis. Faseb J *21*, 1768-1776.

Klinge L, Dean AF, Kress W, Dixon P, Charlton R, Müller JS, Anderson LV, Straub V, Barresi R, Lochmüller H, Bushby K. (2008) Late onset in dysferlinopathy widens the clinical spectrum. Neuromuscul Disord *18*, 288-290.

Klinge L, Aboumousa A, Eagle M, Hudson J, Sarkozy A, Vita G, Charlton R, Roberts M, Straub V, Barresi R, Lochmüller H, Bushby K. (2009) New aspects on patients affected by dysferlin deficient muscular dystrophy. J Neurol Neurosurg Psychiatry *81*; 946-953.

Klinge L, Harris J, Sewry C, Charlton R, Anderson L, Laval S, Chiu YH, Hornsey M, Straub V, Barresi R, Lochmüller H, Bushby K. (2010) Dysferln associates with the developing t-tubule system in rodent and human skeletal muscle. Muscle Nerve *41*, 166-173.

Klopfenstein DR, Vale RD. The lipid binding pleckstrin homology domain in UNC-104 kinesin is necessary for synaptic vesicle transport in Caenorhabditis elegans. (2004). Mol Biol Cell *15*, 3729-3739.

Koenig M, Monaco AP, Kunkel LM. (1988). The complete sequence of dystrophin predicts a rod-shaped cytoskeletal protein. Cell *53*, 219-228.

Komazaki S, Ito K, Takeshima H, Nakamura H. (2002). Deficiency of triad formation in developing skeletal muscle cells lacking junctophilin type 1. FEBS Lett *524*, 225-229.

Krahn M, Béroud C, Labelle V, Nguyen K, Bernard R, Bassez G, Figarella-Branger D, Fernandez C, Bouvenot J, Richard I, Ollagnon-Roman E, Bevilacqua JA,Salvo E, Attarian S, Chapon F, Pellissier JF, Pouget J, Hammouda el H, Laforêt P, Urtizberea JA, Eymard B, Leturcq F, Lévy N. (2009). Analysis of the DYSF mutational spectrum in a large cohort of patients. Hum Mutat *30*, 345-375.

Krahn M, Wein N, Bartoli M, Lostal W, Courrier S, Bourg-Alibert N, Nguyen K, Vial C, Streichenberger N, Labelle V, DePetris D, Pécheux C, Leturcq F, Cau P, Richard I, Lévy N. (2010) A naturally occurring human minidysferlin protein repairs sarcolemmal lesions in a mouse model of dysferlinopathy. Sci Transl Med *2*, 50-69.

Kramerova I, Kudryashova E, Wu B, Ottenheijm C, Granzier H, Spencer MJ. (2008). Novel role of calpain-3 in the triad-associated protein complex regulating calcium release in skeletal muscle. Hum Mol Genet *17*, 3271-3280.

Krause T, Gerbershagen MU, Fiege M, Weisshorn R, Wappler F, (2004). Dantrolene - a review of its pharmacology, therapeutic use and new developments. Anaesthesia *59*, 364-373.

Kurebayashi N, Ogawa Y. (2001). Depletion of Ca^{2+} in the sarcoplasmic reticulum stimulates Ca^{2+} entry into mouse skeletal muscle fibres. J Physiol *533*, 185-99.

Kuru S, Yasuma F, Wakayama T, Kimura S, Konagaya M, Aoki M, Tanabe M, Takahashi T. (2004). A patient with limb girdle muscular dystrophy type 2B (LGMD2B) manifesting cardiomyopathy]. Rinsho Shinkeigaku *44*, 375-378.

Laval SH, Bushby KM. (2004) Limb-girdle muscular dystrophies - from genetics to molecular pathology. Neuropathol Appl Neurobiol *30*, 91-105.

Lee E, Marcucci M, Daniell L, Pypaert M, Weisz OA, Ochoa GC, Farsad K, Wenk MR, De Camilli P. (2002). Amphiphysin 2 (Bin1) and T-tubule biogenesis in muscle. Science *297*, 1193-1196.

Lennon NJ, Kho A, Bacskai BJ, Perlmutter SL, Hyman BT, Brown RH Jr, (2003). Dysferlin interacts with annexins A1 and A2 and mediates sarcolemmal woundhealing. J Biol Chem *278*, 50466-50473.

Lerario A, Cogiamanian F, Marchesi C, Belicchi M, Bresolin N, Porretti L, Torrente Y. (2010). Effects of rituximab in two patients with dysferlin-deficient muscular dystrophy. BMC Musculoskelet Disord *11*, 157.

Li H, Ding X, Lopez JR, Takeshima H, Ma J, Allen PD, Eltit JM. (2010). Impaired Orai1-mediated resting Ca^{2+} entry reduces the cytosolic [Ca^{2+}] and sarcoplasmic reticulum Ca2+ loading in quiescent junctophilin 1 knock-out myotubes. J Biol Chem *285*, 39171-39179.

Liu J, Aoki M, Illa I, Wu C, Fardeau M, Angelini C, Serrano C, Urtizberea JA, Hentati F, Hamida MB, et al. (1998). Dysferlin, a novel skeletal muscle gene, is mutated in myoshi myopathy and limb girdle muscular dystrophy. Nat Genet *20*, 31-36.

Lostal W, Bartoli M, Bourg N, Roudaut C, Bentaïb A, Miyake K, Guerchet N, Fougerousse F, McNeil P, Richard I. (2010). Efficient recovery of dysferlin deficiency by dual adeno-associated vector-mediated gene transfer. Hum Mol Genet *19*, 1897-1907.

Lostal W, Bartoli M, Roudaut C, Bourg N, Krahn M, Pryadkina M, Borel P, Suel L, Roche JA, Stockholm D, Bloch RJ, Levy N, Bashir R, Richard I. (2012). Lack of correlation between outcomes of membrane repair assay and correction of dystrophic changes in experimental therapeutic strategy in dysferlinopathy. PLoS One *7*, 38036.

Louch WE, Mørk HK, Sexton J, Strømme TA, Laake P, Sjaastad I, Sejersted OM. (2006). T-tubule disorganization and reduced synchrony of Ca^{2+} release in murine cardiomyocytes following myocardial infarction. J Physiol *574*, 519-533.

Luo X, Hojayev B, Jiang N, Wang ZV, Tandan S, Rakalin A, Rothermel BA, Gillette TG, Hill JA. (2012). STIM1-dependent store-operated Ca2+ enty is required for pathological cardiac hypertrophy. J Mol Cell Cardiol *52*, 136-147.

Lyfenko AD, Dirksen RT.(2008). Differential dependence of store-operated and excitation-coupled Ca^{2+} entry in skeletal muscle on STIM1 and Orai1. J Physiol *586*, 4815-4824.

Lyon AR, MacLeod KT, Zhang Y, Garcia E, Kanda GK, Lab MJ, Korchev YE, Harding SE, Gorelik J. (2009). Loss of T-tubules and other changes to surface topography in ventricular myocytes from failing human and rat heart. Proc Natl Acad Sci USA *106*, 6854-6859.

Lyon AR, Nikolaev VO, Miragoli M, Sikkel MB, Paur H, Benard L, Hulot JS, Kohlbrenner E, Hajjar RJ, Peters NS, Korchev YE, Macleod KT, Harding SE, Gorelik J. (2012). Plasticity of surface structures and β(2)-adrenergic receptor localization in failing ventricular cardiomyocytes during recovery from heart failure. Circ Heart Fail *5*, 357-365.

Maier LS, Bers DM. (2002). Calcium, calmodulin, and calcium-calmodulin kinase II: heartbeat to heartbeat and beyond. J Mol Cell Cardiol *34*, 919-39.

Maier LS, Bers DM, Pieske B. (2000). Differences in Ca^{2+}-handling and sarcoplasmic reticulum Ca^{2+}-content in isolated rat and rabbit myocardium. J Mol Cell Cardiol *32*, 2249-2258.

Marty NJ, Holman CL, Abdullah N, Johnson CP. (2013). The c2 domains of otoferlin, dysferlin, and myoferlin alter the packing of lipid bilayers. Biochemistry *52*, 5585-5592.

Marx SO, Marks AR. (2002). Regulation of the ryanodine receptor in heart failure. Basic Res Cardiol *97*, 49-51.

Matsuda C, Hayashi YK, Ogawa M, Aoki M, Murayama K, Nishino I, Nonaka I, Arahata K, Brown RH Jr. (2001). The sarcolemmal proteins dysferlin and caveolin-3 interact in skeletal muscle. Hum Mol Genet, *10*, 1761-1766.

Matsuda C, Kameyama K, Tagawa K, Ogawa M, Suzuki A, Yamaji S, Okamoto H, Nishino I, Hayashi YK. (2005). Dysferlin interacts with affixin (beta-parvin) at the sarcolemma. J Neuropathol Exp Neurol *64*, 334-340.

McMahon HT, Kozlov MM, Martens S. (2010). Membrane curvature in synaptic vesicle fusion and beyond. Cell *140*, 601-605.

McNeil PL, Steinhardt RA. (2003) Plasma membrane disruption: repair, prevention, adaption. Annu Rev Cell Biol *19*, 697-731.

Merritt JE, McCarthy SA, Davies MP, Moores KE. (1990). Use of fluo-3 to measure cytosolic Ca^{2+} in platelets and neutrophils. Loading cells with the dye, calibration of traces, measurements in the presence of plasma, and buffering of cytosolic Ca^{2+}. Biochem J *269*, 513-519.

Milting H, Heilmeyer LM Jr, Thieleczek R. (1994). Phosphoinositides in membranes that build up the triads of rabbit skeletal muscle. FEBS Lett *345*, 211-218.

Min SW, Chang WP, Südhof TC. (2007). E-Syts, a family of membranous Ca^{2+}-sensor proteins with multiple C2 domains. Proc Natl Acad Sci USA *104*, 3823-3828.

Minetti C, Bado M, Broda P, Sotgia F, Bruno C, Galbiati F, Volonte D, Lucania G, Pavan A, Bonilla E, Lisanti MP, Cordone G. (2002). Impairment of caveolae formation and T-system disorganization in human muscular dystrophy with caveolin-3 deficiency. Am J Pathol *160*, 265-270.

Moore SA, Shilling CJ, Westra S, Wall C, Wicklund MP, Stolle C, Brown CA, Michele DE, Piccolo F, Winder TL, Stence A, Barresi R, King N, King W, Florence J, Campbell KP, Fenichel GM, Stedman HH, Kissel JT, Griggs RC, Pandya S, Mathews KD, Pestronk A, Serrano C, Darvish D, Mendell JR. (2006). Limb-girdle muscular dystrophy in the United States. J Neuropathol Exp Neurol *65*, 995-1003.

Muller AJ, Baker JF, DuHadaway JB, Ge K, Farmer G, Donover PS, Meade R, Reid C, Grzanna R, Roach AH, Shah N, Soler AP, Prendergast GC. (2003). Targeted disruption of the murine Bin1/Amphiphysin II gene does not disable endocytosis but results in embryonic cardiomyopathy with aberrant myofibril formation. Mol Cell Biol *23*, 4295-4306.

Murphy RM, Mollica JP, Lamb GD. (2009). Plasma membrane removal in rat skeletal muscle fibers reveals caveolin-3 hot-spots at the necks of transverse tubules. Exp Cell Res *315*, 1015-1028.

Nagaraju K, Rawat R, Veszelovszky E, Thapliyal R, Kesari A, Sparks S, Raben N, Plotz P, Hoffman EP. (2008). Dysferlin Deficiency Enhances Monocyte Phagocytosis: A Model for the Inflammatory Onset of Limb-Girdle Muscular Dystrophy 2B. Am J Pathol *172*, 774-785.

Nakai J, Dirksen RT, Nguyen HT, Pessah IN, Beam KG, Allen PD. (1996). Enhanced dihydropyridine receptor channel activity in the presence of ryanodine receptor. Nature *380*, 72-75.

Nalefski EA, Falke JJ. (1996). The C2 domain calcium-binding motif: structural and functional diversity. Protein Sci *5*, 2375-90.

Nicot AS, Toussaint A, Tosch V, Kretz C, Wallgren-Pettersson C, Iwarsson E, Kingston H, Garnier JM, Biancalana V, Oldfors A, Mandel JL, Laporte J. (2007). Mutations in amphiphysin 2 (BIN1) disrupt interaction with dynamin 2 and cause autosomal recessivecentronuclear myopathy. Nat Genet *39*, 1134-1139.

Nishi M, Komazaki S, Kurebayashi N, Ogawa Y, Noda T, Iino M, Takeshima H. (1999). Abnormal features in skeletal muscle from mice lacking mitsugumin 29. J Cell Biol *147*, 1473-1480.

Nishimura S, Kawai Y, Nakajima T, Hosoya Y, Fujita H, Katoh M, Yamashita H, Nagai R, Sugiura S. (2006). Membrane potential of rat ventricular myocytes responds to axial stretch in phase, amplitude and speed-dependent manners. Cardiovasc Res *72*, 403-411.

Pan Z, Yang D, Nagaraj RY, Nosek TA, Nishi M, Takeshima H, Cheng H, Ma J. (2002). Dysfunction of store-operated calcium channel in muscle cells lacking mg29. Nat Cell Biol *4*, 379-83.

Parton RG, Way M, Zorzi N, Stang E. (1997) Caveolin-3 associates with developing T-tubules during muscle differentiation. J Cell Biol *136*, 137-154.

Patel P, Harris R, Geddes SM, Strehle EM, Watson JD, Bashir R, Bushby K, Driscoll PC, Keep NH. (2008). Solution structure of the inner DysF domain of myoferlin and implications for limb girdle muscular dystrophy type 2b. J Mol Biol *379*, 981-990.

Piccolo F, Moore SA, Ford GC, Campbell KP. (2000). Intracellular accumulation and reduced sarcolemmal expression of dysferlin in limb-girdle muscular dystrophies. Ann Neurol *48*, 902-912.

Picht E, Zima AV, Blatter LA, Bers DM. (2007). SparkMaster: automated calcium spark analysis with ImageJ. Am J Physiol Cell Physiol *293*, 1073-1081.

Pieske B, Schlotthauer K, Schattmann J, Beyersdorf F, Martin J, Just H, Hasenfuss G. (1997): Ca^{2+}-dependent and Ca^{2+}-independent regulation of contractility in isolated human myocardium. Basic Res Cardiol *92*; 75-86.

Pinniger GJ, Bruton JD, Westerblad H, Ranatunga KW. (2005). Effects of a myosin-II inhibitor (N-benzyl-p-toluene sulphonamide, BTS) on contractile characteristics of intact fast-twitch mammalian muscle fibres. J Muscle Res Cell Motil *26*, 135-141.

Posey AD Jr, Pytel P, Gardikiotes K, Demonbreun AR, Rainey M, George M, Band H, McNally EM. (2011). Endocytic recycling proteins EHD1 and EHD2 interact with fer-1-like-5 (Fer1L5) and mediate myoblast fusion. J Biol Chem *286*, 7379-7388.

Pressmar J,Brinkmeier H, Seewald MJ, Naumann T, Rüdel R. (1994). Intracellular Ca^{2+} concentrations are not elevated in resting cultured muscle from Duchenne (DMD) patients and in MDX mouse muscle fibres. Pflügers Arch *426*, 499- 505.

Rayavarapu S, Van der Meulen JH, Gordish-Dressman H, Hoffman EP, Nagaraju K, Knoblach SM. (2010). Characterization of dysferlin deficient SJL/J mice to assess preclinical drug efficacy: fasudil exacerbates muscle disease phenotype. PLoS One *5*, 12981.

Razzaq A, Robinson IM, McMahon HT, Skepper JN, Su Y, Zelhof AC, Jackson AP, Gay NJ, O'Kane CJ. (2001). Amphiphysin is necessary for organization of the excitation-contraction coupling machinery of muscles, but not for synaptic vesicle endocytosis in Drosophila. Genes Dev *15*, 2967-79.

Rechsteiner M, Rogers SW. PEST sequences and regulation by proteolysis. (1996). Trends Biochem Sci *21*, 267-271.

Rizo J, Südhof TC. C2-domains, structure and function of a universal Ca^{2+}-binding domain. (1998). J Biol Chem *273*, 15879-15882.

Roux I, Safieddine S, Nouvian R, Grati M, Simmler MC, Bahloul A, Perfettini I, Le Gall M, Rostaing P, Hamard G, Triller A, Avan P, Moser T, Petit C. (2006). Otoferlin, defective in a human deafness form, is essential for exocytosis at the auditory ribbon synapse. Cell *127*, 277-289.

Royer L, Ríos E. Deconstructing calsequestrin. (2009). Complex buffering in the calcium store of skeletal muscle. J Physiol *587*, 3101-311.

Schiaffino S, Cantini M, Sartore S. (1977). T-system formation in cultured rat skeletal tissue. Tissue Cell *9*, 437-446.

Schwinger RH, Böhm M, Müller-Ehmsen J, Uhlmann R, Schmidt U, Stäblein A, Uberfuhr P, Kreuzer E, Reichart B, Eissner HJ. (1993). Effect of inotropic stimulation on the negative force-frequency relationship in the failing human heart. Circulation *88*, 2267-2276.

Shin OH, Han W, Wang Y, Südhof TC. (2005). Evolutionarily conserved multiple C2 domain proteins with two transmembrane regions (MCTPs) and unusual Ca^{2+} binding properties. J Biol Chem *280*, 1641-1651.

Shinozaki-Narikawa N, Kodama T, Shibasaki Y. (2006). Cooperation of phosphoinositides and BAR domain proteins in endosomal tubulation. Traffic *7*, 1539-1550.

Shao X, Li C, Fernandez I, Zhang X, Südhof TC, Rizo J. (1997). Synaptotagmin-syntaxin interaction: the C2 domain as a Ca^{2+}-dependent electrostatic switch. Neuron *18*, 133-142.

Song LS, Sobie EA, McCulle S, Lederer WJ, Balke CW, Cheng H. (2006). Orphaned ryanodine receptors in the failing heart. Proc Natl Acad Sci USA *103*, 4305-4310.

Straub V, Campbell KP, (1997). Muscular dystrophies and the dystrophin-glycoprotein complex. Curr Opin Neurol *10*, 168-175.

Sutton RB, Davletov BA, Berghuis AM, Südhof TC, Sprang SR. (1995). Structure of the first C2 domain of synaptotagmin I: a novel Ca^{2+}/phospholipid-binding fold. Cell *80*, 929-938.

Takekura H, Nishi M, Noda T, Takeshima H, Franzini-Armstrong C. (1995). Abnormal junctions between surface membrane and sarcoplasmic reticulum in skeletal muscle with a mutation targeted to the ryanodine receptor. Proc Natl Acad Sci USA *92*, 3381-3385.

Takekura H, Flucher BE, Franzini-Armstrong C. (2001a). Sequential docking, molecular differentiation, and positioning of T-Tubule/SR junctions in developing mouse skeletal muscle. Dev Biol *239*, 204-214.

Takekura H, Fujinami N, Nishizawa T, Ogasawara H, Kasuga N. (2001b). Eccentric exercise-induced morphological changes in the membrane systems involved in excitation-contraction coupling in rat skeletal muscle. J Physiol *533*, 571-583.

Takeshima H, Komazaki S, Nishi M, Iino M, Kangawa K. (2000). Junctophilins: a novel family of junctional membrane complex proteins. Mol Cell *6*, 11-22.

Therrien C, Dodig D, Karpati G, Sinnreich M. (2006). Mutation impact on dysferlin inferred from database analysis and computer-based structural predictions. J Neurol Sci *250*, 71-78.

Therrien C, Di Fulvio S, Pickles S, Sinnreich M. (2009) Characterization of lipid binding specificities of dysferlin C2 domains reveals novel interactions with phosphoinositides. Biochemnistry *48*, 2377-84.

Tjondrokoesoemo A, Park KH, Ferrante C, Komazaki S, Lesniak S, Brotto M, Ko JK, Zhou J, Weisleder N, Ma J. (2011). Disrupted membrane structure and intracellular Ca2+ signalling in adult skeletal muscle with acute knockdown of Bin1. PLoS One *6*, 25740.

Toussaint A, Cowling BS, Hnia K, Mohr M, Oldfors A, Schwab Y, Yis U, Maisonobe T, Stojkovic T, Wallgren-Pettersson C, Laugel V, Echaniz-Laguna A, Mandel JL, Nishino I, Laporte J. (2011). Defects in amphiphysin 2 (BIN1) and triads in several forms of centronuclear myopathies. Acta Neuropathol *121*, 253-266.

Vafiadaki E, Reis A, Keers S, Harrison R, Anderson LV, Raffelsberger T, Ivanova S, Hoger H, Bittner RE, Bushby K, Bashir R. (2001). Cloning of the mouse dysferlin gene and genomic characterization of the SJL-Dysf mutation. Neuroreport *12*, 625-629.

Vandré DD, Ackerman WE 4th, Kniss DA, Tewari AK, Mori M, Takizawa T, Robinson JM. (2007). Dysferlin is expressed in human placenta but does not associate with caveolin. Biol Reprod *77*, 533-542.

Van Deurs B, von Bũlow F, Vilhardt F, Holm PK, Sandvig K. (1996). Destabilization of plasma membrane structure by prevention of actin polymerization. Microtubule-dependent tubulation of the plasma membrane. J Cell Sci *109*, 1655-1665.

Van Oort RJ, Garbino A, Wang W, Dixit SS, Landstrom AP, Gaur N, De Almeida AC, Skapura DG, Rudy Y, Burns AR, Ackerman MJ, Wehrens XH. (2011). Disrupted junctional

membrane complexes and hyperactive ryanodine receptors after acute junctophilin knockdown in mice. Circulation *123*, 979-988.

Veratti E. (1961). Investigations on the fine structure of striated muscle fiber read before the Reale Istituto Lombardo, 13 March 1902. J Biophys Biochem Cytol *10*, 1-59.

Wagner E, Lauterbach MA, Kohl T, Westphal V, Williams GS, Steinbrecher JH, Streich JH, Korff B, Tuan HT, Hagen B, Luther S, Hasenfuss G, Parlitz U, Jafri MS, Hell SW, Lederer WJ, Lehnart SE. (2012). Stimulated emission depletion live-cell super-resolution imaging shows proliferative remodeling of T-tubule membrane structures after myocardial infarction. Circ Res *111*, 402-414.

Wang X, Weisleder N, Collet C, Zhou J, Chu Y, Hirata Y, Zhao X, Pan Z, Brotto M, Cheng H, Ma J. (2005). Uncontrolled calcium sparks act as a dystrophic signal for mammalian skeletal muscle. Nat Cell Biol *7*, 525-530.

Washington NL, Ward S. (2006) FER-1 regulates Ca^{2+}-mediated membrane fusion during C. elegans spermatogenesis. J Cell Sci *119*, 2552-2562.

Wehrens XH, Lehnart SE, Huang F, Vest JA, Reiken SR, Mohler PJ, Sun J, Guatimosim S, Song LS, Rosemblit N, D'Armiento JM, Napolitano C, Memmi M, Priori SG, Lederer WJ, Marks AR. (2003). FKBP12.6 deficiency and defective calcium release channel (ryanodine receptor) function linked to exercise-induced sudden cardiac death. Cell *113*, 829-840.

Wenzel K, Carl M, Perrot A, Zabojszcza J, Assadi M, Ebeling M, Geier C, Robinson PN, Kress W, Osterziel KJ, Spuler S. (2006). Novel sequence variants in dysferlin-deficient muscular dystrophy leading to mRNA decay and possible C2-domain misfolding. Hum Mutat *27*, 599-600.

Wenzel K, Geier C, Qadri F, Hubner N, Schulz H, Erdmann B, Gross V, Bauer D, Dechend R, Dietz R, Osterziel KJ, Spuler S, Ozcelik C. (2007) Dysfunction of dysferlin-deficient hearts. J Mol Med *85*, 1203-1214.

Yan M, Rachubinski DA, Joshi S, Rachubinski RA, Subramani S. (2008). Dysferlin domain-containing proteins, Pex30p and Pex31p, localized to two compartments, control the number and size of oleate-induced peroxisomes in Pichia pastoris. Mol Biol Cell *19*, 885-898.

Yao A, Matsui H, Spitzer KW, Bridge JH, Barry WH. (1997). Sarcoplasmic reticulum and Na^{+}/Ca^{2+} exchanger function during early and late relaxation in ventricular myocytes. Am J Physiol *273*, 2765-2773.

Yasunaga S, Grati M, Cohen-Salmon M, El-Amraoui A, Mustapha M, Salem N, El-Zir E, Loiselet J, Petit C. (1999). A mutation in OTOF, encoding otoferlin, a FER-1-like protein, causes DFNB9, a nonsyndromic form of deafness. Nat Genet *21*, 363-369.

Acknowledgements

I would like to thank Prof. Jutta Gärtner for giving me the wonderful opportunity to join the department of pediatrics and for her support during my PhD thesis. I am very thankful for the use of the well-equipped laboratory of the department of pediatrics.

I am sincerely grateful to PD Dr. Lars Klinge and PD Dr. Sven Thoms for giving me the opportunity to work on this really interesting and challenging project and for their excellent supervision. I appreciate their never failing encouragement and their valuable criticisms and feedback. This work would not have been possible without you.

I would also like to thank Prof. Lars Maier and Dr. Stefan Wagner for the excellent collaboration and for giving me the opportunity to use the equipment of the cardiology lab. I am very grateful for their scientific support, helpful ideas and discussions. Further I would like to thank Timo Schulte, Thomas Sowa and all other members of the AG Maier for technical assistance and encouragement.

I would like to give special thanks to Irmgard Cierny and Marc Ziegenbein for excellent technical assistance in the lab, help and encouragement. I would also like to give special thanks to all members of the “pediatrics lab” for creating a pleasant atmosphere, scientific team work, help, and accompany.

I thank Dr. Viacheslav Nicolaev for excellent collaboration and scientific support.

I would like to thank Prof. David Liebetanz for the collaboration and for making the running wheel experiment possible.

I thank the members of my thesis committee, Prof. Jutta Gärtner, Prof. Peter Schu and Prof. Wolfgang Brück for helpful discussions, ideas and support.

I would also like to thank the coordination team from the Molecular Medicine Graduate Program PD Dr. Werner Albig and Dr. Erik Meskauskas for their support in administrative matters during the last three years.